UNIVERSITY OF SOUTHAMPTON

FACULTY OF ENGINEERING, SCIENCE AND MATHEMATICS

School of Ocean and Earth Science

Modelling the seasonal succession of *Emiliania huxleyi* and other phytoplankton in the Bering Sea

by

Agostino Merico

Thesis for the degree of Doctor of Philosophy

November 2003

UNIVERSITY OF SOUTHAMPTON

ABSTRACT

FACULTY OF ENGINEERING, SCIENCE AND MATHEMATICS
SCHOOL OF OCEAN AND EARTH SCIENCE

Doctor of Philosophy

MODELLING THE SEASONAL SUCCESSION OF EMILIANIA HUXLEYI AND OTHER PHYTOPLANKTON IN THE BERING SEA

by Agostino Merico

Several years of physical and biological anomalies have affected the Bering Sea shelf ecosystem since 1997. Such anomalies reached their peak in a striking visual phenomenon: the first appearance in the area of bright waters caused by massive blooms of the coccolithophore *Emiliania huxleyi* (*E. huxleyi*). This study provides an insight into the mechanisms of phytoplankton succession in the south-eastern part of the shelf during such years and addresses the causes of *E. huxleyi* success by means of a 1/2-dimensional time-dependent ecosystem model, field data and satellite-derived information. A number of potential hypotheses are identified based on field observations conducted in the area and on previous knowledge of *E. huxleyi* general ecology. The key hypotheses are then considered as causative factors and explored with the model. The model also includes carbon chemistry routines in order to investigate the relations between phytoplankton and the carbonate system.

Archived satellite imagery (from 1978 to 1997), examined with the aim of establishing the history of the presence of *E. huxleyi* in the Bering Sea, revealed that a small bloom was already present in 1996, a precursor of the big blooms which occurred the following years. No blooms were detected before 1996.

The modelling study suggests that *E. huxleyi* blooms were initiated in 1997 by a shallow mixed layer depth in conjunction with a lack of photoinhibition in this species. A top-down control by microzooplankton selectively grazing phytoplankton other than *E. huxleyi* appears to be responsible for the unusual long persistence of the blooms (from three to four months). Compelling evidence is also provided that can potentially explain the typical diatom-coccolithophore succession sequence in terms of calcite saturation state (a variable recently shown to be crucial for the production of calcium carbonate by all marine calcifying organisms). Therefore, a simple ecological mechanism is proposed: **"microzooplankton grazing responds to frustule silicification and coccosphere calcification"** so that lightly (or heavily) silicified frustules make diatoms susceptible of higher (or lower) grazing pressure by microzooplankton and lightly (or heavily) calcified coccospheres make coccolithophore susceptible of higher (or lower) grazing pressure by microzooplankton.

It is also shown that the high N:P ratio hypothesis, regarded as crucial in the formation of blooms of this species in previous studies, does not hold in the Bering Sea shelf. Evidence is provided which suggests that *E. huxleyi* is able to exploit situations where either phosphorus or nitrogen is limiting to competing species, both in mesocosm experiments and in the ocean.

Contents

List of Figures

List of Tables

Acknowledgements

I offer great thanks and appreciation to my supervisor, Toby Tyrrell, for his support, guidance and useful advices. Thanks are also extended to Rachel Mills, for her assistance and encouragement in her role as second supervisor, and to Martin Sinha, for the enthusiasm demonstrated for my work as the chair person of my advisory panel.

I am profoundly indebted to Evelyn Lessard who provided a great hospitality and valuable insights into the biology of microplankton during a three-month visit to the School of Oceanography of the University of Washington in Seattle (USA).

Thanks to Mike Fasham, Tom Anderson, Patrick Holligan, John Shepherd and Paolo Cipollini, with whom I have had many fruitful and stimulating discussions during all my time at Southampton Oceanography Centre. Very helpful conversation pertaining the work of this thesis were had also with Jeremy Young, Sandra Broerse, Joanna Waniek, Andrew Yool, Adrian Martin and Boris Kelly-Gerreyn. I am indebted to Joanna Waniek and Alice Stuart-Menteth for their comments on a draft of this thesis. My thanks to Chris Brown and Steve Groom for their collaboration and helpful advice on the part of this study concerning the remote sensing of phytoplankton from space. I wish to thank Temel Oguz for his hospitality at the Institute of Marine Science of the Middle East Technical University in Erdemli (Turkey) and for the fruitful discussions we had on ecosystem modelling, and Tulay Cokacar for her help with SeaWiFS-derived calcite data.

I am very grateful to Sei-ichi Saitoh, who gave me the possibility to take part to a cruise in the Bering Sea in August 2002 where I had the great chance to observe closely the complex ecosystem I have been trying to model. Many thanks to Takahiro Iida for his help during the cruise and to Jun Yamamoto for giving me access to the "secrets" of the T/V Oshoro Maru and for making some of the Oshoro Maru public data easily available in electronic formats. Modelling efforts in marine ecology are only as meaningful as the availability of data to constrain and validate them. I am therefore deeply grateful to officers and crew of the T/V Oshoro Maru and R/V Alpha Helix, to all technicians involved in sampling, carrying out analyses and measuring concentrations.

This thesis was funded by a research grant from the University of Southampton, and I acknowledge the World University Network scholarship for giving me the financial support for a three-month visit to the University of Washington where I could get in contact with the major experts of the Bering Sea ecosystem (of whom I wish to mention in particular Phyllis Stabeno and Terry Whitledge). I am very grateful to my friends and colleagues at the Southampton Oceanography Centre and elsewhere, who have helped no end in making these years really enjoyable with the benefit of shared experience. It is a long list but you know who you are.

Finally, I wish to give a special thank to my wife and our parents for all they have done for me, for their faith in me, for their support and for their encouragement.

This thesis is dedicated to the memory of my mother, Rosa.

Phytoplankton succession is a series of false starts in ever-changing directions toward a momentarily defined unispecific specificity which is never achieved because the environment immediately changes and alters the direction of competitive pressure.

Hutchinson G. E. (1967). A treatise on Limnology. Vol. II, John Wiley, New York

Chapter 1

Introduction

This thesis is concerned with understanding the functioning of the lowest trophic levels of the Bering Sea shelf ecosystem, and in particular with one phytoplankton species: the coccolithophore *Emiliania huxleyi* (*E. huxleyi*).

The Bering Sea shelf is one of the richest and most productive ecosystems of the world (Walsh *et al.*, 1989), providing almost half of the fish and shell-fish caught in the United States (Macklin, 1999). However, it has undergone significant perturbations, which have been most evident after the mid '90s (Stabeno *et al.*, 2001). The temporal disturbances in the Bering Sea have been linked to a series of climate-induced anomalies (Overland *et al.*, 2001). These climatic anomalies were accompanied by several disruptions to the biotic components of the ecosystem (Stockwell *et al.*, 2001; Baduini *et al.*, 2001; Brodeur *et al.*, 2002) including a massive bloom of the coccolithophore *E. huxleyi* (Vance *et al.*, 1998; Sukhanova & Flint, 1998). *E. huxleyi* blooms of such magnitude, covering an area of at least 200,000 km^2 and as intensive as 2.1-2.8x10^6 cells L^{-1}, have never been observed in this area before 1997 and they seem they have disappeared since 2001. Their seasonal persistence was also a great surprise (from three to four months as compared to one to two months for instance in the north Atlantic, where this species is more common).

Notwithstanding the importance of the specific consequences that the unprece-

dented massive *E. huxleyi* presence might have had on the Bering Sea ecosystem, such blooms have also a global significance in terms of environmental impact through dimethyl-sulphide production, large fluxes of calcium carbonate being exported out of the surface waters and changes in the CO_2 air-sea fluxes (Westbroek *et al.*, 1993).

As said, the massive presence of *E. huxleyi* in the Bering Sea 1997-2000 is an unprecedented case. This makes the region an ideal ground for exploring and testing hypotheses, established through many years of studies, about the major requirements for the formation of these blooms in their natural environment, or to look for new ones. For instance, how and to what extent did the unusual weather conditions contribute to the arrival of *E. huxleyi* in the Bering Sea? What were the reasons for such an atypical seasonal persistence? And ultimately, by studying it in an environment as rich and complex as the Bering Sea ecosystem, what more can we learn about the ecology of a cosmopolitan species like *E. huxleyi* and its interactions with other plankton?

1.1 Aims

The general aims of this study were to understand the conditions that allowed *E. huxleyi* to temporarily "colonize" the area, and to investigate the mechanisms of phytoplankton seasonal succession during years of anomalous climatic forcing.

A mathematical model has been developed (the numerical code being written *ex novo*) and implemented. The model has been constrained with field observations and satellite-derived information. Given that *E. huxleyi* has never been reported in the Bering Sea before 1997, the modelling studies have been accompanied by an initial investigation of archive satellite imagery (from 1978 to 1997) with the aim to establish the history of the presence of *E. huxleyi* in the Bering Sea. Due to the potential impact of this species on the global carbon cycle through calcification, the chemistry of carbon has been also included in the model, in order to investigate the variations of the most important variables of the carbon system in connection with

the biological calcification process.

There are no models that can reproduce the full complexity of a real ecosystem. What, therefore, is the utility of using a model? A model is a tool like any other tool in oceanography and, as such, it does have uncertainties. The model presented here is an ecological model with no explicit spatial dimensions in it. Mesoscale physical features, for example, are not contemplated. The model is applied to a definite location of the Bering Sea shelf with the assumption that all that the model shows of that precise point is valid within a reasonable distance. This same principle is used when the properties shown by a single measuring cast in the field are generalised to the adjacent waters. In this respect, the uncertainty of this model is comparable with the uncertainty related to any measuring exercise in the field, but with the added value of being able to put the observations in the context of the all variables (or many of them) affecting the ecosystem and thus to explore their mutual interactions. Models allow, in a rigorous and quantitative way, to investigate hypotheses and to test if they are broadly compatible with known facts.

1.2 The Bering Sea

1.2.1 Hydrography and physics

The Bering Sea (Fig. 1.1) is a semi-enclosed, high latitude sea. It is divided almost equally in areal extent between a deep basin (maximum depth 3,500 m) and the continental shelf (with depths less than 200 m).

Three hydrographic domains (Coachman, 1986) can be identified over the shelf: coastal, middle and outer (Fig. 1.2).

The domains are separated by fronts, located approximately at the 50 and 100 m isobaths, and at the shelf break (150-200 m). The characteristics of the water columns in these three domains may be very different. Typically, tides and winds keep all the water in the coastal domain fairly mixed throughout the year. Solar

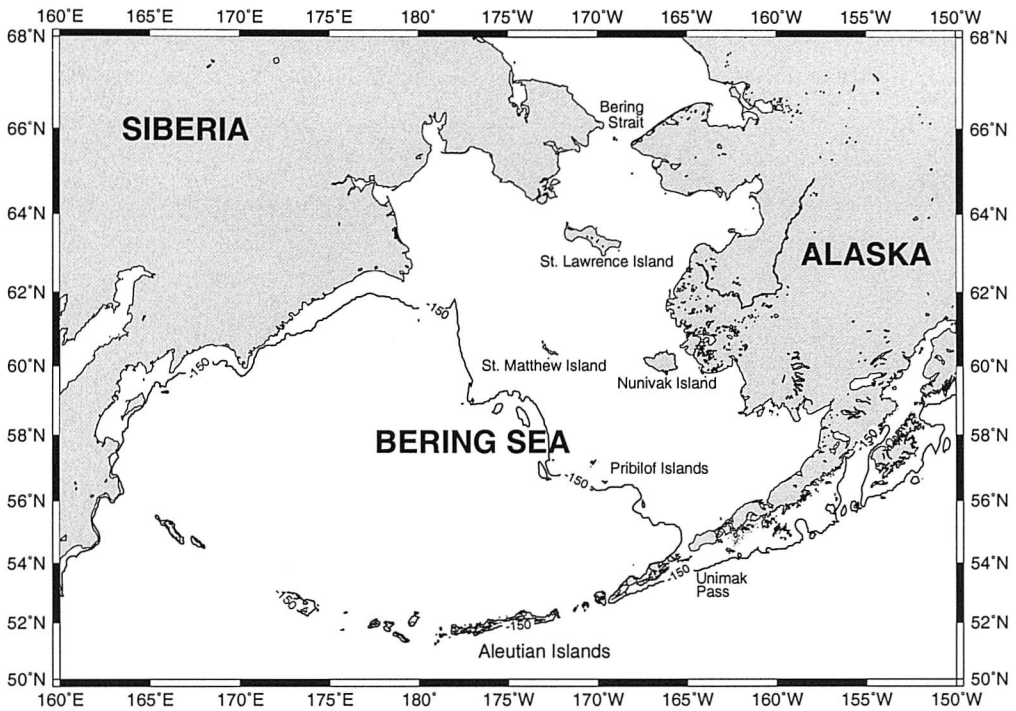

Figure 1.1: Map of the Bering Sea with 150 m isobath indicating approximately the division between the deep basin (western side) and the continental shelf (eastern side).

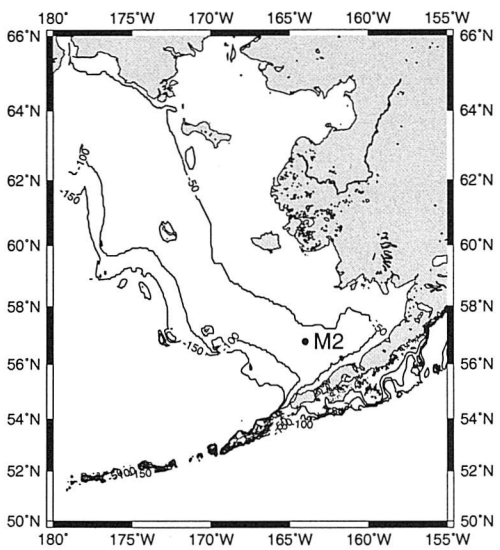

Figure 1.2: Map of the eastern Bering Sea with bathymetric contour lines indicating the three hydrographic domains: 1) the coastal domain from the coast line to the 50 m isobath; 2) the middle domain from the 50 m isobath to the 100 m isobath; and 3) the outer domain approximately between the 100 m and 150 m isobaths. M2 marks mooring station 2 at 56.8°N and 164°W.

heating in the warmer seasons stratifies the middle domain waters into two strongly isolated layers, the upper being mixed by winds and the lower being mixed by tides. The outer domain waters have a more complex structure due to the vertical and horizontal currents along the shelf break. Figure 1.3 shows a schematic diagram of a section of the water column on the shelf.

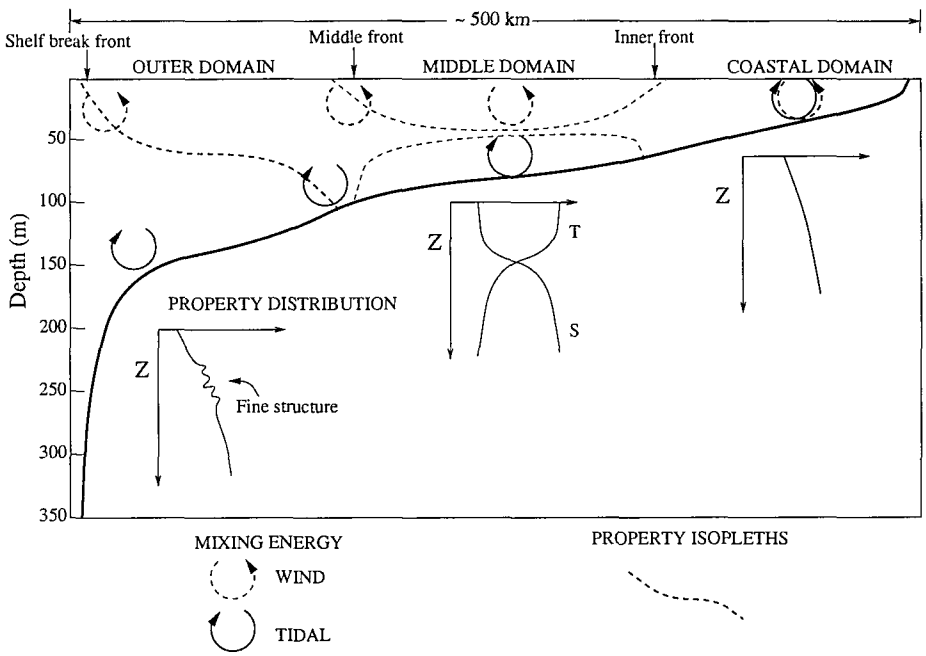

Figure 1.3: Schematic diagram of the water column on the shelf relating the vertical energy distributions to the typical horizontal and vertical property distributions and the fronts. Modified from Coachman (1986).

Interactions among ocean, ice, and atmosphere dominate the physics of the Bering Sea. Seasonal extremes in solar radiation, meteorological forcing, and ice cover, result from these interactions. There are also strong connections between this area and the large interannual fluctuations of the tropical South Pacific, via the El Niño-Southern Oscillation (ENSO) events, and the North Pacific, via the Pacific Decadal Oscillation (PDO) (Niebauer *et al.*, 1999). These two fluctuations appear to perturb the passage of storms along the Aleutian Island chain. The migration of storms results in a statistical feature known as the Aleutian Low Pressure System (Stabeno *et al.*, 1999a).

The circulation in the Bering Sea basin has been described (Stabeno *et al.*, 1999a) as a cyclonic gyre, with the southward flowing Kamchatka Current and the

northward flowing Bering Slope Current. The circulation is strongly influenced by the Alaskan Stream, which enters the Bering Sea through the many passes in the Aleutian Arc and represents the main source water for much of the flow. Circulation on the eastern Bering Sea shelf is generally northwestward. Both circulation and distribution of water properties are highly influenced by the passes through the Aleutian Arc.

During ice formation, cold saline water is produced over the northern shelf and flows through Bering Strait, because of this northward transport an onshelf flux of slope waters is required, which represents a supply of nutrient-rich water that stimulates primary production. This shelf-slope exchange represents the connection mechanism between the basin and the shelf. The exchange can occur virtually anywhere along the shelfbreak but two regions have been identifled (Schumacher & Stabeno, 1998) where preferential transport onto the shelf has been observed. The first is the Bering Canyon, which lies along the Aleutian Islands near Unimak Pass. The enhanced concentration of nutrients observed near Unimak Pass most likely originate from Aleutian North Slope Current waters interacting with canyon topography and coming onto the shelf. The second region occurs west of Pribilof Islands, where the narrowing of the shelf accelerates the flow resulting in water being entrained from the adjacent slope (Stabeno *et al.*, 1999b). It is the combination of nutrient-rich slope waters with summer solar radiation that makes this region one of the world's most productive ecosystems (Walsh *et al.*, 1989).

The appearance of the seasonal sea ice over the Bering Sea shelf in winter and the presence of an isolated cold mass of subsurface water in summer ($< 2\,^{\circ}C$) are other dominant features of this area. The amount of seasonal sea ice in winter is determined by atmospheric temperature and by storm tracks generated by the Aleutian Low Pressure System. The formation of sea ice generally begins in November, with maximum ice extent occurring in March. From June to October the shelf is typically ice-free (Schumacher & Stabeno, 1998). The mechanism of ice formation has been described by a "conveyor belt" analogy (Pease, 1980). Sea ice forms along

the south facing coasts, in the northern region of the shelf, and it is blown south until it reaches warmer waters and melts. The ice edge thus advances southward as the melt water cools and freshens the upper water layer. As water freezes, brine rejection takes place giving origin to a dense, cold saline mass of water and thus to a density-driven flow. The ice melt in turn produces a positive buoyancy flux and assists in the formation of a strong two-layer system over the middle shelf domain. Thus the pool of cold water is related to winter air temperature, bathymetry, currents and sea ice itself (Wyllie-Echeverria & Wooster, 1998). Associated with ice melt is a bloom of phytoplankton (usually in April) that accounts for 10-65% of the total annual primary production over the eastern shelf (Niebauer *et al.*, 1990). During years when the ice is not present, the spring bloom is delayed (usually in May).

In summary, from spring through summer, the vertical structure on the middle shelf is typically two-layered. In autumn and winter, if ice is not present, winds mix the entire water column to about 100 m depth. The melting of ice provides buoyancy for the two-layered structure and the shallow upper layer insulates the lower layer by absorption of heat during spring. The temperature difference between the two layers can be as high as 7 °C. This insulation of the lower layer results in a cold pool, defined as the region of the lower-layer water over the middle shelf below 2 °C.

1.2.2 Previous field and modelling studies

In 1975 the first wide scale, long term systematic study named Processes and Resources of the Bering Sea shelf (PROBES) was launched. The project was designed in order to gain an insight, in the context of an interdisciplinary and multi-institutional research, into the transfer rate of energy from primary producers to higher trophic levels (McRoy *et al.*, 1986). Comprising two phases (phase 1 from 1976 to 1979 and phase 2 from 1980 to 1982), PROBES allowed several important accomplishments. The establishment of the circulation, water masses, and fluxes of the southeastern Bering Sea shelf was achieved (Coachman, 1986). This made it possible to determine

that a single main transect of stations across the shelf, rather than a pattern that sampled the entire region, was well representative of the whole shelf. It was possible then to concentrate efforts focusing on chemical-biological changes that occurred over the spring bloom period along this transect (Codispoti *et al.*, 1986; Whitledge *et al.*, 1986). Interannual and interseasonal differences in primary and secondary production were understood in more detail (Sambrotto *et al.*, 1986; Vidal & Smith, 1986). Analyses of the inorganic carbon system (partial pressure of carbon dioxide, pCO_2, and dissolved inorganic carbon, DIC) in this nitrogen limited environment showed that when nitrogen is limiting, the organic matter synthesised increases substantially its C:N ratio over the Redfield ratio, which gave an important account for the ocean's role in the global carbon cycle (Sambrotto *et al.*, 1993).

Interestingly, during spring 1980 and spring-summer 1981, Codispoti *et al.* (1986) observed changes in carbonate alkalinity which suggested the presence of some calcifying organism in the surface waters. Despite the presence of pteropods among the zooplankton data, Codispoti *et al.* (1986) judged unlikely that this organism could have been totally responsible for the precipitation of the amount of calcium carbonate that they observed. The authors noted that a coccolithophore bloom might have explain those changes but concluded that they had no evidence for this in the phytoplankton data. Unfortunatelly, their phytoplankton sampling scheme was not optimised for collecting small calcareous organisms.

There have been other projects after PROBES and most of them have focused on understanding the spring bloom dynamics or the functioning of the higher trophic levels of the ecosystem, given the high productivity (both ecological and economical) of the area. For example, the Fisheries-Oceanography Coordinated Investigations (FOCI), a collection of the National Ocanic and Atmospheric Administration (NOAA) research programs, attempts now to understand the influence of environment on the abundance of various commercially valuable fish and shellfish stocks in the Bering Sea and their role in the ecosystem.

Despite the great amount of data available since the PROBES project, only a

few mathematical models have been developed that could make use of them to test hypotheses quantitatively. The most important works on biogeochemical modelling, have probably been the ones of Magley (1990), Walsh & Dieterle (1994) and Eslinger & Iverson (2001). With an early model, Magley (1990) suggested that in contrast to the outer shelf domain, zooplankton within the middle shelf domain had little effect on phytoplankton community species composition. Walsh & Dieterle (1994) used a two-dimensional model with a focus on the carbon system to conclude, confirming earlier studies (Walsh *et al.*, 1981), that the shelf ecosystem serves as a sink of atmospheric CO_2. Walsh & Dieterle (1994) also suggested that, as a consequence of the rising levels of atmospheric pCO_2 since the Industrial Revolution, the biophysical CO_2 status of the Bering Sea shelf may have switched over the last 250 years, from a prior source to the present sink. Eslinger & Iverson (2001) concentrated more on the effects of convective and wind-driven mixing on spring phytoplankton dynamics by using a coupled biological and physical model constrained and validated against data of the PROBES project collected in 1980 and 1981.

The model developed for this study makes use of a wide and up-to-date range of data (highly detailed temporal data collected by a mooring station, *in situ* sampled data and satellite-derived information) and aims at addressing a new phenomenon for the Bering Sea: the appearance of the coccolithophore *E. huxleyi*. *E. huxleyi* is also the key species to coccolithophore ecology, and can potentially represent a perturbation to the Bering Sea role as a sink for atmospheric CO_2 shown by Walsh & Dieterle (1994). The investigation of the controls on the phytoplankton succession over a full year cycle with modelling tools is also a new subject for the Bering Sea.

1.2.3 Recent anomalies

It has been recognised that a number of climatic anomalies taking place in 1997 in the Bering Sea combined to create a series of physical perturbations (Overland *et al.*, 2001; Stabeno *et al.*, 2001). The PDO in its positive phase (consisting of higher atmospheric pressure in summer over Alaska), a monthly oscillation of higher-than-

normal atmospheric pressure over the Gulf of Alaska (in May 1997), and a seasonal anomaly connected to the North Pacific atmospheric circulation responding to the 1997/98 El Niño strong event all combined to create unusually warm weather and calm winds in 1997 in the Bering Sea. The sea surface temperatures in turn were higher than usual with a consequent more strongly stratified water column in 1997 as evident from hourly temperature distributions (Fig. 1.4) measured at the mooring station M2.

In combination with these climatic anomalies, also several biotic components of the ecosystem were observed to be disrupted. An increase in jellyfish was reported, although a general increasing trend is known to have been taking place since the early '90s, (Brodeur *et al.*, 2002); a mass mortality of sea birds, with clear indication of starvation as the main cause, was observed (Baduini *et al.*, 2001); a lower than usual number of salmon returned to the Bristol Bay (Vance *et al.*, 1998); a massive bloom of the coccolithophore *E. huxleyi* was observed for the first time ever in the area (Vance *et al.*, 1998; Sukhanova & Flint, 1998); an anomalous high number of sea mammals were also observed in the areas of this bloom (Tynan *et al.*, 2001); and lower euphausiid concentrations were measured as well (Stockwell *et al.*, 2001).

It is not clear how all these perturbations are connected to each other or how they are related to the presence of *E. huxleyi*. However, the study discussed here represents an initial step in the effort to comprehend the functioning of the lowest trophic levels of such a complex ecosystem during years of exceptional physical forcing.

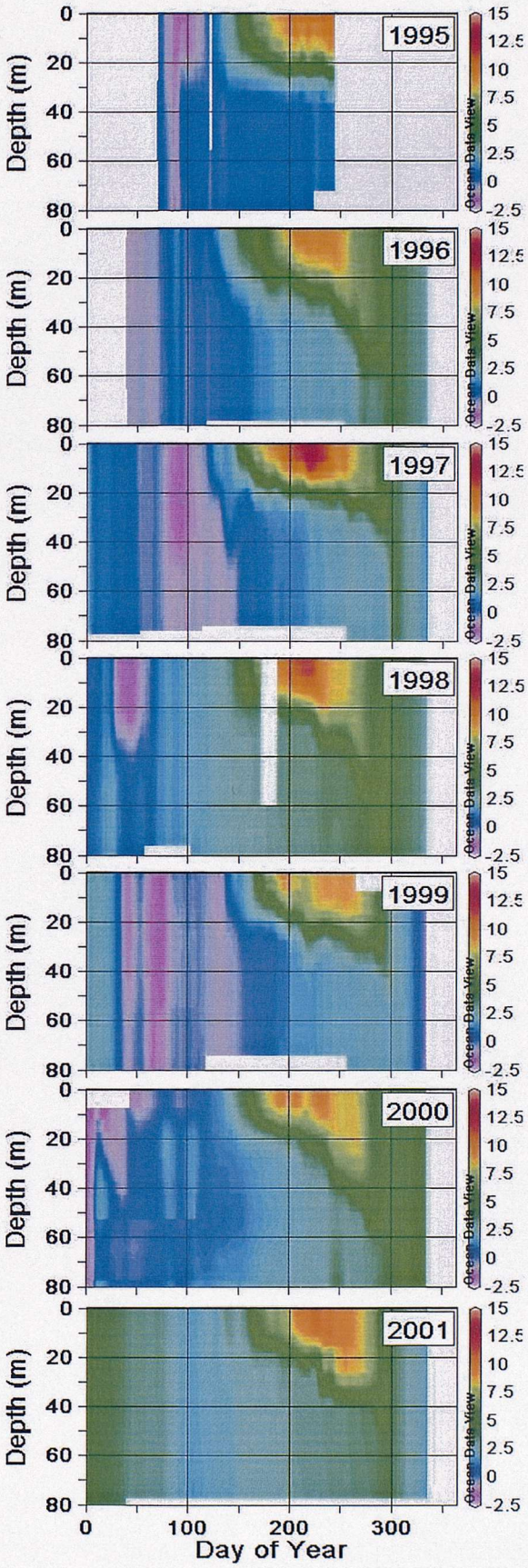

Figure 1.4: Temperature distribution with depth and time in the Bering Sea at mooring station M2 (see Fig 1.2). Purple areas indicate temperatures of approximately -1.7 °C, which occur when ice is over the mooring site. White areas indicate no data. Plot created using Ocean Data View (Schlitzer, 2002).

1.3 Ecophysiology of *E. huxleyi*

A brief review of the ecophysiology of *E. huxleyi* will be given in this section. The aim is to identify those important ecophysiological characteristics that can be included into the model as working hypotheses.

General

The unicellular organism *E. huxleyi* (Fig. 1.5) is a cosmopolitan coccolithophore species. Coccolithophores are a diverse group of marine phytoplankton belonging to the algal class Prymnesiophyceae (Green *et al.*, 1990). The cosmopolitan character of *E. huxleyi* may appear as an ecological versatility. However, it is now well established that the reason for that is an intraspecific diversification into separate ecotypes, with physiologies attuned to their respective growth environments (Paasche, 2002). Molecular-DNA based techniques have revealed a high genetic diversity even between clones from one and the same bloom (Medlin *et al.*, 1996; Iglesias-Rodríguez *et al.*, 2002).

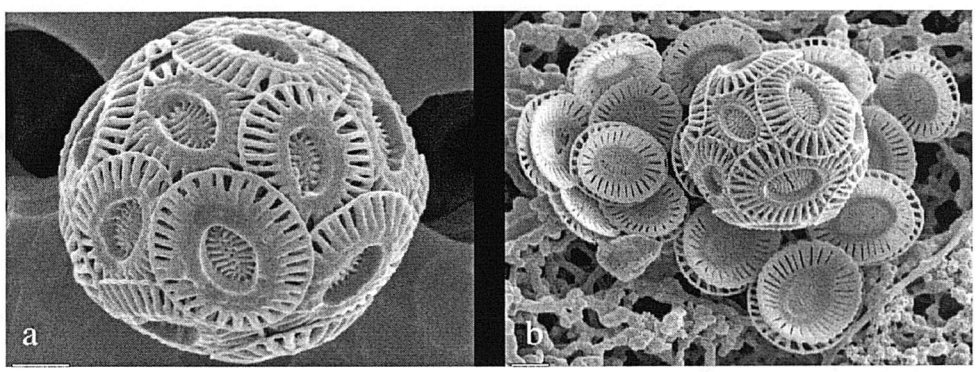

Figure 1.5: *E. huxleyi* cell (a) surrounded by attached coccoliths, and (b) coccoliths shedding off. Image courtesy of Jeremy Young.

In addition to several spectacular blooms, defined as concentration of at least $10^6\,\mathrm{cell\,L^{-1}}$ (Tyrrell & Merico, 2003), which is equivalent to $10\,\mathrm{mg\,C\,m^{-3}}$ when using a time-invariant carbon content of $10\,\mathrm{pg\,cell^{-1}}$ (Holligan *et al.*, 1983), *E. huxleyi* occurs in lesser (but still significant) numbers in all oceans except the Arctic Ocean and high-latitude Southern Ocean (Winter *et al.*, 1994). It is frequently the most

numerous species in phytoplankton cell counts from surface water samples, although because of the rather small size of the cells (5-8 μm in diameter), it makes a lesser contribution to total chlorophyll. Blooms can cover very large areas, for instance at least 200,000 km^2 in the Eastern Bering Sea in 1997 (Sukhanova & Flint, 1998), and 250,000 km^2 in the North Atlantic in 1991 (Holligan *et al.*, 1993a). Cell concentrations vary between blooms and according to the stage of the bloom. Some examples of cell concentrations found in natural blooms are given in Table 1.1. The highest concentration ever reported is 115x10^6 cells L^{-1}, from a Norwegian fjord in 1955 (Berge, 1962), as shown in Table 1.1.

Table 1.1: *E. huxleyi* cell concentrations found in some natural blooms in various locations of the world ocean (after Tyrrell & Merico, 2003).

Bloom location	**Concentration (10^6 cells L^{-1})**	**Year**	**Source**
Norwegian fjords	10 - 100	1950s	Birkenes & Braarud (1952)
	up to 115	1955	Berge (1962)
	up to 7	1992	Kristiansen *et al.* (1994)
Western English Channel	up to 8.5	1980s	Holligan *et al.* (1983)
	up to 2	1992	Garcia-Soto *et al.* (1995)
Gulf of Maine	<0.5 - >2	1988-89	Balch *et al.* (1991)
	>1	1988-90	Townsend *et al.* (1994)
North Sea	<0.1 - >1	1980s	Holligan *et al.* (1993b)
	0.1 - 1.2	1993	van der Wal *et al.* (1995)
	1 - 6	1994	Head *et al.* (1998)
	0.6 - 2.3	1999	Burkill *et al.* (2002)
North Atlantic	up to 4	1987	Malin *et al.* (1993)
	0 - 10	1991	Holligan *et al.* (1993a)
Nova Scotian shelf	up to 1.5	1991	Brown & Yoder (1993)
Bay of Biscay	up to 3	1998	Lampert *et al.* (2002)
Black Sea	4.7,31	1990,93	Mihnea (1997)
	up to 10	1992	Cokacar *et al.* (2001)
Bering Sea[a]	2.1 - 2.8	1997	(Sukhanova & Flint, 1998)
	0.3	1997	(Stockwell *et al.*, 2001)

[a]For data of years following 1997, see chapter 3.

E. huxleyi cells produce peculiar calcareous plates called coccoliths (the complete covering of coccoliths is called a coccosphere), which are approximately 2.5 μm in diameter. Usually, a cell is covered by 10-15 coccoliths in a single layer although very frequently additional coccoliths are found on top of the primary layer (Fig. 1.5b), sometimes forming two or three extra layers (Paasche, 2002). Coccoliths are shed in the surrounding water as the cells grow and, due to their important property to intensely backscatter light, they cause high surface reflectance, which is easily observed with remote sensing techniques (Holligan *et al.*, 1983, 1993a; Balch *et al.*, 1993). These loose calcite ($CaCO_3$) plates eventually sink to the sea floor, either freely or in zooplankton faecal pellets, or dissolve. *E. huxleyi*, being the most abundant calcifying phytoplankton on earth (Westbroek *et al.*, 1993), may have a major influence on the transport of particulate inorganic carbon to the deep waters.

Intrinsic growth rate

In a review of the ecophysiological ecology of coccolithophores, which included *E. huxleyi*, Brand (1994) concluded that this species is more *r*-selected than most other coccolithophores. This is supported by a high intrinsic growth rate and by the predominance of this species in fairly nutrient-rich environments.

Irradiance effects on photosynthesis and growth

Remarkably, photosynthesis in *E. huxleyi* shows no sign of photoinhibition (Nanninga & Tyrrell, 1996). Growth becomes fully light-saturated at about 300 μmol m^{-2} s^{-1} at a temperature of 20-24 °C (Paasche, 1967; Nanninga & Tyrrell, 1996). These data suggest a higher light saturation irradiance for growth in *E. huxleyi* than in diatoms and dinoflagellates using the mean values for these groups of 84 and 47 μmol m^{-2} s^{-1}, respectively (Richardson *et al.*, 1983). It has been suggested that natural blooms of *E. huxleyi* are promoted by high irradiances (Nanninga & Tyrrell, 1996; Tyrrell & Taylor, 1996). As suggested by Paasche (2002), this is partly an indirect effect: periods of particularly high irradiance will favour the creation of a shallow thermocline that favour the growth of *E. huxleyi* not only because it tolerates strong light

but also because of its high affinity for nutrients.

Nutrients and growth

The half-saturation constant for phosphorus-limited growth has been found to be extremely low (about 1 nM) in *E. huxleyi*, which is one to three orders of magnitude lower than in marine flagellates (Smayda, 1997). Mesocosm experiments (Egge & Heimdal, 1994) have shown *E. huxleyi* success in those bags manipulated by adding high quantities of N and low quantities of P rather than vice-versa. From a physiological perspective, *E. huxleyi* is known to synthesize the enzyme alkaline phosphatase (Kuenzler & Perras, 1965) which allows uptake of dissolved organic phosphate and should therefore give an advantage to this species when inorganic phosphate is limiting. With regard to nitrogen, supplied as nitrate plus ammonium, Riegman *et al.* (1992) found *E. huxleyi* to be a poor competitor. Nevertheless, the half-saturation constants for uptake of these nutrients are low, about $0.2\,\mu$M (Riegman *et al.*, 2000). Other nitrogen compunds that can be used by this species include low-molecular-weight amids and, in the presence of nickel ions, also urea and purines (Palenik & Henson, 1997).

Grazing mortality

E. huxleyi cells may be consumed by calanoid copepods as shown in laboratory (Harris, 1994) and in mesocosms experiments (Nejstgaard *et al.*, 1997). These results are consistent with many observations of the occurrence of coccoliths in copepod faecal pellets collected from natural populations (Honjo, 1976; Holligan *et al.*, 1983). The evidence from fieldwork about microzooplankton grazing has been more equivocal suggesting preference for (Holligan *et al.*, 1993a) or rejection of (Nejstgaard *et al.*, 1997) *E. huxleyi* cells. During the developing stage of an *E. huxleyi* bloom in the northern North Sea in June 1999, Archer *et al.* (2001) observed significant grazing on *E. huxleyi* by the microzooplankton (heterotrophic flagellates) and reported a mean grazing rate of $0.54 \pm 0.13\,\mathrm{d}^{-1}$. However, in another bloom, off the Devon (UK) coast during July 1999, Fileman *et al.* (2002) observed that microzooplankton

grazing on *E. huxleyi* was low and that photosynthetic dinoflagellates and cryptophytes were grazed the most. In a very recent study (Strom *et al.*, 2003), it has been shown a lower feeding rates by ciliates and heterotrophic dinoflagellates on *E. huxleyi* strains with high dimethylsulfoniopropionate (DMSP) lyase activity. This result suggests that high levels of DMSP lyase activity somehow promote reduced palatability. Strom *et al.* (2003) hypothesised that the factors promoting reduced grazing in their experiments constitute signals rather than acute toxins.

1.4 *E. huxleyi* in the Bering Sea

In September 1997, the Sea-viewing Wide Field-of-view Sensor (SeaWiFS) on board of the newly launched satellite SeaStar started to collect data of the global ocean bio-optical properties (hereafter, for simplicity, the term "satellite" will be used to indicate the remote-sensing instrument rather than the vector carrying it). Thanks to its high spatial resolution (4.5-9 km) and high level of coverage (possible due to the global network of receiving stations), SeaWiFS soon became the "tool of choice" for studying the milky-turquoise waters associated with *E. huxleyi* blooms. That September, SeaWiFS started to show a very large area of bright waters covering almost all the continental shelf of the Bering Sea, to the great surprise of marine scientists and local fishermen who had never before observed such phenomenon in the region. The bright waters were caused by a bloom of *E. huxleyi*, which had been taking place at least since early July of that year, as field observations confirm (Vance *et al.*, 1998; Sukhanova *et al.*, 1999). The bloom, or the white waters associated with it, lasted up to October 1997 (Sukhanova *et al.*, 1999), and appear to have come back in the following years as early as February. No blooms have been observed since 2001. Figure 1.6 shows true colour images of SeaWiFS monthly composite scenes of the Bering Sea from 1997 to 2001.

Even more surprising was perhaps the fact that SeaWiFS images of the Bering Sea (Fig. 1.6) suggested that blooms were taking place in the middle of winter, as also proposed in a remote sensing study by Iida *et al.* (2002). Given the high latitude

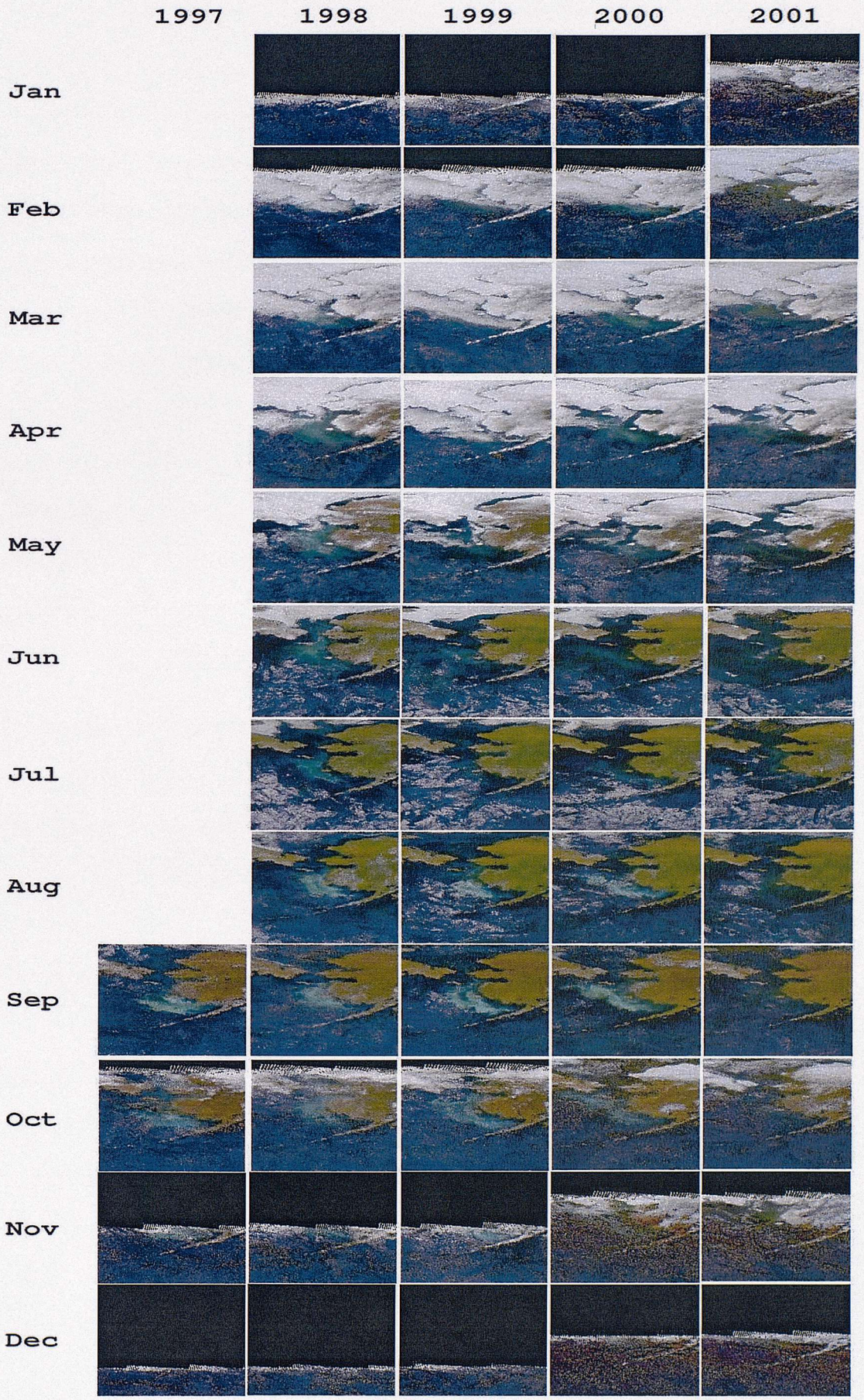

Figure 1.6: True-colour images of SeaWiFS monthly composite scenes of the Bering Sea from 1997 to 2001 (after Broerse *et al.*, 2003).

(56-60°N), winter time blooms of any phytoplankton should be highly unlikely here. In regions like the Bering Sea, deep mixing and very low surface sunlight levels should make net growth of phytoplankton (phothosynthesis exceeding respiration) impossible in wintertime (Sverdrup, 1953). In fact, it became clear later (Broerse *et al.*, 2003) that the winter bright waters in the Bering Sea were not caused by living *E. huxleyi* cells and, very unexpectedly, not even by loose coccoliths. In a sampling campaign conducted in February 2001, Broerse *et al.* (2003) found that at the brightest station of the transect, coccoliths were strongly outnumbered by empty and broken diatom frustules. From several lines of evidence it was determined that frustules were remnants from previous year blooms, that had settled to the sea floor but had been resuspended by strong winds during winter. On the basis of measurements of the scattering properties of opal material, Broerse *et al.* (2003) calculated that the observed concentration of diatom frustules and fragments was sufficient to produce the surface brightness seen in the satellite images.

The annual development of the bright waters in the Bering Sea appears to have been relatively consistent from year to year in the period from 1997-2000 (Fig. 1.6). A reduction in the brightness of the patches usually occurs in June and July, probably when summer stratification and diminishing wind strength prevent resuspension of the sediment into the surface waters (Broerse *et al.*, 2003). The increase in brightness after July is likely the start of the actual *E. huxleyi* summer/autumn bloom (1998 appears to be an exceptional year in which bright waters were present as early as June). The transition from summer to winter bright waters is less clear and may be a continuing process, in which the senescent *E. huxleyi* community is gradually overtaken by detrital and mineral particles as increasing winds stir up the sediments from below (Broerse *et al.*, 2003). The satellite images from November to January (Fig. 1.6) are increasingly obscured by clouds and winter darkness[1] preventing accurate retrieval of radiances.

[1]This occurs in the northern hemisphere during winter, when the sun angle is too low (solar zenith greater than 72.7°). Since SeaWiFS is designed for viewing ocean colour in visible wavelengths, a significant energy saving is made by turning the sensor off over the dark regions (see for example `http://www.sat.dundee.ac.uk/seawifs.html`).

Satellite evidence is an important source of information to this study, provided that it has been accurately validated by ground-truthing observations (as happened for the Bering Sea). Satellite imagery represents a powerful model constraint in terms of temporal and spatial occurrences of *E. huxleyi* blooms and will be used in this study to validate the model results.

1.5 Working hypotheses

A number of potential hypotheses are outlined here about possible causative factors stimulating the blooms of *E. huxleyi* in the Bering Sea. The hypotheses are derived both from the typical conditions found in the past to play an important role in *E. huxleyi* bloom formation (recently reviewed by Tyrrell & Merico, 2003), and also from field observations in the Bering Sea. However, not all of them have been considered as causative factors and investigated with the model. The motivations for considering or discounting individual hypotheses are discussed below.

1.5.1 Reduced vertical exchange

A reduced vertical exchange in 1997, because of sunnier weather (Fig. 1.4), might have given a competitive advantage to *E. huxleyi*. This is based on the observation that waters stripped of nutrients and with no (or scarce) possibilities of being replenished may be a good environment for *E. huxleyi* (Brand, 1994). In particular, waters with very low silicate concentrations ($<2\,\mu$M) are thought to represent an ideal environment for this species when in competition with diatoms (Egge & Aksnes, 1992). Temperature distributions (Fig. 1.4) show a higher difference in temperature between the upper and bottom layer of water in the summer of 1997 (about 12 °C) compared to other summers when it remained approximately constant (between 7-8 °C). According to these data, the temperature gradient in 1997 is about 1.5 times higher than other years. A stronger stratification in 1997 might have acted as a barrier for vertical advection of nutrients allowing *E. huxleyi* to establish a very high population. This hypothesis has been investigated.

1.5.2 Photoinhibition

Several authors have studied the effect of light saturation and inhibition on phytoplankton (Platt *et al.*, 1980; Kirk, 1994). It appears from these studies that photosynthesis saturates in diatoms at levels of irradiance of about $120\,W\,m^{-2}$, with a rather sharp decline of the photosynthetic rate at higher light intensities. For example, a reduction to only 20% of the maximum photosynthetic rate is observed in natural diatom assemblages at $360\,W\,m^{-2}$ (see Fig. 10.1 in Kirk, 1994). Nanninga & Tyrrell (1996) measured the light saturation level for *E. huxleyi* and noticed a slight photoinhibiting effect (reduction to between 80-95% of maximum rate) only at very high light values (between 240 and $360\,W\,m^{-2}$). In the Bering Sea, moreover, photoinhibition has been indicated in the past as a factor that could affect the spring bloom (Eslinger & Iverson, 2001). On the basis of these observations, it can be expected that the unusually clear sky conditions of the Bering Sea in 1997 might have created a favourable niche for *E. huxleyi*. Such a possibility has been investigated in this study.

1.5.3 Zooplankton selective grazing

There is a growing body of evidence in oligotrophic regions (Lessard & Murrell, 1998; Quevedo & Anadón, 2001), but also in eutrophic areas (Strom *et al.*, 2001), that microzooplankton (i.e. protists and metazoan, sizes $<200\,\mu m$) can be the dominant consumers of phytoplankton production, capable of consuming more than 100% of daily primary production (Verity & Smetacek, 1996). Although some previous studies have indicated that *E. huxleyi* was readily grazed by microzooplankton (Holligan *et al.*, 1993a; Levasseur *et al.*, 1996), others have found reduced grazing by microzooplankton on *E. huxleyi*. Based on pigment analysis in dilution experiments, Fileman *et al.* (2002) observed that photosynthetic dinoflagellates rather than *E. huxleyi* were selectively grazed within an *E. huxleyi* bloom off the Devon (UK) coast. Low microzooplankton grazing on *E. huxleyi* cells relative to total chlorophyll was also

found in a bloom in the North Sea (Archer *et al.*, 2001). In the Bering Sea, within the *E. huxleyi* bloom of 1999, Olson & Strom (2002) found that microzooplankton selectively grazed phytoplankton >10 μm (i.e. larger than *E. huxleyi*), but this differential grazing was not found outside bloom waters. That selective grazing might have favoured *E. huxleyi* in proliferating and in maintaining high abundances for a relatively long time, has been investigated.

1.5.4 Effect of coccoliths

In a recent study, Tyrrell *et al.* (1999) found that coccoliths cause the surface waters to become brighter (more irradiance available in the top few metres due to the fact that coccoliths scatter light rather than absorbing it) and the deeper waters to become darker. According to this finding, in the current model of the upper mixed layer ecosystem in which there is no phytoplankton activity in the bottom box (see section 2.2), it is assumed that coccoliths will not increase the extinction of light in the (relatively shallow) upper box. In any case, given that coccoliths are shed only during the senescent phase of the bloom, they will not have any impact on the establishment of the bloom. Therefore, the processes of production and shedding of coccoliths are simulated in this study only in order to compare model output with satellite brightness and to assess their impact on carbon chemistry.

1.5.5 N:P ratio

High N:P ratio has been suggested as crucial for *E. huxleyi* success, either by modelling studies forced with field (Tyrrell & Taylor, 1996) and mesocosm data (Aksnes *et al.*, 1994), and by culture experiments (Riegman *et al.*, 2000). This hypothesis is based on the observation that *E. huxleyi* has a high affinity for inorganic phosphate and on its high ability to express a strong alkaline phosphatase activity, which makes this species able to access phosphorus contained in organic matter.

From a compilation of data (Fig. 1.7), it has become clear that inorganic phosphate is never more limiting than inorganic nitrate in the Bering Sea, neither before

1996, when *E. huxleyi* was not present in the area in blooming concentrations, nor after, when the massive blooms took place. These data suggest that alkaline phosphatase activity by *E. huxleyi* did not play any role for its success in the Bering Sea, therefore this hypothesis has not been considered as a causative factor in the model and phosphate, being rarely limiting (see Fig. 3.1d), has not been included as a state variable of the model. However, given the attention that the high N:P hypothesis has received in the past, an analysis of archive data has been carried out (and past studies have been reviewed) for those areas of the world ocean where blooms of *E. huxleyi* are commonly found in order to evaluate if the Bering Sea case is unique in this respect (the results are given in chapter 4).

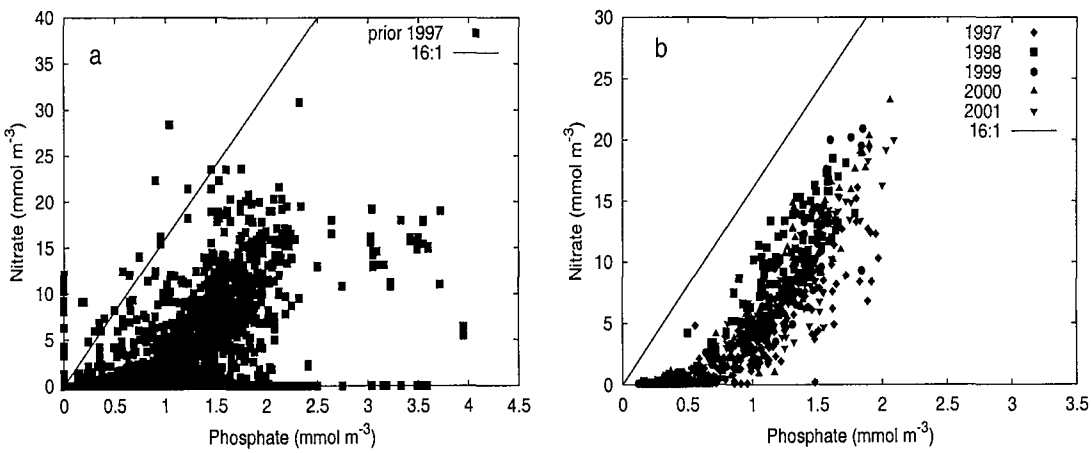

Figure 1.7: N:P ratios in the whole water column of the Bering Sea shelf a) before 1997 (*E. huxleyi* not present) and b) after 1997 (*E. huxleyi* present). Data source a) World Ocean Database and b) T/V Oshoro Maru public reports (Anonymous, 2002). The 16:1 line represents the Redfield ratio.

1.5.6 Calcite saturation state

As mentioned in section 1.3, the development of a coccolithophore bloom is a major local process for the export of $CaCO_3$ to the deep water. Calcification also causes a shift in the equilibrium of the carbonate system toward higher CO_2 concentrations and can cause seawater to emit CO_2 to the atmosphere (Holligan *et al.*, 1993a).

The processes of precipitation and dissolution of $CaCO_3$ in seawater appear to

be driven by the saturation state of seawater with respect to calcite (Ω_{cal}), where:

$$\Omega_{cal} = \frac{[Ca^{2+}][CO_3^{2-}]}{k_{sp}} \tag{1.1}$$

k_{sp} is the stoichiometric solubility product for a particular mineral phase [calcite (*cal*), aragonite (*arag*), or high-magnesian calcite (*hmc*)] and depends on temperature, salinity and pressure. Brackets represent total stoichiometric concentrations. Values of $\Omega_{cal} < 1$ indicate undersaturation and values > 1 indicate supersaturation. In the open ocean, mineral calcium carbonate is formed almost exclusively by biological processes, despite the fact that these waters are supersaturated with respect to this mineral[2]. Given that $[Ca^{2+}]$ can be considered constant in today's ocean, Ω_{cal} is largely determined by $[CO_3^{2-}]$.

Ω seems to have an important influence on calcifying organisms. For instance, coral reefs are restricted to low latitudes most likely because of a dependence on the aragonite saturation state (Kleypas *et al.*, 1999), which attains highest values between about 0-30° of latitude and becomes smaller towards the pole (Fig. 1.8).

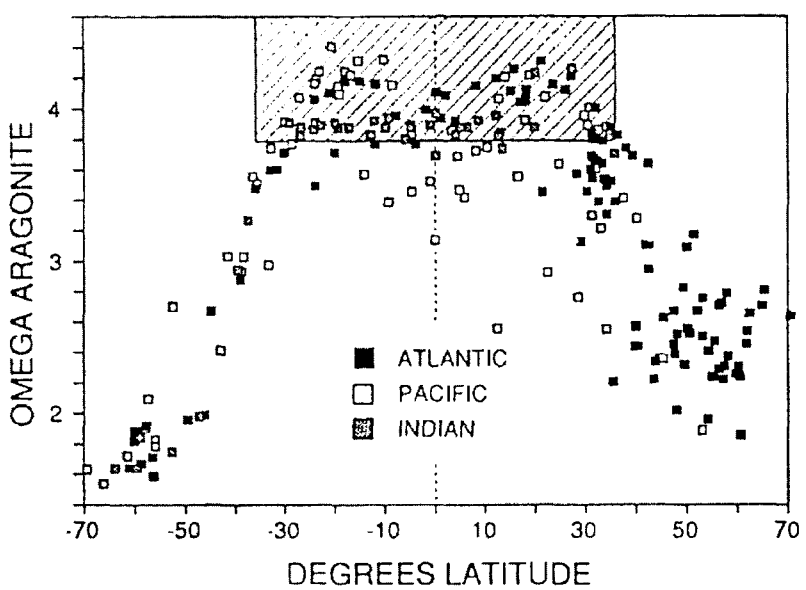

Figure 1.8: Latitudinal distribution of aragonite saturation state in different oceans (from Opdyke & Wilkinson, 1990).

[2]The lack of inorganic precipitation of $CaCO_3$ is generally thought to be due to nucleation barriers; the necessary seeds crystals may be absent, or magnesium ions, phosphate or organic compounds may act as surface inhibitors for nucleation (see p. 316 in Stumm & Morgan, 1981).

Laboratory experiments have shown that the shell weight in foraminifera is strongly dependent on $[CO_3^{2-}]$ (Spero *et al.*, 1997). Coccolithophores showed a decline in calcification rates when cultured at low Ω_{cal} (i.e. the calcification to phytosynthesis ratio, C/P, decreased by 20% when pCO_2 was increased from 100 to 750 ppm by acid addition, Riebesell *et al.*, 2000). Coccolith malformations were also apparent as a consequence of such growing conditions. Very recently, also Sciandra *et al.* (2003) showed that net cell calcification can be significantly and rapidly reduced in coccolithophores following an increase of the pCO_2 in the medium. However, in contrast with Riebesell *et al.* (2000), they found that this effect was not accompanied by a significant decrease in the C/P ratio, since organic C production decreased roughly in proportion to inorganic C production. The main difference between the two studies was that in Sciandra *et al.* (2003) experimental growth was nitrogen-limited.

If the biogeography of calcifiers is controlled by $[CO_3^{2-}]$, it may be expected that alterations of $[CO_3^{2-}]$ distribution in the global ocean may alter the environment of these organisms possibly forcing them to migrate towards new locations, where Ω is more suitable. Given the strong correlation between sea surface temperature (SST) and $[CO_3^{2-}]$ in the world ocean (see Figs. 1 and 2 in Opdyke & Wilkinson, 1993), it is reasonable to suppose that this migration can be also initiated in connection with temperature changes and hence global warming. Such phenomenon might have therefore occurred in the Bering Sea in 1997.

Understanding the effects of $[CO_3^{2-}]$ on calcifiers is vitally important if we are to clarify the possible consequences on these organisms of the almost three-fold increase in surface ocean $[CO_2]$ (and the consequent $[CO_3^{2-}]$ decrease, see for example Fig. 1.9) expected by the end of the next century, according to the "business as usual" scenario (Houghton *et al.*, 2001).

The calculation of the carbonate system variables has been implemented in the model in order to investigate (in a "descriptive" rather than a "predictive" fashion) the possible relations between Ω and *E. huxleyi* seasonal abundances. Such a mod-

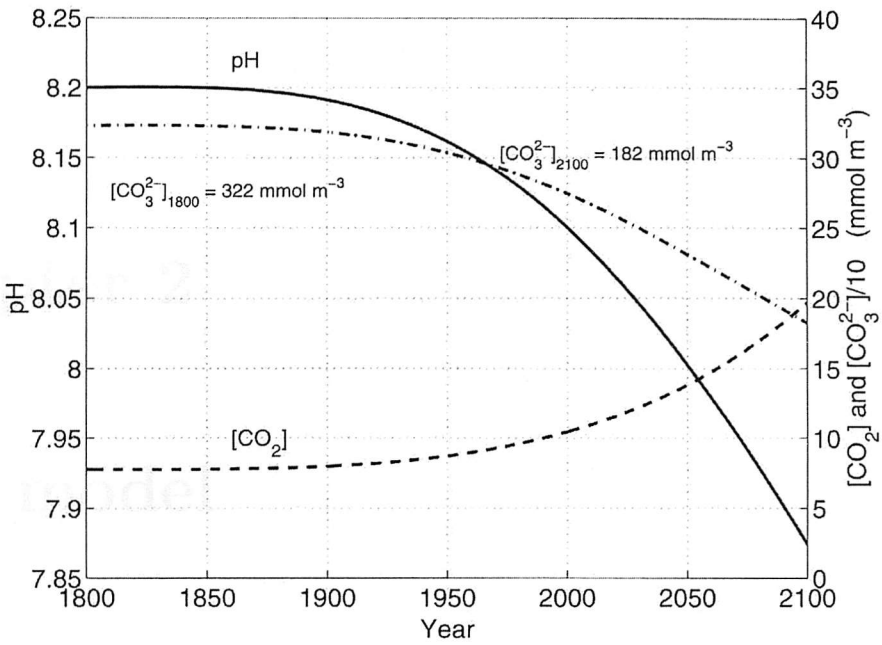

Figure 1.9: Changes of $[CO_2]$, $[CO_3^{2-}]$ and pH in the surface ocean calculated according to the "business as usual" scenario (from Zeebe & Wolf-Gladrow, 2001).

elling study of the ecological importance of the calcite saturation state to *E. huxleyi* success is a new area of research.

1.6 Summary

The hypotheses that have been considered as causative factors and implemented into the model are: 1) reduced vertical exchange, 2) photoinhibition, 3) zooplankton selective grazing and 4) calcite saturation state. While these hypotheses represent conditions that have been observed in the field or in culture and mesocosm experiments, their investigation with a mathematical model that explicitly includes *E. huxleyi* as a state variable is new.

The following chapter will be dedicated to the description of the model and the mathematical equations will be introduced. In chapter 3 the data to constrain, validate and compare the model results are presented. The results of the present study, the sensitivity analyses and a detailed discussion of the outcomes are given in the chapters 4, 5 and 6, respectively. Conclusions are presented in chapter 7.

Chapter 2

The model

2.1 Introduction

The models of Aksnes *et al.* (1994) and Tyrrell & Taylor (1996) are the only ones in the published literature that include *E. huxleyi* explicitly as an extra state variable of the ecosystem. These two models together with the one of Fasham (1995) provided the basic structure for the ecosystem model presented here. The computational code has been newly written in order to provide software that can be as representative of the Bering Sea case as possible. It was also decided to devote an important part of this study to writing the code because the hypotheses outlined in the previous chapter have not been contemplated before in an ecosystem model that would include *E. huxleyi* or that would be written in the context of the Bering Sea ecosystem with several phytoplankton functional groups. Such effort, on the another hand, will provide the scientific community of the Bering Sea with a new tool for future studies.

Below, the physical aspects of the model are described, together with the structure of the ecosystem and the key factors that characterise *E. huxleyi*. The complete set of equations is presented in section 2.3.

2.2 Model description

2.2.1 Physical aspects

In common with Tyrrell & Taylor (1996), a simple 1/2-dimensional physical scheme has been adopted. This does not include lateral advection effects on phytoplankton succession. Such an approximation is reasonable when considering that long-term average current speeds within the Bering Sea middle shelf domain are on the order of $1\,\mathrm{cm\,s^{-1}}$ (Coachman, 1986). Blooms of *E. huxleyi* are usually found in stabilised and well stratified waters (Nanninga & Tyrrell, 1996). In the Bering Sea the blooms took place predominantly in the middle shelf domain (as shown in Fig. 2.1) where the water column is typically stratified into two layers during the warm seasons (see Fig. 1.4) and where tides have no direct effect on the upper box (see section 1.2.1 and Fig. 1.3). The model is intended to represent the southern part of the middle shelf region around station M2 (Fig. 1.1). The water column is therefore simulated with two boxes. The biological activity takes place only in the upper box. The lower box represents the nutrient pool with nutrient concentrations kept constant throughout the year (N_0 and S_0 for nitrate and silicate, respectively) as well as the carbon state variables (DIC_0 and Alk_0 for dissolved inorganic carbon and alkalinity, respectively). Nutrients are supplied to the upper box by entrainment or turbulent diffusive mixing ("diffusive mixing" is hereafter used as for "turbulent diffusive mixing") across the interface (the method is as in Fasham, 1993). Diffusive mixing is parameterised by means of a constant factor, k.

On top of the water column a box representing the atmosphere has been considered in order to allow exchanges of CO_2 at the air/sea interface. The partial pressure of CO_2 in air, $pCO_{2(air)}$, has been assumed constant (Peng *et al.*, 1987) and equal to $358\,\mu$atm (Murata & Takizawa, 2002). A scheme of the physical structure of the model is presented in Figure 2.2 with a simplified diagram of the food web.

The model is forced with variable photosynthetic active radiation (PAR) and

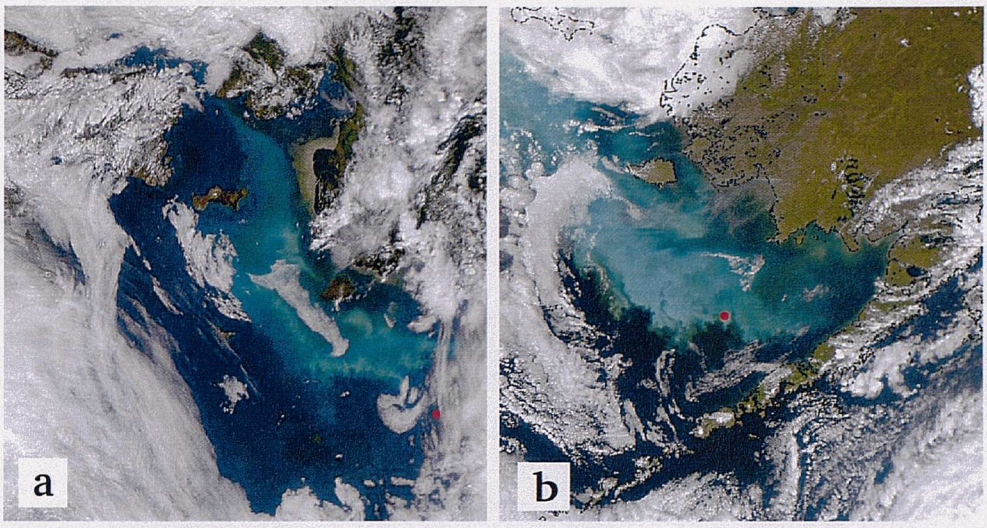

Figure 2.1: *E. huxleyi* blooms in the Bering Sea on a) 20 July 1998 and b) 16 September 2000. Images show areas of different size. The red dots mark the location of station M2. Note how the bright water patches stretch along the middle shelf domain (compare with Fig. 1.1). Images provided by the SeaWiFS Project, NASA/Goddard Space Flight Center, and ORBIMAGE.

wind speed by using 6-hourly climatology data from the European Centre for Medium-Range Weather Forecasts (ECMWF). PAR attenuation through depth is then simulated using the attenuation model of Anderson (1993). Wind speed data are used in order to calculate the gas transfer velocity at the air-sea interface (see appendix A). A variable mixed layer depth (MLD) is also used to force the model. The MLD has been reconstructed from mooring temperature (T) data (Fig. 1.4) as the depth at which T differs by 0.5 °C from its sea surface value (SST). SST is also used to control phytoplankton growth. Seasonal variations of noon PAR (weekly running average), wind speed (weekly running average), MLD and SST from 1995 to 2001 are shown in Fig. 3.3.

2.2.2 Food web structure

The compartments (i.e. state variables) to include into the ecosystem have been chosen according to the aim of this study which is the understanding of the factors that contributed to the seasonal succession of the most important phytoplankton groups of the Bering Sea from 1995 to 2001. The necessity to have sufficient complexity, in order to produce realistic simulations, but avoiding an excessive number

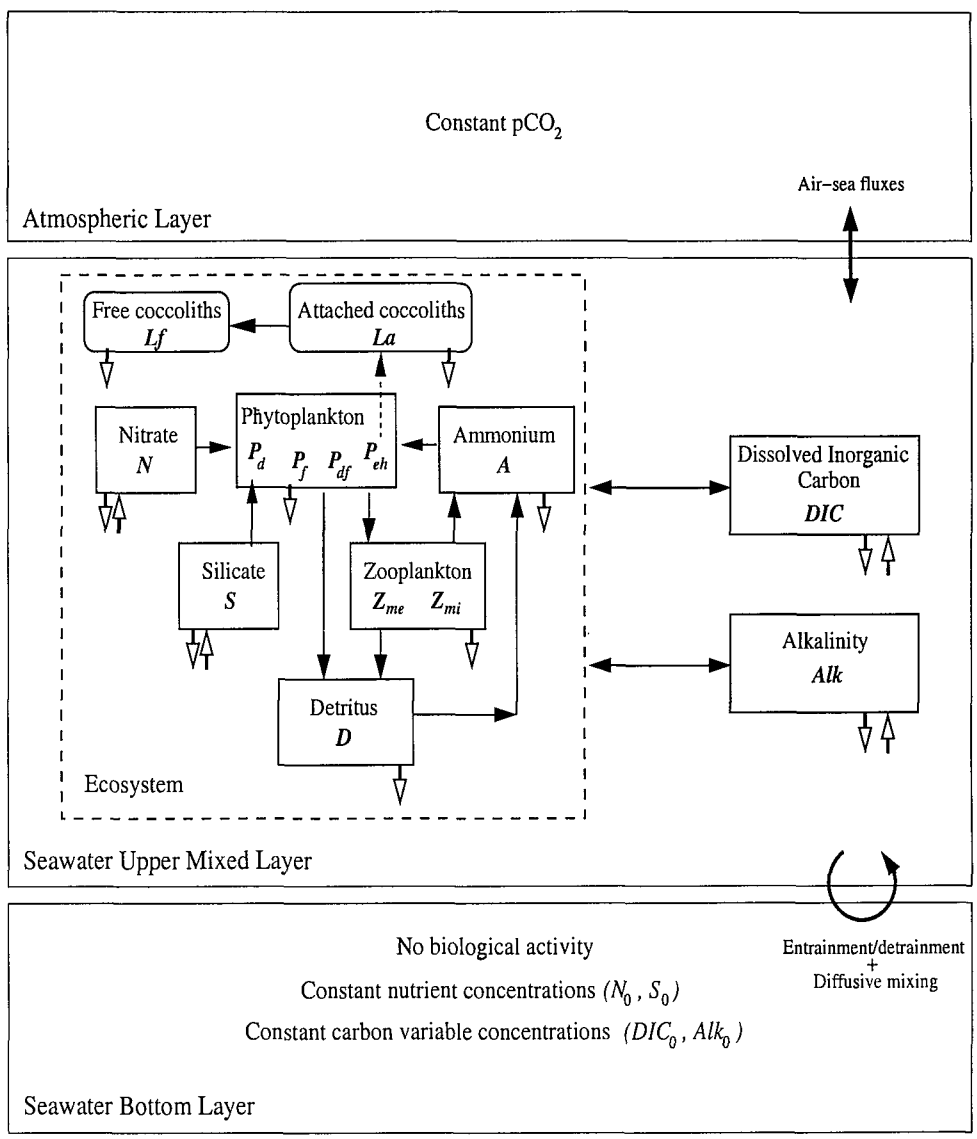

Figure 2.2: Physical structure of the model with main biological and chemical components. Arrows represent exchange of materials. Empty arrows indicate the material flowing between mixed layer depth and bottom layer. The arrow from *E. huxleyi* (P_{eh}) to attached coccoliths (L_a) is dashed indicating that attached coccoliths are produced proportionately to the *E. huxleyi* concentration rather than with a real flow of material between these two compartments. Note that mesozooplankton (Z_{me}) grazes also on microzooplankton (Z_{mi}). See text for more details.

of parameters has also shaped the model.

The food web (Fig. 2.2) takes into account 3 typical phytoplankton groups of the region (Sukhanova *et al.*, 1999): diatoms (P_d), flagellates (P_f) and dinoflagellates (P_{df}), as well as the species *E. huxleyi* (P_{eh}). Three main nutrients are considered: silicate (S), nitrate (N) and ammonium (A), with silicate used only by diatoms. Two different classes of zooplankton are included: microzooplankton (Z_{mi}) and mesozooplankton (Z_{me}). Diatoms, dinoflagellates and microzooplantkon are the food sources for mesozooplankton; flagellates and *E. huxleyi* are the food sources for microzooplankton. Under certain conditions (see below), microzooplankton can also graze on diatoms. The problem of how to realistically simulate the remineralisation of zooplankton faecal pellets and dead plankton into ammonium has been tackled by including a detrital compartment (D) with a fixed sinking rate. The breakdown of detritus (i.e. ammonification) to ammonium is also represented. In order to reduce complexity, the role of bacteria as a mediator of this process has not been included, following Fasham (1995). The nitrogen flux through the simplified foodweb of the ecosystem considered here is shown in Fig. 2.3. Coccoliths are included in the model as attached (i.e. part of the coccosphere) and free coccoliths (i.e. those which have become detached from the coccosphere), L_a and L_f, respectively. Their modelling is discussed in more detail in subsection 2.2.4.

2.2.3 *E. huxleyi* advantages

An extra grazing term is included in the diatom equation ($G_{d,mi}P_d$ in equation 2.11) in order to simulate the effect of microzooplankton selectively "switching" from *E. huxleyi* or other flagellates to diatoms (Olson & Strom, 2002). This term is introduced when silicate concentrations fall below the threshold of 3 μM. When this is the case, the maximum ingestion rate of diatoms (see equation 2.15), $g_{d,mi}$, is switched from 0 to 0.7 d^{-1} and the one of *E. huxleyi*, $g_{eh,mi}$, from 0.7 to 0.175 d^{-1}. This scenario has its ecological foundation in the fact that when waters are depleted with silicate, diatoms frustules are more weakly silicified (Ragueneau *et al.*, 2000;

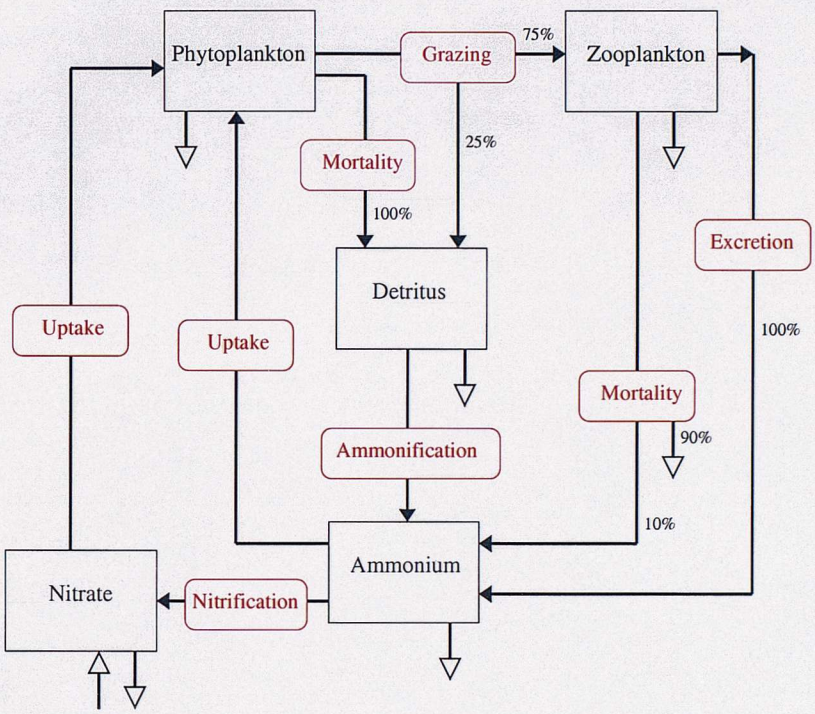

Figure 2.3: Nitrogen cycle through the simplified foodweb. The text in red indicates the process responsible for the flow of nitrogen from one compartment to another. Empty arrows represent exchanges between upper and bottom boxes. Zooplankton grazing efficiency is set to 75%, the remaining flows into detritus; 100% of zooplankton excretion is directly remineralised into ammonium; 90% of dead zooplankton is rapidly lost out of the upper box, while 100% of phytoplankton mortality is recycled into detritus. Breakdown of detritus into ammonium (ammonification) takes place at a rate of $0.05\,\mathrm{d}^{-1}$, and ammonium is nitrified at a rate of $0.05\,\mathrm{d}^{-1}$.

Rousseau *et al.*, 2002; Goering & Iverson, 1981, observed in the Bering Sea) and this may increase their susceptibility to grazing. The reduction in grazing on *E. huxleyi* is based on evidence from field studies (e.g. Olson & Strom, 2002) as well as laboratory studies that have shown that *E. huxleyi* uses chemical defence (Strom *et al.*, 2003). The underlying assumption here is that the newly-arrived *E. huxleyi* in the Bering Sea represented a sub-optimal prey for microzooplankton as compared to the lightly-silicified summer diatom population. Figure 2.4 illustrates the modelling of the zooplankton-phytoplankton interactions just described.

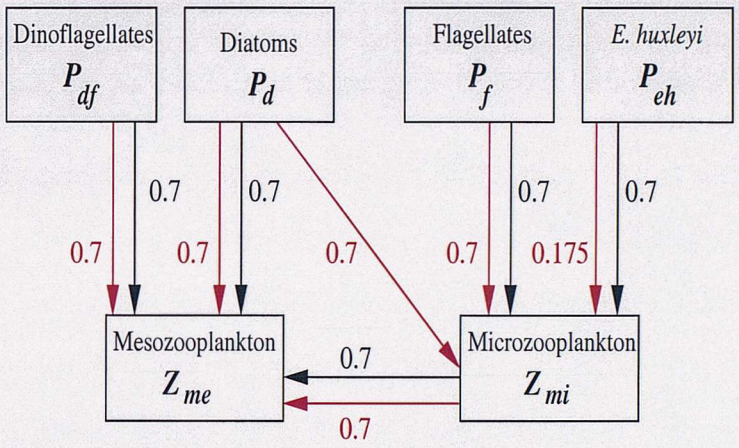

Figure 2.4: Schematic representation of the zooplankton-phytoplankton interactions. The model switches from interactions indicated with black arrows to interactions indicated with red arrows when silicate concentration fall below 3 μM. The numbers indicate the ingestion rates for the two cases in d^{-1}.

Photoinhibition is incorporated in the model by calculating light-limited growth using a Steele's function (equation 2.6). The growth of *E. huxleyi* is assumed to saturate at higher irradiances than for all other phytoplankton (see Table 2.1 for exact values). In combination with different maximum growth rates (at 0 °C), this formulation of light limitation will give *E. huxleyi* a relative disadvantage at low light levels and a relative advantage at high light levels (see Fig. 2.5).

Young (1994) observed that *E. huxleyi* predominates in areas of upwelling and in coastal and shallow sea assemblages. In addition, Hurlburt (1990) classified *E. huxleyi* together with diatoms as fast growing, *r*-selected species. These indications suggest a higher maximum growth rate for *E. huxleyi* with respect to other small phytoplankton such as flagellates. It was for this reason that Tyrrell & Taylor (1996)

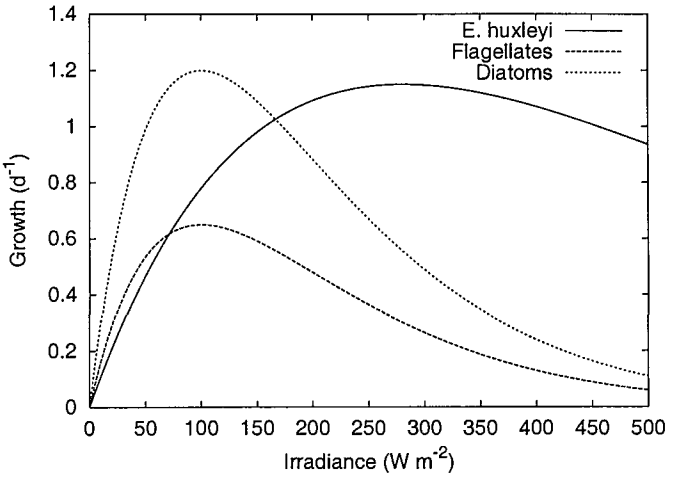

Figure 2.5: Comparison of PI-curves for *E. huxleyi*, flagellates and diatoms in the model. Saturation level is set to $280\,\mathrm{W\,m^{-2}}$ for *E. huxleyi*, and to $100\,\mathrm{W\,m^{-2}}$ for all other phytoplankton and with maximum growth rates as in Table 2.1.

adopted a high growth rate for *E. huxleyi* in their ecosystem model, comparable to the one for diatoms but somewhat smaller. In this study, a maximum growth rate of $1.15\,\mathrm{d^{-1}}$ has been assumed for *E. huxleyi*, $1.2\,\mathrm{d^{-1}}$ for diatoms, $0.65\,\mathrm{d^{-1}}$ for flagellates and $0.6\,\mathrm{d^{-1}}$ for dinoflagellates. During the diatom spring blooms of the years 1980 and 1981 a maximum growth rate in the range of $1.2\,\mathrm{d^{-1}}$ was determined in the Bering Sea (Eslinger & Iverson, 2001).

In the modelling studies by Tyrrell & Taylor (1996) and Aksnes *et al.* (1994) the high competitive ability of *E. huxleyi* in phosphorus-limited environments was expressed by assuming for this species a higher affinity for phosphorus (i.e. lower half-saturation constant for phosphorus uptake) but same affinity for nitrogen (i.e. same half-saturation constant for nitrogen uptake) with respect to other phytoplankton. The affinity for a certain nutrient, α, is mathematically expressed as μ_{max}/N_h, where μ_{max} is the temperature-dependent intrinsic growth rate and N_h the half-saturation constant for the nutrient uptake. In some ecosystem models (Aksnes *et al.*, 1994, 1995) the growth of phytoplankton is formulated in terms of affinities, $\mu = \mu_{max}\frac{N}{(\mu_{max}/\alpha)+N}$, rather than half-saturation constants, $\mu = \mu_{max}\frac{N}{N_h+N}$. The use of a constant affinity implies the use of a variable half-saturation constant (as μ_{max} varies with temperature) which may be a more appropriate approach when growth is calculated at low nutrient regimes (Aksnes *et al.*, 1995). However, since phosphorus

is never present in limiting concentrations in the Bering Sea (see subsection 1.5.5), neither the N:P ratio nor phosphorus are included as state variables in the present model and the growth is expressed in terms of half-saturation constants rather than affinities.

2.2.4 Other major processes and parameters

Half saturation constants for phytoplankton nutrient uptake are equal for all groups and species and set to $1.5\,\mathrm{mmol\,m^{-3}}$ for nitrate uptake, which is within the range of 0.5-2.75 $\mathrm{mmol\,m^{-3}}$ determined by Sambrotto *et al.* (1986) in the Bering Sea, and $0.05\,\mathrm{mmol\,m^{-3}}$ for ammonium uptake (Tyrrell & Taylor, 1996). Phytoplankton natural mortality is modelled linearly with a constant rate set to $0.08\,\mathrm{d^{-1}}$ for all groups and species (slightly higher than $0.05\,\mathrm{d^{-1}}$ used by Fasham, 1995). Among phytoplankton, only diatoms are assumed to sink. Sinking takes place at a minimum velocity of $0.5\,\mathrm{m\,d^{-1}}$, as silicate becomes depleted ($< 2\,\mu$M) this velocity is increased as described by Tyrrell & Taylor (1996). The grazing processes have been simulated as in Fasham (1993). Zooplankton losses are by excretion (directly remineralised into ammonium), mortality (of which 10% is remineralised directly into ammonium and the rest is assumed to sink rapidly out of the system) and faecal pellets (which are assumed to be produced during grazing and remineralised through detritus according to the given assimilation efficiencies, B, of 75%, as in Fasham, 1993). Detritus is lost out of the system by sinking (at a constant rate of $1\,\mathrm{m\,d^{-1}}$, Fasham, 1993), and is remineralised into ammonium through a constant breakdown rate of $0.05\,\mathrm{d^{-1}}$ (Fasham, 1993). Nitrification has been considered by including a constant ammonium oxidation rate term of $0.05\,\mathrm{d^{-1}}$ (Denman, 2003; Ward, 2000). The processes involving the flow of nitrogen in the model are illustrated with a simplified foodweb scheme in Fig. 2.3.

Since the details of how and why the coccoliths are produced and afterward detached in nature are not fully understood, it is very difficult to give a realistic representation of this processes. The only attempt so far to model such mechanisms

is represented by the study of Tyrrell & Taylor (1996). The same formulation is adopted here. The production of attached coccoliths is made proportional to *E. huxleyi* concentration. Under optimal conditions coccolith production takes place at a maximum calcification rate, C_{max}, of $0.2\,\mathrm{mg\,cal\,C\,(mg\,org\,C)^{-1}\,d^{-1}}$ (Fernández *et al.*, 1993). The process is limited by temperature and light, not by nutrients (Paasche, 2002). Attached coccoliths are lost into the free coccolith compartment by detachment, by grazing of the whole cell and by cell natural mortality. Since one calcified cell can hold a maximum of 10-50 coccoliths (Balch *et al.*, 1993), the detachment is calculated by comparing the concentration of attached coccoliths with the concentration of *E. huxleyi* cells. When the ratio of these two variables is greater than Π_{max} coccoliths per cell (set to 30), than the coccoliths in excess are shed and transferred into the free coccolith compartment. The grazing of attached and free coccoliths is assumed to take place at the same rate as for cells ($G_{eh,mi}$). Grazed coccoliths (attached and free) are not assimilated by zooplankton (Honjo & Roman, 1978). Based on this observation, it is assumed that ingested coccoliths are egested and lost rapidly out of the system (in the form of large aggregates and faecal pellets). There are strong indications that calcite dissolution can take place at depths well above the chemical lysocline through biologically mediated processes (Harris, 1994; Milliman *et al.*, 1999). Therefore free coccoliths are also dissolved in the model at a constant rate of $0.05\,\mathrm{d^{-1}}$ (Tyrrell & Taylor, 1996).

As said, diffusive vertical exchange between the two boxes has been parameterised with a multiplicative factor. Although in a rather simplistic fashion, k does take into account those processes like breaking internal waves, convective mixing and storm events. A low value of this parameter, typically $0.01\,\mathrm{m\,d^{-1}}$ (Fasham, 1993), corresponds to strong stratification and therefore less diffusive exchange between the two boxes.

The model uses nitrogen as currency (i.e. plankton and nitrogen nutrient differential equations are in units of $\mathrm{mmol\,N\,m^{-3}}$) and, where necessary to compare results with carbon or chlorophyll equivalents, a Redfield C:N ratio of 6.625 for

phytoplankton and 5.625 for zooplankton, with a C:Chlorophyll ratio of 50 (Taylor *et al.*, 1997). The attached and free coccoliths equations are in units of carbon as is *DIC*. Alkalinity is modelled in units of charge-equivalent[1] (Eq).

2.2.5 The carbonate system

In the ocean, carbon dioxide can be found in three different forms: as free carbon dioxide, $CO_{2(aq)}$, as bicarbonate, HCO_3^-, and as carbonate ion, CO_3^{2-} (see Fig. 2.6). The sum of these dissolved forms is called total dissolved inorganic carbon (DIC). While DIC tends to remain constant over long time scales, the relative concentrations of its component species are subject to change over much shorter periods. Under normal seawater conditions (pH=8.0-8.2), there is roughly 6-10 times more HCO_3^- than CO_3^{2-}. When CO_2 dissolves in seawater, less than 1% remains as CO_2; most dissociates into HCO_3^- and CO_3^{2-}. The carbon chemistry of the upper mixed layer of the ocean responds thermodynamically to any increase in atmospheric pCO_2. Therefore, as more CO_2 is driven into the ocean, it quickly forms carbonic acid, which is a weak acid. Most of this rapidly dissociates to either HCO_3^- or CO_3^{2-}. Alkalinity (Alk), i.e. the excess of positively charged ions in the seawater, is balanced by the proportion of these two ions. If more negative charge is needed, then some of the HCO_3^- is converted to CO_3^{2-}, and if less is needed, then some of the CO_3^{2-} is converted to HCO_3^-.

As suggested by Broecker (1974), to a first approximation, the carbonate ion concentration can be estimated as follows:

$$[CO_3^{2-}] \approx \text{Alk} - \text{DIC} \tag{2.1}$$

[1] Alkalinity can be expressed in molar concentration units, but it is more convenient to use charge-equivalent units (i.e. Eq). That is because the doubly charged carbonate ion carries a double weighting, such that its contribution to alkalinity is twice its molar concentration. For example, if the molar value of $[CO_3^{2-}]$ is $0.2\,\mu\text{mol}\,\text{kg}^{-1}$, then its contribution to alkalinity will be $0.4\,\mu\text{Eq}\,\text{kg}^{-1}$

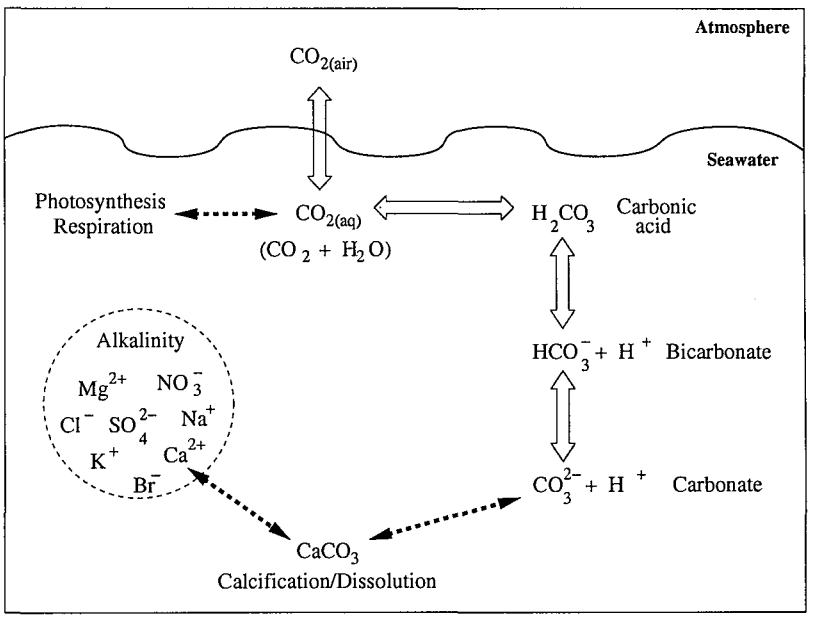

Figure 2.6: Carbonate system in seawater. See appendix A for a detailed description of this system. See also note 2 (next page) for a clarification on the substrates for calcification.

with:

$$\mathrm{DIC} = [CO_{2(aq)}] + [HCO_3^-] + [CO_3^{2-}] \tag{2.2}$$

$$\mathrm{Alk} \approx [HCO_3^-] + 2[CO_3^{2-}] + [B(OH)_4^-] + [OH^-] - [H^+] \tag{2.3}$$

See appendix A for a derivation of these relations. According to equation 2.1, as alkalinity decreases (for instance during calcification through Ca^{2+} removal) or as DIC increases (for instance through respiration and/or input from the atmosphere), $[CO_3^{2-}]$ decreases.

E. huxleyi (and calcifiers in general) require Ca^{2+} and CO_3^{2-} ions for calcification[2]. $[Ca^{2+}]$ in seawater is much higher than $[CO_3^{2-}]$ and it can be considered constant in today's ocean, hence $[CO_3^{2-}]$ is considered the limiting factor to calcification.

[2]Calcification ultimately involves the precipitation of $CaCO_3$ from Ca^{2+} and CO_3^{2-} ions. However, despite much intense investigation (see, for example, the reviews of Brownlee & Taylor, 2003; Paasche, 2002), the precise mechanisms and transport routes of substrates leading to the precipitation reaction are still unclear. Also, there is good evidence that HCO_3^- is the external inorganic carbon source for calcification in coccolithophores (Berry *et al.*, 2002; Paasche, 2002), nevertheless experimental evidence (Riebesell *et al.*, 2000) indicates CO_3^{2-} ion as the limiting element. This apparent paradox seems to be also evident in corals and coralline algae (J. Kleypas, personal communication).

The calculation of the carbon system variables was implemented in the model on the base of the carbon system equations of Millero (1995) and Peng *et al.* (1987). In the model, carbon is consumed by phytoplankton by assuming a C:N ratio equal to 6.625. The exchange of CO_2 across the air-sea interface is computed by using the formulation of Wanninkhof (1992). The effects of calcification and dissolution are taken into account as well. Deep DIC and alkalinity concentrations (DIC_0 and Alk_0) are set to 2,100 μmol kg^{-1} and 2,250 μEq kg^{-1}, respectively (Walsh & Dieterle, 1994).

2.2.6 Method

The approach used in finding the model configuration that could best reproduce the observations from 1995 to 2001 comprises two steps. The first step, the "calibration", consisted in running the model without *E. huxleyi* in order to explore its behaviour with respect to the seasonal succession patterns and other aspects of the ecosystem observed before the increased *E. huxleyi* activity (i.e. before 1995). The forcing functions for this case (SST, MLD and PAR) are obtained as the average functions that have been affecting the ecosystem in the last 20 years (before 1995) and the model results compared with multi-year composites of observations (for the variables available). This step also allowed to make initial estimations of poorly known parameters and optimise them to produce results consistent with the observed data. The second step, the "main simulation", with *E. huxleyi* included into the model, consisted in running the model from the year 1995 to the year 2001 continuously. The appropriate forcing functions for each year have been used and the results are compared to the observations for the same time period.

The system of differential equations has been solved numerically using the fourth-order Runge-Kutta method with a time step of one hour. A linear interpolation of ECMWF data (i.e. PAR and wind speed) for the runs related to years from 1995 to 2001, which are 6-hourly, is used to match the time step of the model.

In order to minimise the dependency of the model results on the initial conditions

of the state-variables, the model was run repeatedly over a full seasonal cycle of the physical forcing prior to 1995. Only once it developed a repeatable annual cycle, was it then run with the forcing from 1995 to 2001.

2.3 Model equations

All state variables and parameters used in the model are given at the end of this chapter in Tables 2.1 and 2.2 along with their symbols, units and values.

The effect of the physical forcing (and therefore the connection with the climate) on the ecosystem is modelled implicitly by using the seasonal dynamics of the mixed layer depth $M(t)$. Temperature data (as detailed functions of time and depth) have been used to reconstruct the MLD, $M(t)$. $h(t) = dM(t)/dt$ was used to calculate the time rate of change of the MLD. Exchange between the two layers was modelled as two processes, vertical diffusion and entrainment or detrainment caused by deepening or shallowing of the MLD. According to Fasham (1993), the variable $h^+(t) = max[h(t), 0]$ was used in order to take into account the effects of entrainment and detrainment. The two zooplankton variables were considered capable of maintaining themselves within the mixed layer and thus the function $h(t)$ was used in that case. Diffusive mixing across the thermocline, k, has been parameterised by means of a constant factor. The whole diffusion term can finally be written as:

$$K = \frac{k + h^+(t)}{M(t)} \tag{2.4}$$

2.3.1 Phytoplankton

The phytoplankton growth rate, μ_d (for example in the case of diatoms), is a function of light, nutrients and temperature. These terms are assumed to limit growth independently so that:

$$\mu_d = \mu_{0,d} f(T) \Psi_d(I) \Phi_d(N, A, S) \tag{2.5}$$

Where $\mu_{0,d}$ is the maximum intrinsic growth rate at temperature $T = 0°$ C, $f(T) = e^{0.063T}$, and the term $\mu_{0,d}f(T)$ represents the Eppley (1972) formulation of temperature-dependent growth. The light limitation term, is calculated by integrating PAR over the depth z by using two formulations: 1) the Steele formulation (in the calibration and standard runs):

$$\Psi_d(I) = \frac{1}{M}\int_0^M \frac{I(z)}{I_{s,d}} e^{1-\frac{I(z)}{I_{s,d}}} dz \tag{2.6}$$

where $I_{s,d}$ is the light level at which photosynthesis saturates in the case of diatoms, and 2) the Michaelis-Menten formulation (in the sensitivity analysis run):

$$\Psi_d(I) = \frac{1}{M}\int_0^M \frac{I(z)}{I_{h,d} + I_z} dz \tag{2.7}$$

where $I_{h,d}$ is the half saturation constant of growth with respect to light. In both formulations, $I(z)$ is calculated with Anderson's model (Anderson, 1993), which formulation is presented in Appendix B.

Following Fasham (1995), the nutrient limitation term $\Phi_d(N, A, S)$ is given by:

$$\Phi_d(N, A, S) = min\left(n_d + a_d, \frac{S}{S_h + S}\right) \tag{2.8}$$

with:

$$n_d = \frac{N/N_{h,d}}{1 + N/N_{h,d} + A/A_{h,d}} \tag{2.9}$$

for nitrate limitation and

$$a_d = \frac{A/A_{h,d}}{1 + N/N_{h,d} + A/A_{h,d}} \tag{2.10}$$

for ammonium limitation. $S_h, N_{h,d}$ and $A_{h,d}$ are the half saturation constants for diatom uptake of silicate, nitrate and ammonium, respectively. For phytoplankton other than diatoms, the limitation due to nutrient is simply given by the sum of

equations 2.9 and 2.10.

The equations for phytoplankton can now be written as:

$$\frac{dP_d}{dt} = \mu_d P_d - m_d P_d - G_{d,me} P_d - G_{d,mi} P_d - \left(\frac{v_d}{M} + K\right) P_d \quad (2.11)$$

$$\frac{dP_f}{dt} = \mu_f P_f - m_f P_f - G_{f,mi} P_f - K P_f \quad (2.12)$$

$$\frac{dP_{df}}{dt} = \mu_{df} P_{df} - m_{df} P_{df} - G_{df,me} P_{df} - K P_{df} \quad (2.13)$$

$$\frac{dP_{eh}}{dt} = \mu_{eh} P_{eh} - m_{eh} P_{eh} - G_{eh,mi} P_{eh} - K P_{eh} \quad (2.14)$$

Where (for example in the case of diatoms, equation 2.11) m_d is the constant mortality rate, $G_{d,me}$ the grazing rate of mesozooplankton on diatoms and $G_{d,mi}$ the grazing rate of microzooplankton on diatoms (which is different than zero only under particular conditions, see subsection 2.2.3).

2.3.2 Zooplankton

Following Fasham (1993), the grazing rate of, for example, mesozooplankton on diatoms is assumed to take the following form:

$$G_{d,me} = \frac{g_{d,me} p_{d,me} Z_{me} P_d}{Z_{h,me}(p_{d,me} P_d + p_{df,me} P_{df} + p_{mi,me} Z_{mi}) + p_{d,me} P_d^2 + p_{df,me} P_{df}^2 + p_{mi,me} Z_{mi}^2} \quad (2.15)$$

Where $g_{d,me}$ is the maximum ingestion rate, $Z_{h,me}$ is the half saturation constant for ingestion and $p_{d,me}$ is the mesozooplankton preference for diatoms. The grazing rates on other food sources are analogous. The equations for zooplankton are therefore:

$$\frac{dZ_{mi}}{dt} = \left(B_{f,mi} G_{f,mi} + B_{eh,mi} G_{eh,mi} + B_{d,mi} G_{d,mi}\right) Z_{mi} - e_{mi} Z_{mi} - m_{mi} Z_{mi}^2 - G_{mi,me} Z_{mi} - \frac{h(t)}{M} Z_{mi} \quad (2.16)$$

$$\frac{dZ_{me}}{dt} = \left(B_{d,me} G_{d,me} + B_{df,me} G_{df} + B_{mi,me} G_{mi}\right) Z_{me} - e_{me} Z_{me} - m_{me} Z_{me}^2 - \frac{h(t)}{M} Z_{me} \quad (2.17)$$

$B_{f,mi}$ is, for example, the assimilation efficiency of flagellates by microzooplankton, and e_{mi} and m_{mi} are the microzooplankton excretion and mortality rates, respectively. Note that zooplankton mortality is represented by a quadratic function of zooplankton biomass, which constitutes the so-called closure term (Steele & Henderson, 1992). This may be interpreted as representing either cannibalism within the same group, or an unmodelled higher predator whose biomass is assumed to be proportional to that of the zooplankton. Such formulation reduces the likelihood of obtaining solutions with short-term oscillations or multi-year cycles (Edwards & Yool, 2000).

2.3.3 Nutrients

The nutrient equations are as follow:

$$\begin{aligned}
\frac{dN}{dt} &= -\mu_{0,d} f(T)\Psi_d(I)\Phi_d(N,A,S)\frac{n_d}{n_d+a_d}P_d - \mu_{0,f} f(T)\Psi_f(I)n_f P_f \\
&\quad -\mu_{0,df} f(T)\Psi_{df}(I)n_{df} P_{df} - \mu_{0,eh} f(T)\Psi_{eh}(I)n_{eh} P_{eh} \\
&\quad +\Omega A + K\left(N_0 - N\right) \qquad (2.18) \\
\frac{dA}{dt} &= -\mu_{0,d} f(T)\Psi_d(I)\Phi_d(N,A,S)\frac{a_d}{n_d+a_d}P_d - \mu_{0,f} f(T)\Psi_f(I)a_f P_f \\
&\quad -\mu_{0,df} f(T)\Psi_{df}(I)a_{df} P_{df} - \mu_{0,eh} f(T)\Psi_{eh}(I)a_{eh} P_{eh} + m_D D \\
&\quad +(e_{mi} + \delta_{mi} m_{mi} Z_{mi})Z_{mi} + (e_{me} + \delta_{me} m_{me} Z_{me})Z_{me} \\
&\quad -\Omega A - KA \qquad (2.19) \\
\frac{dS}{dt} &= -\mu_d P_d + K\left(S_0 - S\right) \qquad (2.20)
\end{aligned}$$

The constant terms N_0 and S_0 represent the concentrations below the mixed layer depth of nitrate and silicate, respectively. Note that ammonium concentration below the MLD is assumed to be zero (Fasham, 1993). The equation for ammonium (2.19) shows the balance between the loss due to ammonium uptake by phytoplankton and due to nitrification (ΩA) and gains from zooplankton excretion and detrital remineralisation (see below). A Si:N ratio of 1:1 is assumed in equation 2.20 (Brzezinski, 1985; Dugdale *et al.*, 1995).

2.3.4 Detritus

The equation for detritus is:

$$\begin{aligned}\frac{dD}{dt} &= (1-B_{d,me})G_{d,me}+(1-B_{df,me})G_{df,me}+(1-B_{mi,me})G_{mi,me}\\ &+(1-B_{eh,mi})G_{eh,mi}+(1-B_{f,mi})G_{f,mi}+(1-B_{d,mi})G_{d,mi}\\ &+m_dP_d+m_fP_f+m_{df}P_{df}+m_{eh}P_{eh}-m_DD-\left(\frac{v_D}{M}+K\right)D \quad (2.21)\end{aligned}$$

Where m_D is the breakdown rate of detritus to ammonium. The source of detritus in the mixed layer are assumed to be dead phytoplankton and zooplankton faecal pellets.

2.3.5 Coccoliths

Coccoliths are represented in the model as attached (i.e. part of the coccosphere) and free coccoliths (i.e. which have become detached from the coccosphere), L_a and L_f, respectively.

The synthesis of new coccoliths is made proportional to the number of *E. huxleyi* cells and the changes in the two state variables are represented by:

$$\frac{dL_a}{dt} = \rho_{CN}CP_{eh}-G_{eh,mi}L_a-m_{eh}L_a-\Gamma-KL_a \quad (2.22)$$

$$\frac{dL_f}{dt} = \Gamma+m_{eh}L_a-\delta_fG_{eh,mi}L_f-\Theta L_f-KL_f \quad (2.23)$$

Where ρ_{CN} is the C:N Redfield ratio. $C = C_{max}f(T)\Psi(I)$, with C_{max} the constant rate of calcification (i.e. coccolith production) under optimal conditions, $f(T)$ and $\Psi(I)$ representing temperature and light dependence of calcification, respectively (analogous to temperature- and light-limited photosynthesis functions). δ_f is the fraction of free coccoliths lost during microzooplankton grazing. Θ represents the constant dissolution rate. The transfer from attached to free coccoliths, Γ, is calculated by comparing the concentration of attached coccoliths with the concentration

of *E. huxleyi* cells. When the ratio of these two variables is greater than the maximum number of coccoliths allowed per cell (Π_{max}), then all the excess coccoliths are transferred to the pool of free coccoliths. The number of coccoliths in excess is calculated with:

$$\Gamma = \gamma \left(L_a - \Pi_{max} C_L \frac{\rho_{CN} P_{eh}}{C_{eh}} \right) \tag{2.24}$$

Where γ is the rate of detachment (i.e.: 100% of coccoliths in excess per time step).

2.3.6 Dissolved inorganic carbon

The change in total inorganic carbon in the upper box of the water column is affected by the utilisation of inorganic carbon by phytoplankton, the breakdown of detritus, the zooplankton excretion, the fraction of zooplankton mortality that rapidly decomposes into ammonium, and diffusive fluxes. The DIC cycle is affected also by $CaCO_3$ formation and dissolution. In the model, these processes are described by:

$$\begin{aligned} \frac{dDIC}{dt} &= -\rho_{CN}(\mu_d P_d + \mu_f P_f + \mu_{df} P_{df} + \mu_{eh} P_{eh} + C P_{eh}) + \\ &+\rho_{CN}[m_D D + (e_{mi} + \delta_{mi} m_{mi} Z_{mi}) Z_{mi} + (e_{me} + \delta_{me} m_{me} Z_{me}) Z_{me}] + \\ &+\Theta L_f + v_g S_{CO_2} \left[\frac{p\mathrm{CO}_{2(air)} - p\mathrm{CO}_{2(sea)}}{M(t)} \right] + K(DIC_0 - DIC) \end{aligned} \tag{2.25}$$

Where the term $v_g S_{CO_2} \left[(p\mathrm{CO}_{2(air)} - p\mathrm{CO}_{2(sea)})/M(t) \right]$ describes the CO_2 fluxes at the air-sea interface, with v_g gas transfer velocity, S_{CO_2} solubility of CO_2 (expressed in units of concentration per pressure), and $p\mathrm{CO}_2$ (partial pressure of CO_2 in air and seawater[3]).

The gas transfer velocity is given by equation 8 in Wanninkhof (1992). The solubility of CO_2 is obtained with a least squares polynomial fit vs. temperature and salinity with a method described first by Weiss (1974). As mentioned above,

[3] A more correct form of this equation is written in terms of fugacity (fCO_2), which incorporates the changes of chemical potential as a function of pressure and temperature, rather than partial pressure. However, fugacity is approximately equal to partial pressure at sea level, and $p\mathrm{CO}_2$ is more commonly used in the literature (Weiss, 1974).

$pCO_{2(air)}$ is assumed to be constant at 358 μatm (as measured in 2000 in the Bering Sea by Murata & Takizawa, 2002). The partial pressure of CO_2 in seawater was calculated from model variables of total alkalinity, temperature and DIC along with apparent dissociation constants of carbon acid, boric acid, the solubility of CO_2 and the hydrogen ion activity by using the iterative method presented by Peng *et al.* (1987).

Note that Alkalinity and DIC are independent from temperature and pressure; pCO_2, and pH are not. The knowledge of any two of these parameters, along with the temperature, salinity, pressure, abundances of other constituents of seawater, and the relevant equilibrium constants, allow the determination of the other two. A detailed description of the calculation of these variables is given in appendix A.

2.3.7 Alkalinity

Alkalinity is formally defined as the amount of hydrogen ions (H^+) needed to convert all the weak acid anions back to their non-ionised acids. Another definition is the equivalent sum of all the bases that can accept a proton to the carbonic acid endpoint. It can be seen from equation 2.26 that the precipitation of one unit of calcium carbonate lowers alkalinity by two units, due to the double negative charge of the concentration of the carbonate ions. Therefore, in the model, changes of alkalinity are simply given by the balances between calcification, dissolution and diffusive fluxes:

$$\frac{dAlk}{dt} = -2\rho_{CN}CP_{eh} + 2\Theta L_f + K(Alk_0 - Alk) \tag{2.26}$$

It is assumed that the effects of nitrate and ammonium ions are negligible (Peng *et al.*, 1987).

Table 2.1: Parameters used in the model for calibration and main simulation runs. References for these values are given in the text.

Parameter	Symbol	Unit	Value
Diatoms (P_d)			
Maximum growth rate at 0°C	$\mu_{0,d}$	d^{-1}	1.2
Minimum sinking speed	v_d	$\mathrm{m\,d}^{-1}$	0.5
Mortality rate	m_d	d^{-1}	0.08
Light saturation constant	$I_{s,d}$	$\mathrm{W\,m}^{-2}$	15
Nitrate half-saturation const.	$N_{h,d}$	$\mathrm{mmol\,m}^{-3}$	1.5
Ammonium half-saturation const.	$A_{h,d}$	$\mathrm{mmol\,m}^{-3}$	0.05
Silicate half-saturation const.	S_h	$\mathrm{mmol\,m}^{-3}$	3.5
Flagellates (P_f)			
Maximum growth rate at 0°C	$\mu_{0,f}$	d^{-1}	0.65
Mortality rate	m_f	d^{-1}	0.08
Light saturation const.	$I_{s,f}$	$\mathrm{W\,m}^{-2}$	15
Nitrate half-saturation const.	$N_{h,f}$	$\mathrm{mmol\,m}^{-3}$	1.5
Ammonium half-saturation const.	$A_{h,f}$	$\mathrm{mmol\,m}^{-3}$	0.05
Dinoflagellates (P_{df})			
Maximum growth rate at 0°C	$\mu_{0,df}$	d^{-1}	0.6
Mortality rate	m_{df}	d^{-1}	0.08
Light saturation const.	$I_{s,df}$	$\mathrm{W\,m}^{-2}$	15
Nitrate half-saturation const.	$N_{h,df}$	$\mathrm{mmol\,m}^{-3}$	1.5
Ammonium half-saturation const.	$A_{h,df}$	$\mathrm{mmol\,m}^{-3}$	0.05
E. huxleyi (P_{eh})			
Maximum growth rate at 0°C	$\mu_{0,eh}$	d^{-1}	1.15
Mortality rate	m_{eh}	d^{-1}	0.08
Light saturation const.	$I_{s,eh}$	$\mathrm{W\,m}^{-2}$	45
Nitrate half-saturation const.	$N_{h,eh}$	$\mathrm{mmol\,m}^{-3}$	1.5
Ammonium half-saturation const.	$A_{h,eh}$	$\mathrm{mmol\,m}^{-3}$	0.05
Nitrate (N)			
Deep concentration	N_0	$\mathrm{mmol\,m}^{-3}$	20
Nitrification rate	Ω	d^{-1}	0.05
Silicate (S)			
Deep concentration	S_0	$\mathrm{mmol\,m}^{-3}$	35
Microzooplankton (Z_{mi})			
Assimilation efficiency ($S < 3\mu$M)	$B_{eh,mi}, B_{f,mi}, B_{d,mi}$	– –	0.75, 0.75, 0.75
Assimilation efficiency ($S > 3\mu$M)	$B_{eh,mi}, B_{f,mi}, B_{d,mi}$	– –	0.75, 0.75, 0.0
Grazing preferences ($S < 3\mu$M)	p_{eh}, p_f, p_d	– –	0.33, 0.33, 0.33
Grazing preferences ($S > 3\mu$M)	$p_{eh,mi}, p_{f,mi}, p_{d,mi}$	– –	0.5, 0.5, 0.0
Max. ingestion rates ($S < 3\mu$M)	$g_{eh,mi}, g_{f,mi}, g_{d,mi}$	d^{-1}	0.175, 0.7, 0.7
Max. ingestion rates ($S > 3\mu$M)	$g_{eh,mi}, g_{f,mi}, g_{d,mi}$	d^{-1}	0.7, 0.7, 0.0
Grazing half-saturation const.	$Z_{h,mi}$	$\mathrm{mmol\,m}^{-3}$	1.0
Mortality rate	m_{mi}	$\mathrm{d}^{-1}(\mathrm{mmol\ m}^{-3})^{-1}$	0.05
Excretion rate	e_{mi}	d^{-1}	0.025
Fract. of mort. going into amm.	δ_{mi}	– –	0.1
Mesozooplankton (Z_{me})			
Assimilation efficiency	$B_{d,me}, B_{mi,me}, B_{df,me}$	– –	0.75, 0.75, 0.75
Grazing preferences	$p_{d,me}, p_{mi,me}, p_{df,me}$	– –	0.33, 0.33, 0.33
Max. ingestion rates	$g_{d,me}, g_{mi,me}, g_{df,me}$	d^{-1}	0.7, 0.7, 0.7
Grazing half-saturation const.	$Z_{h,me}$	$\mathrm{mmol\,m}^{-3}$	1.0
Mortality rate	m_{me}	$\mathrm{d}^{-1}(\mathrm{mmol\ m}^{-3})^{-1}$	0.2
Excretion rate	e	d^{-1}	0.1
Fract. of mort. going into amm.	δ_{me}	– –	0.1
Detritus (D)			
Sinking speed	v_D	$\mathrm{m\,d}^{-1}$	0.4
Breakdown rate	m_D	d^{-1}	0.05
Cross-thermocline mixing rate	k	$\mathrm{m\,d}^{-1}$	0.01

Table 2.2: Parameters used to model the calcification process. References for these values are given in the text.

Parameter	Symbol	Unit	Value
Attached coccolith (L_a)			
Calcification rate	C_{max}	mg cal C (mg org C)$^{-1}$ d^{-1}	0.2
Light half-saturation constant	I_h	W m^{-2}	40
Max. number of coccoliths on a cell	Π_{max}	coccolith cell^{-1}	30
Rate of detachment	γ	d^{-1}	24.0
Calcite C content of a coccolith	C_L	g cal C coccolith^{-1}	0.25 10^{-12}
Organic C content of an *E. huxleyi* cell	C_{eh}	g org C cell^{-1}	10.0 10^{-12}
C:N ratio	ρ_{CN}	–	6.625
Free coccolith (L_f)			
Dissolution rate	Θ	d^{-1}	0.05
Fraction of grazed free coccoliths	δ_f	–	0.5
Carbonate system (DIC, Alk)			
DIC deep concentration	DIC_0	μmol kg^{-1}	2,100
Alkalinity deep concentration	Alk_0	μEq kg^{-1}	2,250
Atmospheric pCO$_2$	pCO$_{2(air)}$	μatm	358

Chapter 3

The observations

Ecosystem models are only as meaningful as the availability of data to constrain and validate them. As explained in section 2.2.6, the approach adopted in this modelling study comprised two steps: calibration and main simulation. The calibration, consisted of running and constraining the model with pre-1995 data. The main simulation consisted of constraining and fitting the model results with data from 1995 to 2001. All the data used are presented in this chapter.

The sampling of data described in the following was carried out by technicians and scientists of the cited institutions. The acquisition and processing of the satellite data was part of the work of this thesis.

3.1 Archive data

Data for nitrate, silicate, phosphate, total chlorophyll, SST and salinity in the Bering Sea for the period prior to 1995 have been obtained from the National Oceanographic Data Center of the National Oceanic and Atmospheric Administration. These data are available on the web at `http://www.nodc.noaa.gov/OC5/wod98.html` under the collection called: World Ocean Database 1998 (hereafter referred to as WOD98). The MLD data have also been obtained from the same source and are available on the web at `http://www.nodc.noaa.gov/OC5/mixdata.html`. The pre-1995 data

(shown in Fig. 3.1) have been used for the calibration of the model, i.e. to find an initial set of values for the poorly known parameters so that the results can best reproduce the Bering Sea shelf conditions in terms of phytoplankton seasonal succession and nutrient cycles prior to the appearance of *E. huxleyi*.

Nutrient enrichment processes on the shelf have their origins in the interaction with the deep water of the basin (Whitledge *et al.*, 1988). This nitrate-rich water originates from as deep as 300-400 m. High nitrate levels have been often observed near the bottom at the shelf break, 35 μM, and at the surface, 25 μM, (Whitledge *et al.*, 1986). Typical values for the shelf concentrations of nitrate range between 15 and 20 μM as the spring phytoplankton bloom starts, with a rapid decline during the spring bloom to almost undetectable values or as high as 2 μM (see Figs. 3.1a and 3.1b). The highest concentrations of nitrate observed in surface waters over the eastern Bering Sea shelf occur in late winter and early spring (Whitledge & Luchin, 1999). Winter fluxes of nitrate onto the shelf raises concentrations to as high as 20 μM in surface waters of the outer shelf, while the middle shelf usually only reaches about 15 μM (Whitledge *et al.*, 1986). As the thermocline develops, a two-layered system is produced with nitrate depletion in the upper layer and a uniform but higher concentration in the bottom layer (Fig. 3.2). In the autumn period a stronger mixing weakens the thermocline and enriches the surface with as much as 10 μM of nitrate.

Winter concentrations of dissolved silicon (silicate) usually are as high as 40 μM in both the middle and outer shelf area (Whitledge & Luchin, 1999). During summer, the concentrations of silicate are much lower due to diatom activity. In the middle shelf region, the surface may be depleted to values less than 1 μM while the bottom layer maintains 20-30 μM (Figs. 3.1c and 3.2). Bottom concentrations on the outer shelf are usually as high as 60 μM during late summer and early autumn periods. In the southeastern part of the shelf, summer values (usually around 3-5 μM) are higher than in spring probably because of the deepening of the layer of the seasonal thermocline and the inflow of water from the Pacific. Due to the effect of mixing, in

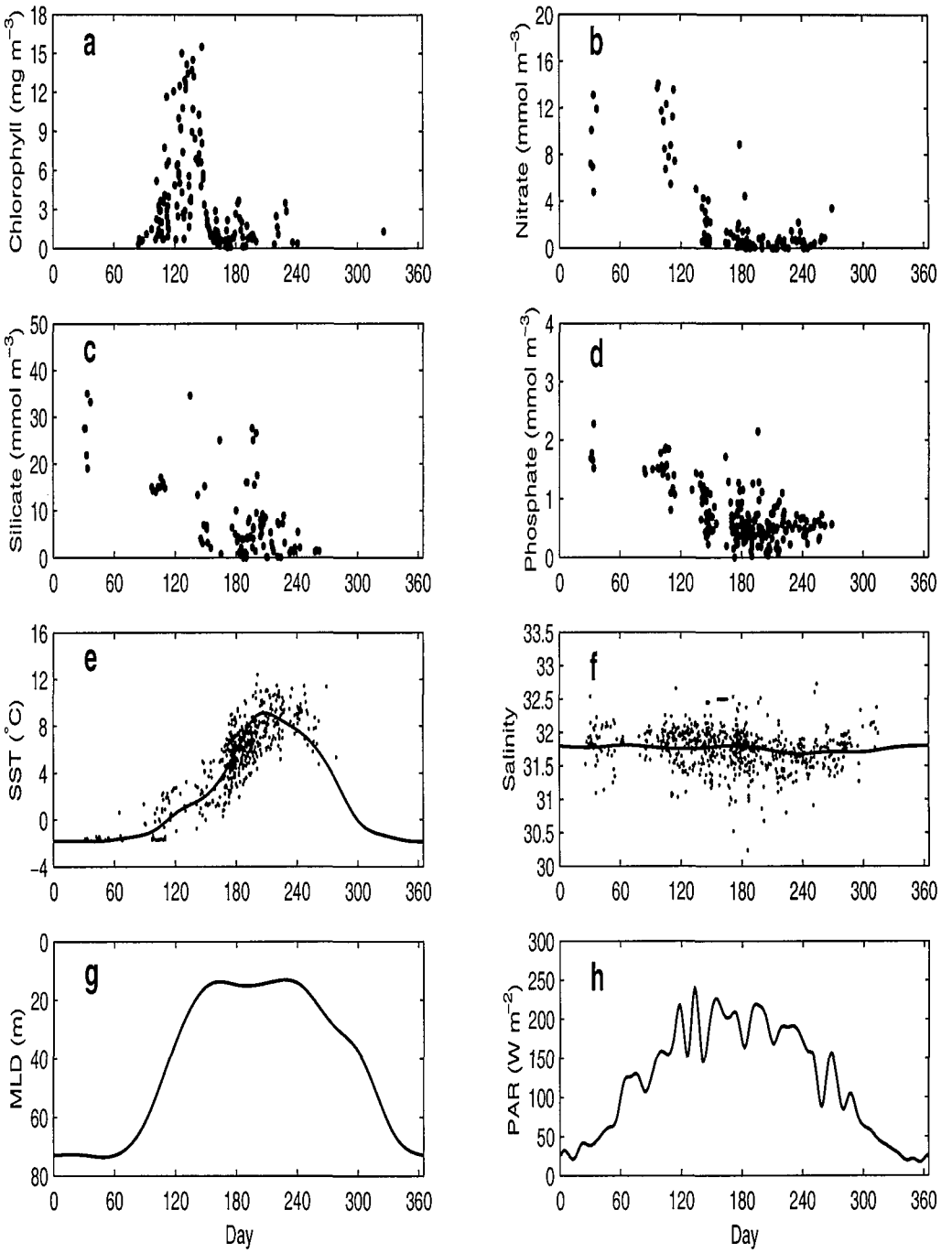

Figure 3.1: Data used for calibrating the model (for the period prior to 1995). SST (e) and Salinity (f) functions have been obtained as the best lines representing the data. All data are multi-year composites of the surface values of the southeastern middle shelf region.

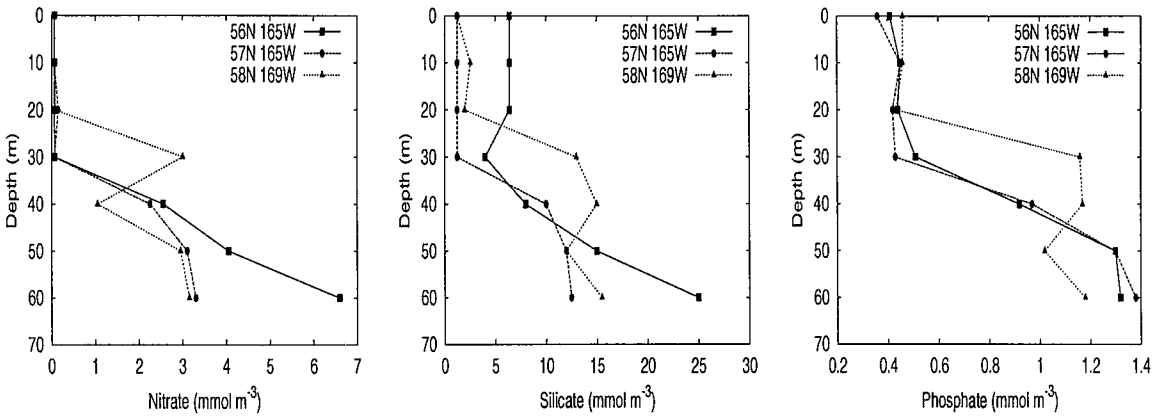

Figure 3.2: Typical summer (July 1987) profiles of nutrients in three different locations on the southern Bering Sea middle shelf region. Data from WOD98.

autumn there is an increase of these values (Whitledge & Luchin, 1999). Near the continental slope instead, the intensification of currents and the formation of eddies increases the silicate content to as much as 70-90 μM in winter.

The vertical distribution of phosphate tends to be different through the water column. In the surface waters, where the productive processes take place, low concentrations are observed (up to 0.3-0.4 μM as shown in Fig. 3.2). From intermediate to deep waters, phosphate concentration increases (to values as high as 2-2.25 μM Whitledge & Luchin, 1999). Bottom water concentrations tend to remain constant throughout the year (Whitledge & Luchin, 1999).

3.2 Field data

Observations for 1995-2001 have been obtained from Hokkaido University, T/V Oshoro Maru public data, which are published in annual reports (Anonymous, 2002), and by several cruises of the R/V Alpha Helix conducted in the area in the context of the following projects: Southeast Bering Sea Carrying Capacity, Process Studies of the Inner Shelf and Longterm Mooring Measurements in the Bering Sea and Plankton Processes.

3.2.1 Physical forcing

For the years from 1995 to 2001, SST, MLD, PAR and wind speed data are used to force the model as described in section 2.2 (data shown in Fig. 3.3). It is worthwhile to note that SST and reconstructed MLD are local data (taken at station M2). It is therefore assumed that they are representative of the whole southern middle shelf domain.

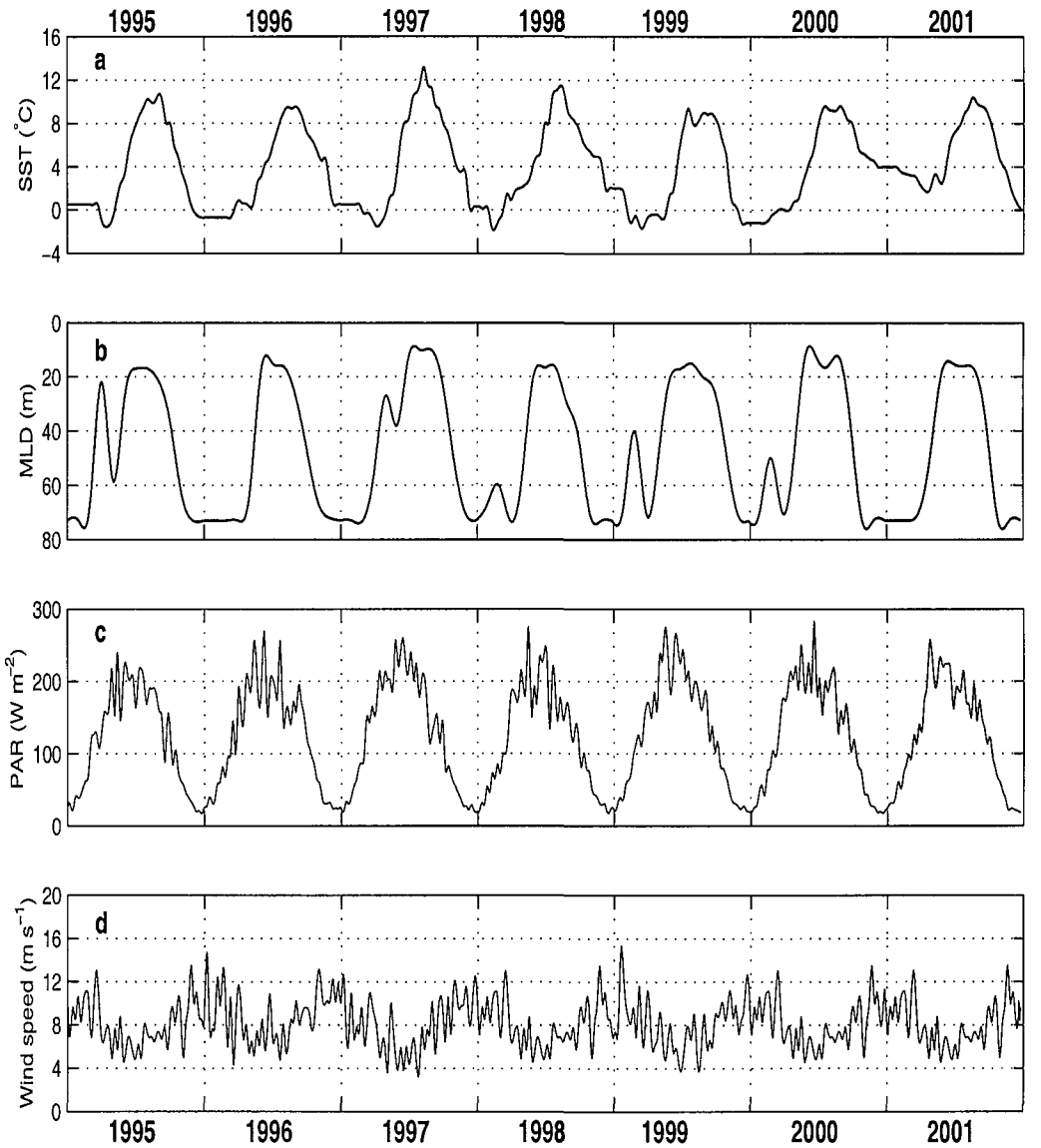

Figure 3.3: Forcing function used as input in the ecosystem model. a) SST, b) MLD and weekly running average of c) noon PAR and d) wind speed.

It may be argued that the stratification of the water column is not only temperature-driven. However, it has since long been recognised (Sambrotto *et al.*, 1986) that

temperature is always the stronger factor influencing water density in the Bering Sea in summer. Salinity changes may play a role during winter or spring time, though, when the process of ice formation or retreat takes place.

3.2.2 Nutrient, chlorophyll and plankton variables

Nitrate and phosphate, for the years after 1995, have been obtained from T/V Oshoro Maru public data (Anonymous, 2002). Silicate and ammonium data were obtained partly from T/V Oshoro Maru public data, partly from cruises sampling in the vicinity of station M2 and partly from published figures in the literature.

Oshoro Maru's seawater samples were collected with Niskin bottles on the CTD system during cruises in the eastern Bering Sea shelf. The samples were stored in polyethylene bottles and kept in a freezer at -20 °C until analysis. Nutrient concentrations were measured at Hokkaido University laboratories with Technicon Auto-analyzer. Samples specifically at the M2 site were also collected with a CTD rosette sampler and the nutrients readily measured onboard. The data are shown in Fig. 3.4.

Phytoplankton samples were collected during cruises with R/V Alpha Helix with Niskin samplers on a CTD rosette. Collections were made at the surface and, usually, at 5 m intervals to 40 m, preserved in neutral Lugol's iodine, and kept in the dark until counted. Cell counts were made using standard Utermöhl settling chamber and inverted-microscope techniques. Counts were made on four random strips of a 10 mL chamber at 450X. Species were identified to lowest possible taxon, and enumerated by counting 200-400 cells per sample. Additional phytoplankton samples were also collected on membrane filters, air-dried in a vacuum chamber and observed under oil immersion with normal microscopy or with scanning electron microscopy for identification. The data are reported in Fig. 3.5. Additional data points are included for *E. huxleyi* biomass (Fig. 3.5b, marked with triangular symbol) and obtained from: 1) values reported by Stockwell *et al.* (2001) for September 1997 and 2) samples of 31 July 1998 obtained by the T/V Oshoro Maru in areas of white waters. The latter

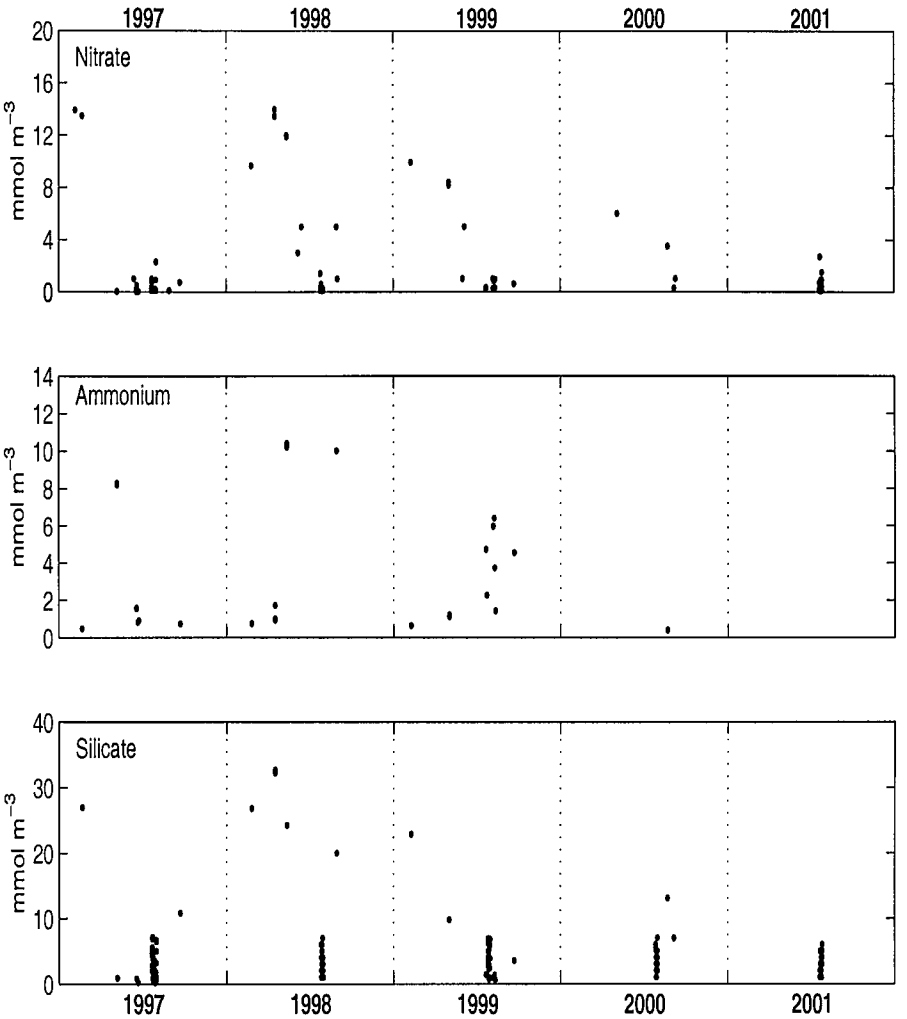

Figure 3.4: Nutrient data collected in the Bering Sea middle shelf region around station M2.

were analysed by preserving the samples in buffered formalin and counted in settled samples. An additional data point is also included in the flagellates' plot (Fig. 3.5c, triangular symbol). This was obtained from samples of 31 July 1998 on the T/V Oshoro Maru and estimating the biomass by using actual cell sizes.

In order to compare cell counts with model results (in nitrate or carbon units), time-invariant carbon content of $10\,\mathrm{pg\,cell^{-1}}$ has been assumed for *E. huxleyi* (Holligan *et al.*, 1983; Balch *et al.*, 1992). For other groups, counts have been converted into biovolume first by assuming a mean diameter of $3\,\mu$m for flagellates and $30\,\mu$m for diatoms. The general protist plankton conversion equation of Menden-Deuer & Lessard (2000) was then used for the volume to carbon conversion, $\mathrm{C} = 0.216\,\mathrm{V}^{0.939}$, where C is the carbon content per cell in pg and V is the biovolume in $\mu\mathrm{m}^3$. It is

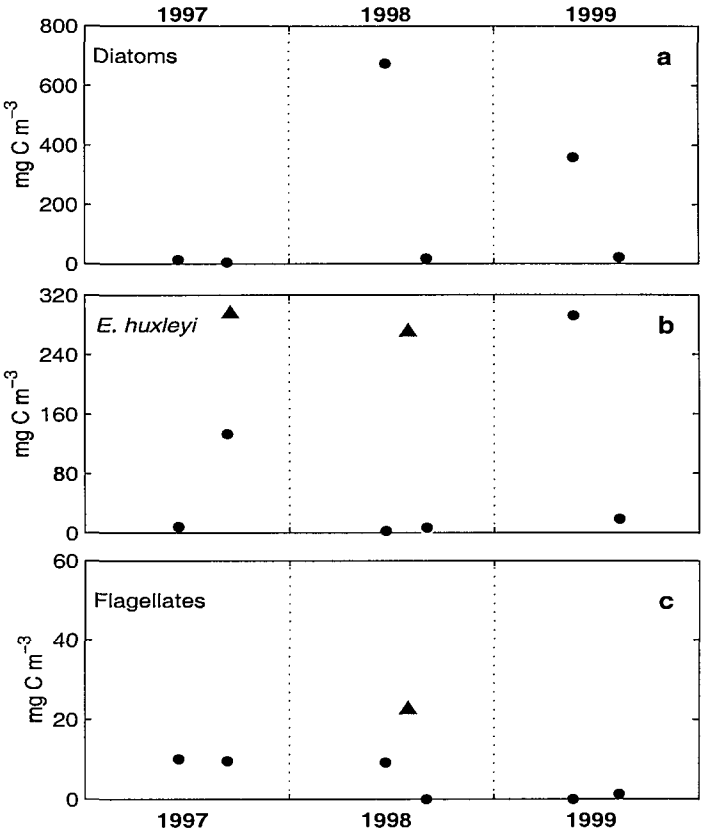

Figure 3.5: Phytoplankton data collected in the Bering Sea middle shelf region around station M2 (dots). E. huxleyi value of 1997 (triangle) are after Stockwell *et al.* (2001). E. huxleyi and Flagellates values of 1998 (triangles) were obtained by T/V Oshoro Maru samples collected in areas of bright waters.

worthwhile to keep in mind that such cell number to biomass conversion is only an approximation and comparisons of these data with model results cannot be considered in absolute terms.

Estimates of mesozooplankton biomass (preserved wet weight) were also obtained from T/V Oshoro Maru public reports (Anonymous, 2002). Over the length of the time series considered here (1995-2001), sampling in the Bering Sea began in early June and ended in early August. The samples were collected with 45 cm mouth diameter NORPAC nets (with a 0.33 mm mesh) towed vertically from 150 m or near bottom (estimated by wire angle) to the surface at about 1 m s^{-1}. Flowmeters mounted inside the net mouth were annually calibrated using vertical tows at several ocean stations. Only samples from the southeastern middle shelf stations (at water depths between 60 and 10 m) have been considered here. Samples that data reports noted as biased by predominance of taxa with high water content (e.g. salps) or

calcareous materials (coccolithophores) have been excluded. Wet weight has been converted into carbon units by assuming a zooplankton water content of 83% and a carbon to ash-free dry weight ratio of 0.45, which gives a carbon to wet weight relationship of 0.092 (see, for example, Table 1.5b in Raymont, 1983). Data are shown in Figure 3.6.

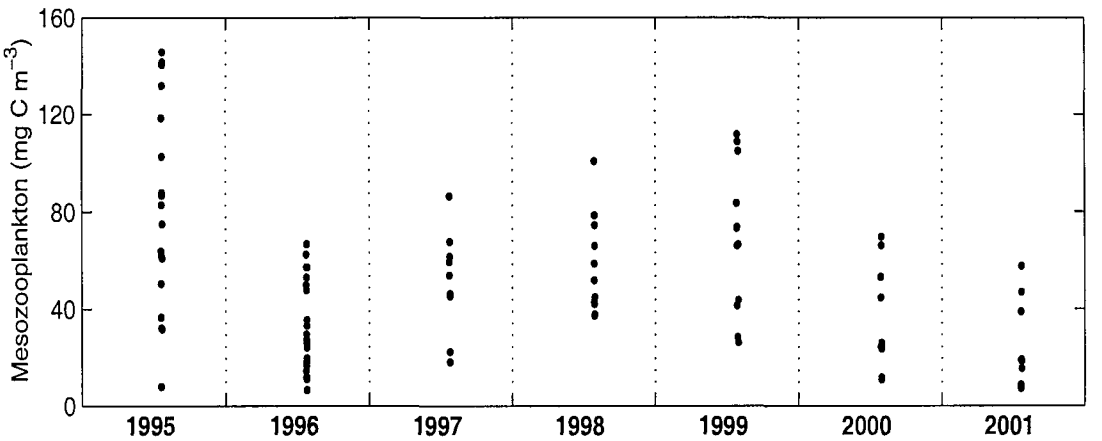

Figure 3.6: Mesozooplankton biomass relatively to the southeastern middle shelf region of the Bering Sea.

3.3 Satellite-derived information

The first satellite instrument to detect an *E. huxleyi* bloom was the LAND remote-sensing SATellite (LANDSAT) in 1977 (Le Fevre *et al.*, 1983). Since then, several other instruments have been used to look for these blooms (see Table 3.1). However, the best results have been probably obtained with the Coastal Zone Color Scanner and the Advanced Very High Resolution Radiometer (AVHRR), at least before SeaWiFS and other high-resolution colour sensors were launched. Another pioneering satellite work, where a coccolithophore bloom shown by CZCS was confirmed by *in situ* observations, was published later by Holligan *et al.* (1983).

In order to study the history of *E. huxleyi* blooms in the Bering Sea before 1997, CZCS and AVHRR archive images have been obtained. Bright water occurrences and chlorophyll concentration from 1997 to 2001 have been obtained from SeaWiFS imagery.

Table 3.1: Satellites used for *E. huxleyi* bloom observation (after Tyrrell & Merico, 2003).

Acronym	Full name	Dates of operation	Number of visible bands	Resolution (km)	Radiometric sensitivity[a] (W m^{-2} st^{-1} μm^{-1})
LANDSAT[b]	LAND remote-sensing SATellite	1972 - still operating	3	0.03	0.9-1.0
CZCS	Coastal Zone Color Scanner	1978 - 1986	4	18[c]	0.166
AVHRR	Advanced Very High Resolution Radiometer	1978 - still operating	1	4[c]	S:N=9:1 at 5% albedo
OCTS	Ocean Color and Temperature Scanner	08/1996 - 06/1997	6	0.7	0.091
SeaWiFS	Sea viewing Wide Field of view Sensor	1997 - still operating	6	4.5 or 9[c]	0.043
MODIS	MODerate resolution Imaging Spectroradiometer	1999 - still operating	10	1 or 5[c]	0.019
MERIS	MEdium Resolution Imaging Spectrometer instrument	2002 - still operating	8	1 or 5[c]	0.016

[a]The radiometric sensitivity represents the smallest radiance which can be detected by certain channel. The values here reported are relative to a waveband centered at about 550 nm (Adapted from IOCCG, 1999). It should be noted that the radiometric sensitivity for LANDSAT-7 is reported here (see NASA's LANDSAT-7 Users Handbook at `http://ltpwww.gsfc.nasa.gov/IAS/handbook/handbook_htmls/chapter8/chapter8.html`) in terms of Relative Spectral Response (unitless) and for AVHRR channel 1 (see http://www2.ncdc.noaa.gov/docs/klm/html/c3/sec3-1.htm) in terms of Signal to Noise ratio (S:N) at 5% albedo.

[b]There have been several generations of LANDSAT sensors. LANDSAT-1 started its operation in 1972 and ended in 1978. The last one, LANDSAT-7, was launched in 1999.

[c]The resolution of images frequently examined for the presence of coccolithophore blooms, rather than the maximum resolution of the instrument (e.g. see Fig. 3 in Brown & Yoder, 1994).

3.3.1 CZCS and AVHRR pre-1997 data

An early satellite work on *E. huxleyi* blooms involved the development of an automatic technique to scan CZCS images for the presence of coccolithophore blooms (Brown & Yoder, 1994). CZCS images were rather low resolution (each individual pixel corresponded to about 18x18 km^2 of the Earth's surface, see Table 3.1) but CZCS's global coverage allowed the construction of a global map of where *E. huxleyi* blooms occur (Brown & Yoder, 1994). The global map of Brown & Yoder (1994) revealed that patches of water possessing spectral characteristics indistinguishable from *E. huxleyi* were evident in the eastern Bering Sea (this map is here reported in Fig. 6.3a), in contradiction with several years of sea surface measurements over the period. The same automatic technique has been used in this study but concentrating the analysis only to the Bering Sea region and checking visually all the scenes which were automatically identified as containing *E. huxleyi* blooms. One hundred and seventy-seven daily composites of normalized water-leaving radiances (*nLw*) at 440, 520, 550 nm from CZCS dating from 1978 to 1986 were examined for the presence of *E. huxleyi*. Scenes with excessively high aerosol content or cloud cover were excluded during initial browsing.

AVHRR data for the months of June to October (inclusive) from 1987 to 1996 were obtained from the NOAA Satellite Active Archive, and processed using software developed by Plymouth Marine Laboratory (Groom & Holligan, 1987). AVHRR raw visible and infra-red channels 1 and 2 were converted into 'remote sensing' reflectance. An average of three daily AVHRR scenes for the period from June to October were inspected for all the years between 1987 and 1996 (i.e. approximately 4,500 scenes in total). Winter months have been neglected because, as explained in section 1.4, *E. huxleyi* blooms are not expected in this period at these latitudes.

Table 3.2: Monthly occurrences of *E. huxleyi* blooms in the southeastern Bering Sea region from 1997 to 2001.

	1997	1998	1999	2000	2001
January	no	no	no	no	no
February	no	no	no	no	no
March	no	no	no	no	no
April	no	no	no	no	no
May	no	no	no	no	no
June	no	no	no	no	no
July	YES	YES	no	no	no
August	YES	YES	YES	YES	no
September	YES	YES	YES	YES	no
October	YES	YES	YES	YES	no
November	no	no	no	no	no
December	no	no	no	no	no

3.3.2 SeaWiFS bright waters: 1997-2001

In addition to *in situ* measurements of phytoplankton abundance at different period of the years, true-colour SeaWiFS imagery has been used to derive the seasonal occurrence of bright waters and to relate them to *E. huxleyi* blooms for the period from 1997 to 2001. It must be stressed that bright images shown by satellite pictures do not necessarily reflect an ongoing bloom of *E. huxleyi* (Broerse *et al.*, 2003). Moreover, bright waters are usually associated with the late stage of the bloom (Holligan *et al.*, 1993a) when nutrient stresses cause the cells to overcalcify (Paasche, 2002). Effectively, in the Bering Sea a strongly isolated upper layer (i.e. shallow depth of mixing) during summer may well have contributed to keep coccoliths in suspension for a long time and thus mimicking a long-lasting bloom. However, despite these caveats, there is evidence (see Fig 3.5 but also Olson & Strom, 2002) that the bright waters shown by SeaWiFS in the Bering Sea in late summer and early autumn do possess high concentrations of living cells. The monthly occurrences of *E. huxleyi* blooms have been inferred from the true-colour SeaWiFS composites (Fig. 1.6) and summarised in Table 3.2. It is reiterated that bright waters in the early times of the years are not considered to be *E. huxleyi* blooms here for the reasons discussed in section 1.4

3.3.3 SeaWiFS chlorophyll: 1997-2001

Chlorophyll has been derived from the 8-day composites of SeaWiFS data (from September 1997 to 2001). Satellite data offer a wide coverage and give an integrated estimate of this variable for the whole southeastern Bering Sea shelf, cloud cover permitting. Data are reported in Fig. 3.7.

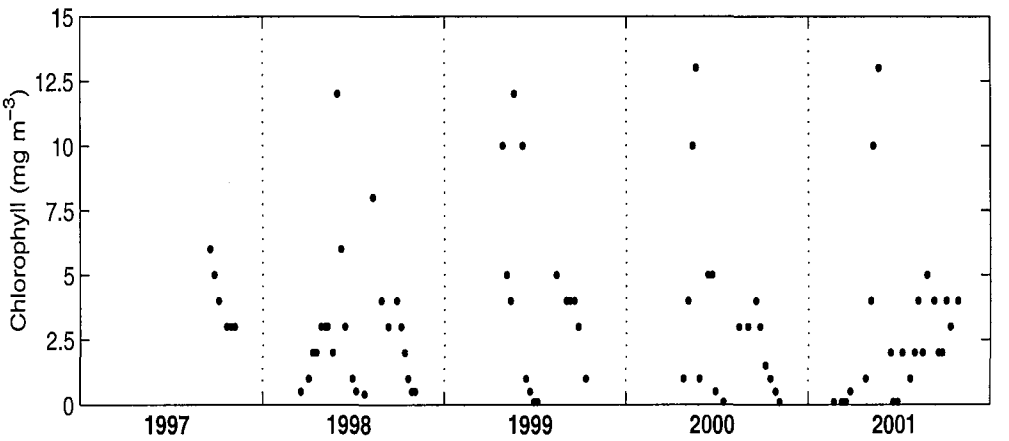

Figure 3.7: SeaWiFS-derived chlorophyll data of the southeastern middle shelf region of the Bering Sea, in the vicinity of station M2. It should be noted that high reflectance waters are excluded from the satellite determination of chlorophyll.

3.3.4 SeaWiFS calcite: 1997-2000[1]

Daily SeaWiFS normalized water leaving radiances data were utilized in order to obtain estimates of calcite concentrations during *E. huxleyi* blooms in the Bering Sea (1997-2000). The radiance data were processed with the SeaWiFS Data Analysis System (SeaDAS) software (Baith *et al.*, 2001) according to the coccolithophore detection algorithm proposed by Gordon *et al.* (2001). The essence of this algorithm is to minimize the influence from the absorption by chlorophyll and dissolved organic material in the visible channels in Case 1 waters and to empirically relate the backscatter coefficient at 550 nm to calcite concentration. The algorithm, however, does overestimate calcite concentrations in Case 2 waters (Cokacar *et al.*, 2003),

[1]The raw data utilized in this subsection have been obtained from the NASA-Distributed Active Archive Center. Tulay Cokacar of the Institute of Marine Science of the Middle East Technical University, Turkey, kindly offered her expertise to process the data and produce the calcite concentrations.

such as the Bering Sea shelf waters. Therefore, although these data represent the best information that can be obtained in order to constrain the carbon chemistry routines, their significance must be carefully interpreted. Selected calcite data can be viewed in the next chapter in Fig. 4.12.

Chapter 4

Results

4.1 Introduction

The modelling studies have been accompanied by an investigation of archived satellite imagery (from 1978 to 1997) to establish the history of the presence of *E. huxleyi* in the Bering Sea. In this chapter, the results of the archived satellite image analysis are presented (published in Merico *et al.*, 2003a) along with the modelling results (submitted to DSR-I, Merico *et al.*, 2003b), the studies related to the high N:P hypothesis as a prerequisite for *E. huxleyi* success are reviewed, and the N:P survey of areas of the world ocean where satellite-detected *E. huxleyi* blooms occur is presented (submitted to LO, Lessard, Merico & Tyrrell, 2003).

4.2 *E. huxleyi* in the Bering Sea before 1997

Daily composites of CZCS imagery (1978-1986) were both inspected visually in true-colour and also categorised to coccolithophore bloom and nonbloom classes using the multispectral classification scheme of Brown & Yoder (1994). The classification method decides whether to assign a CZCS pixel to the *E. huxleyi* bloom class. The corresponding true-colour image was then visually inspected to check the result. Visual inspection was performed because it may identify incorrect results obtained

by the multispectral classification technique. Fig. 4.1 shows an example of this approach.

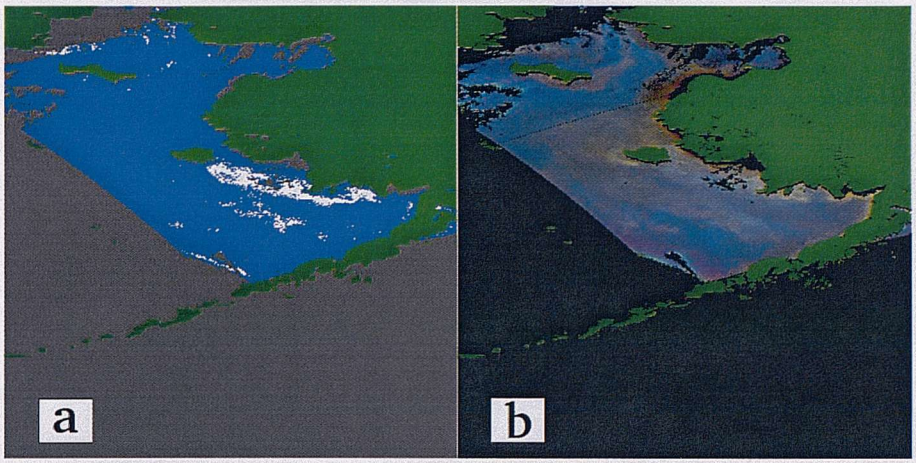

Figure 4.1: Example of CZCS image processing with the classification algorithm (a), compared with the true-colour image (b). White areas are pixels classified by the algorithm as coccolithophore blooms. Data taken by CZCS on 20 July 1980.

The histogram in Fig. 4.2 shows a summary of the results obtained with the automated classification algorithm applied to CZCS imagery. A '+1' value indicates that the algorithm detected an *E. huxleyi* bloom; '-1' indicates a negative response by the algorithm on the presence of the bloom; no bars for a certain month means no data available (during most days examined, clouds obscured large portions of the sea surface). Note that blooms were never detected among the available summer data (May and July '79, April and May '80, May '83, and March '84 were all found, upon visual inspection, to be false positives due to cloud-edge effects), with the sole exception of 20 July 1980. The results of the classification and the equivalent true-colour image for the 20 July 1980 are shown in Fig. 4.1. In this case, although the algorithm does detect a patch of bright water (Fig. 4.1a), from the true-colour image (Fig. 4.1b) it is not at all clear whether this is really an *E. huxleyi* bloom. Proximity of the high reflectance waters to the coastline suggests that suspended sediment is the cause.

The histogram in Fig. 4.2 shows several winter positives. It is unlikely, however, that *E. huxleyi* can bloom during the winter months at these high latitudes. Much more likely is that these winter-time 'blooms' are false positives generated

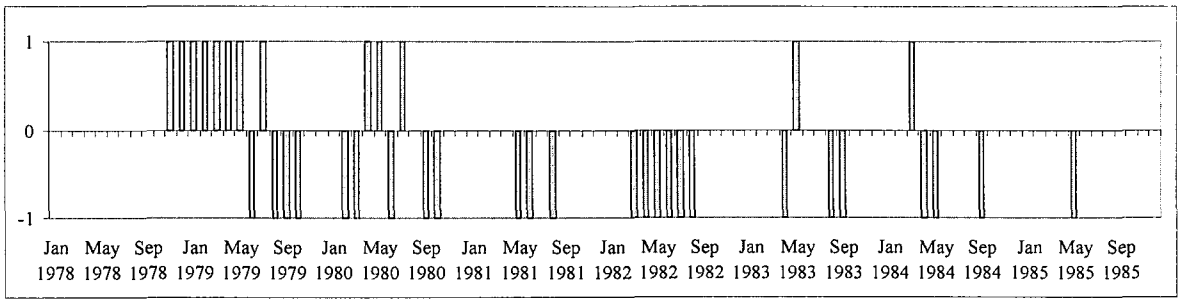

Figure 4.2: Histogram summarizing the results with CZCS. A '+1' value indicates that the algorithm detected an *E. huxleyi* bloom. '-1' indicates a negative response on the presence of a bloom by the algorithm. No bars for a certain date means no data available or no cloud-free images. All summer months, with the exception of July '80, have been visually ascertained to be false-positive due to cloud-edge effects.

by spectrally mimicking conditions, in particular the resuspension of empty diatom frustules (Broerse *et al.*, 2003)

From the data available and acknowledging the uncertainty related to the heavy cloud-cover in the area, this analysis indicates that there is no conclusive evidence from CZCS images for the presence of *E. huxleyi* blooms in the Bering Sea in the years between 1978 and 1986. The scattered white patches in the eastern Bering Sea that appear in the often used global climatology of *E. huxleyi* blooms (Brown & Yoder, 1994) are therefore the presence of conditions that the classification algorithm could not distinguish from actual *E. huxleyi* blooms.

In AVHRR imagery, no evidence for blooms was found in any year except 1996. Indeed, the "footprint" of *E. huxleyi* is evident from August 1996 and, quite strikingly, lasts until the middle of October 1996. It is worthwhile to note that while most days were cloudy, preventing conclusive evidence of the absence of *E. huxleyi* in the area, yet the experience of 1997-2000 is that the blooms in this area persist from three to four months, and so they should be detectable even if there were only a few cloud-free days during the summer.

In Fig. 4.3 the temporal and spatial structure of the small bloom taking place in summer 1996 in the Bering Sea shelf, just south of St. Matthew Island (see Fig. 1.1), is shown. The fact that the bright patch in the image is a bloom is plausible for at least three reasons: 1) its location is in the centre of the bloom area 1997-2000;

2) it persists for at least two months, as did the larger blooms in following years; and 3) it occurs at the same time of the year as the other blooms. A check of the equivalent scene recorded by the AVHRR infrared channel assures that those bright patches are not clouds.

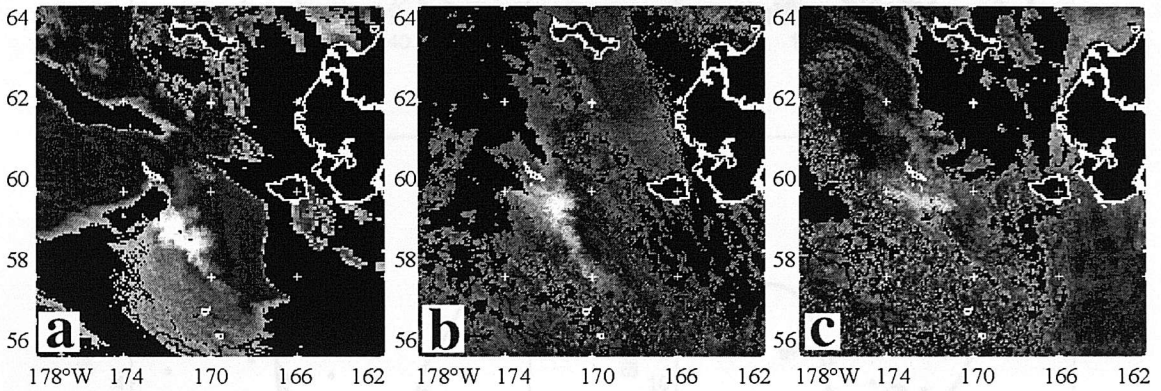

Figure 4.3: Coccolithophore bloom on the Bering Sea shelf in summer 1996. The AVHRR pictures show the persistence of the bloom (to the south of St. Matthew Island) for more than a month: a) 26 August, b) 18 September, and c) 3 October.

In summary, CZCS and AVHRR archive image analysis suggests that no appreciable *E. huxleyi* activity can be inferred from 1978 to 1995. However, a small bloom is clearly evident in the year 1996, which has not been documented before. This suggests that *E. huxleyi* increased its activity in the area gradually rather than abruptly (as erroneously suggested by Napp & Hunt Jr, 2001).

4.3 Modelling studies

The strategy adopted for the modelling studies consisted of two steps. With the first step, the model has been "calibrated" by running it in conditions antecedent to the year 1995 (i.e. without *E. huxleyi*). In the second step, the main simulation (or standard run) is implemented by including *E. huxleyi* as state variable and by examining the years from 1995 to 2001.

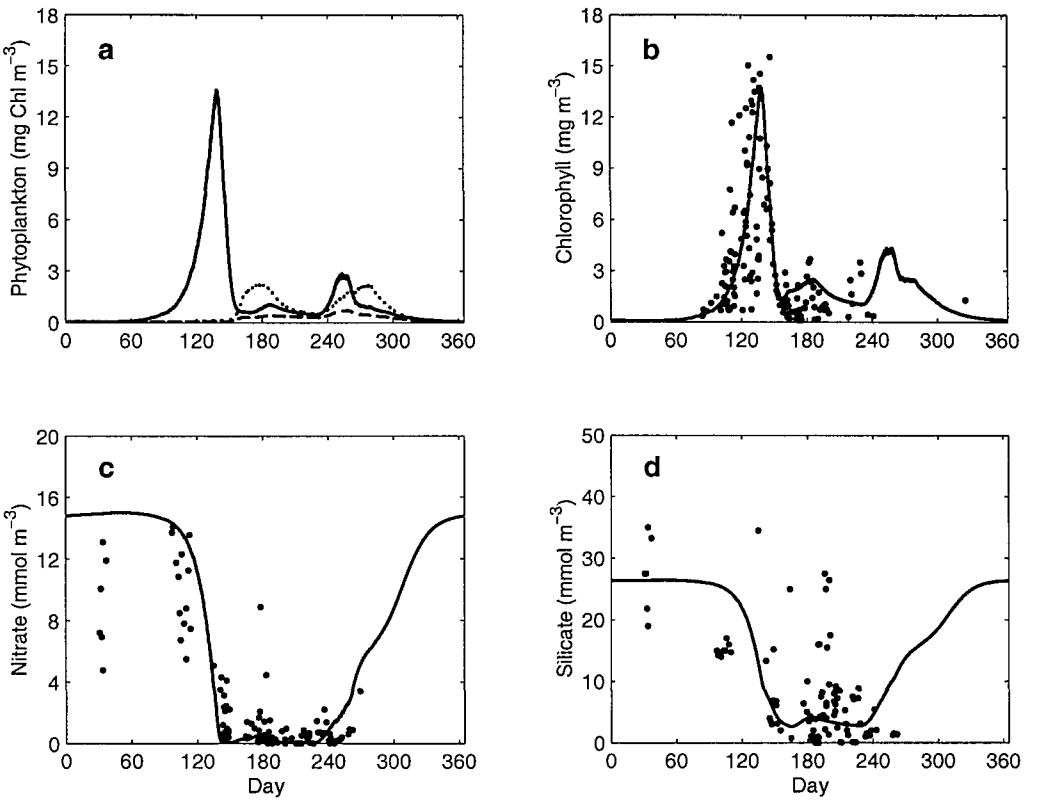

Figure 4.4: Calibration run. Outputs obtained with forcing conditions prior to 1995 (*E. huxleyi* is not included into the model). The plots show: a) modelled phytoplankton seasonal succession following the sequence of diatoms (solid line), flagellates (dotted line) and dinoflagellates (dashed line) and b) simulated total chlorophyll, c) nitrate and d) silicate (continuous lines) as compared with WOD98 data (dots). See text for discussion.

4.3.1 Model calibration

A calibration run has been provided without *E. huxleyi* in order to explore the model behaviour with respect to the seasonal succession patterns and other aspects of the ecosystem observed before the increased *E. huxleyi* activity (i.e. before 1996). Parameters for this run are reported in Table 2.1. The forcing functions for this case (SST, MLD, PAR) are extrapolated from the average functions that have been affecting the ecosystem in the last 20 years (before 1995). The model results are compared with multi-year composites of observations for the variables available in Fig. 4.4. The observations are obtained from the WOD98, as described in chapter 3. The extra grazing pressure on diatoms by microzooplankton when silicate becomes depleted ($< 3\,\mu$M) is also taken into account in this run because such a condition has been suggested in the Bering Sea in the past (Goering & Iverson, 1981).

The model reproduces the typical nutrient seasonal cycles (Fig. 4.4c and Fig. 4.4d). The typical Bering Sea shelf characteristic of a pronounced diatom spring bloom (Goering & Iverson, 1981; Sukhanova *et al.*, 1999) is also predicted (Fig. 4.4a). The autumn diatom peak produced in the simulation is also characteristic of the area, as reported by Sukhanova *et al.* (1999). The deepening of the mixed layer depth at the end of summer provides by entrainment nutrient resources to the best competitors in conditions of declining PAR and weakening of water column stability. Diatoms are the fastest growers in the model (and in reality, see for example Furnas, 1990; Egge & Aksnes, 1992). The general result of phytoplankton succession (Fig. 4.4a), diatoms-flagellates-dinoflagellates, is in agreement with the most common sequence observed in the area and described by Sukhanova *et al.* (1999). Total chlorophyll also compares well with the WOD98 data (Fig. 4.4b).

4.3.2 Main simulation

The standard run (SR), i.e. the run that best fits the data available from 1995 to 2001, and gives the best predictions in terms of phytoplankton succession is presented in this section. Fig. 4.5a shows modelled total chlorophyll compared with SeaWiFS-derived data. All the data are compilations of observations carried out within a reasonable distance from station M2 and representative of the southern middle shelf domain. The simulated seasonal succession is shown in Fig. 4.5b. The black horizontal line represent periods when *E. huxleyi* blooms were seen in satellite images. This information has been obtained from the duration of bright waters seen in monthly-composites of SeaWiFS true-colour images (see Fig. 1.6 and Table 3.2). The concentration of free coccoliths in the model follows that of *E. huxleyi*, but with a slight time lag (Fig. 4.5c). Nitrate and silicate seasonal cycles are reported in Figs. 4.5d and 4.5e, respectively. The model results compare well with chlorophyll (Fig. 4.5a) and nutrient data (Figs. 4.5d and 4.5e).

Modelled mesozooplankton is presented in Fig. 4.6 as compared with biomass data. The misfit between simulated mesozooplankton and data may be due to

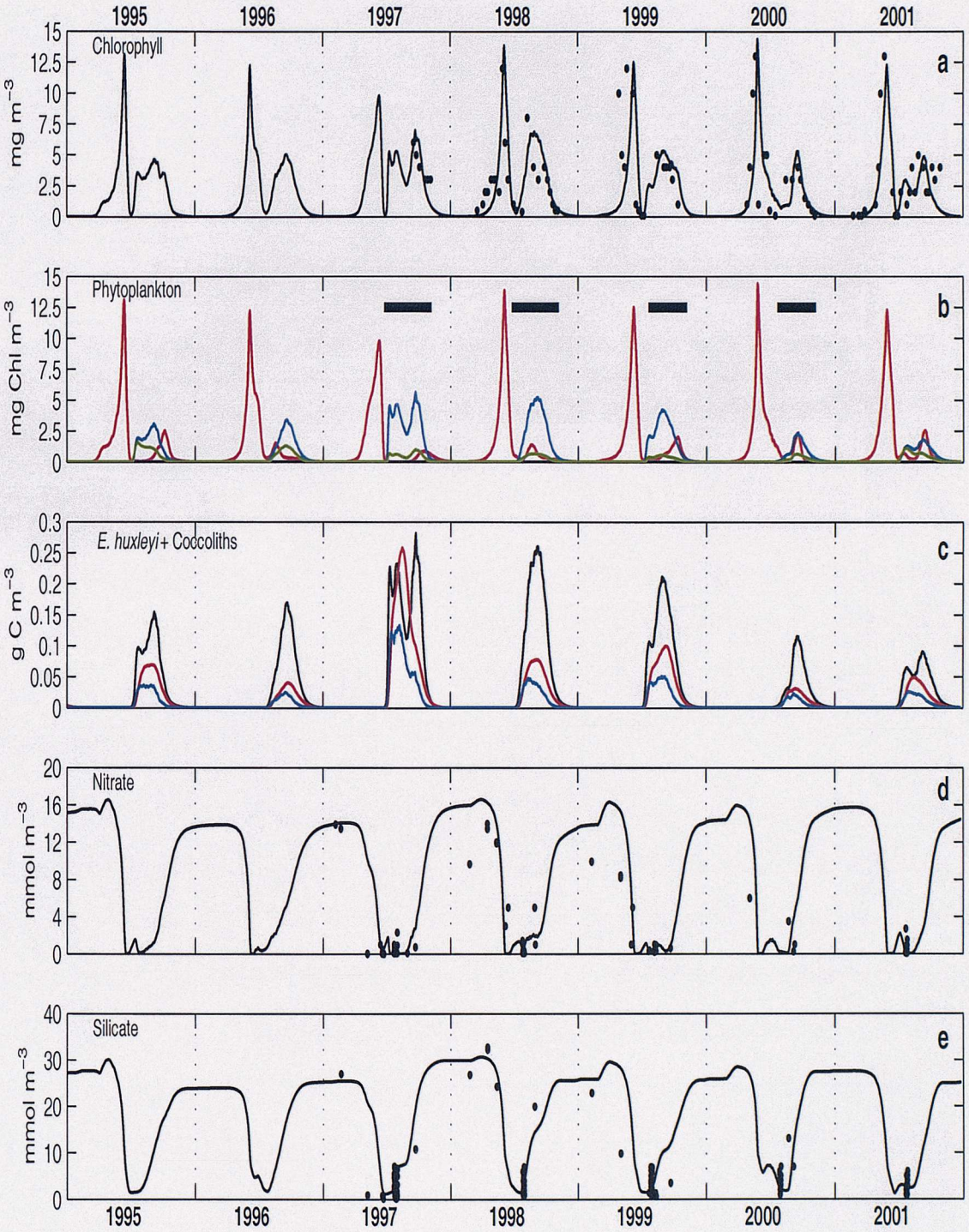

Figure 4.5: Standard run. a) Modelled total chlorophyll (solid line) as compared with SeaWiFS-derived chlorophyll (symbol); b) phytoplankton succession with diatoms represented by red line, *E. huxleyi* by blue line and flagellates by green line, and with horizontal black line indicating the duration of *E. huxleyi* blooms as observed in SeaWiFS true-colour images; c) *E. huxleyi* concentration (black line) as compared with attached coccoliths (blue line) and free coccoliths (red line), d) modelled nitrate cycles (solid line) as compared with data (symbol); and e) silicate cycles (solid line) as compared with data (symbol).

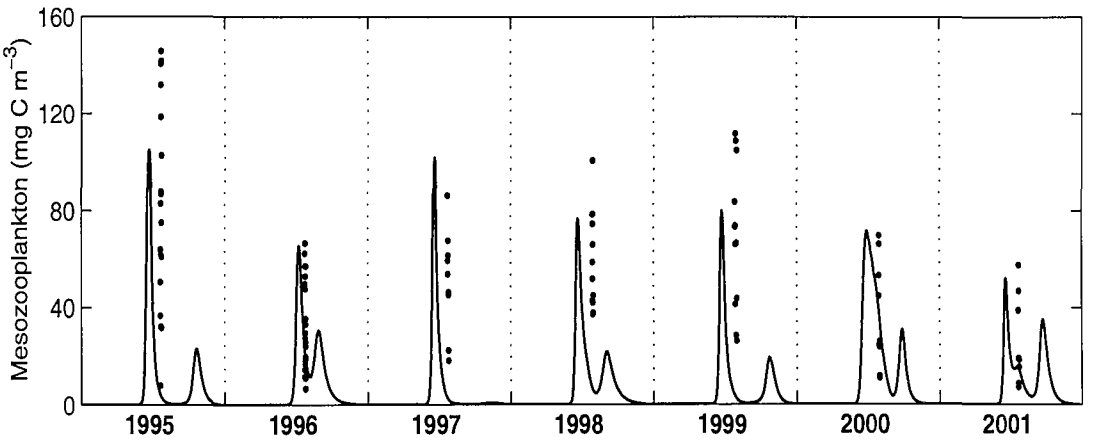

Figure 4.6: Standard run. Modelled mesozooplankton (solid line) as compared with zooplankton biomass data (symbol). Biomass data, originally in wet weight, have been converted into carbon units by assuming a carbon to wet weight relationship of 0.092 (see subsection 3.2.2 for details).

different reasons. Given that the data are a compilation of samples taken over the southern middle shelf domain and during a limited period (from one to two weeks), patchiness may likely be the main explanation for this misfit. Uncertainties in the wet weight to carbon conversion, however, may also account for the differences in the maximum concentrations.

Simulated and observed phytoplankton abundance (data only available for the period 1997-1999) are shown in Fig. 4.7. Note that very low *E. huxleyi* concentrations (68 cells mL^{-1}) were observed at the end of July 1998 (Fig. 4.7b, circular symbol). This because sampling was carried out just outside the bright water patch, on the spot marked by the red dot in Fig. 2.1a. The lack of fit in 1999 between modelled *E. huxleyi* and data is also due to patchiness, indeed sampling in July 1999 was carried outside the bright waters (Zeeman, personal communication). However, simulated *E. huxleyi* bloom timing and duration agrees well with observed SeaWiFS temporal patterns (represented with a black bar in Fig. 4.5b).

A low *E. huxleyi* concentration in the years 1995 and 2001 is not however reproduced by the model. Although *E. huxleyi* cells have been found in the area since the early '90s (but always lower than 1,000 cells L^{-1}, Flint, unpublished observations), the model does overestimate those observations. Despite this, the model gives strong

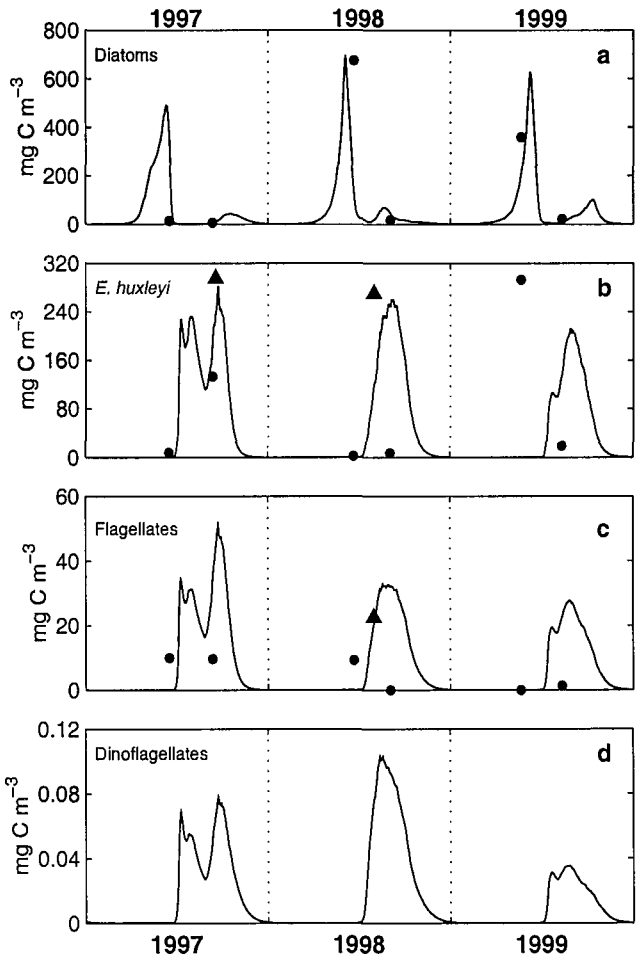

Figure 4.7: Standard run. Phytoplankton abundances as compared with data. Note that in order to compare cell counts with model results (in carbon units), time-invariant carbon content has been assumed for *E. huxleyi*. For other groups, counts have been converted into biovolume first and then into carbon by using the method of Menden-Deuer & Lessard (2000). Note that no data are available to compare dinoflagellates with model results.

suggestions as to the possible causes for *E. huxleyi* massive bloom in the Bering Sea in 1997, as it is evident from the results of the following simple experiment. The model has been run as in the SR configuration from 1995 to 2001 but by forcing the year 1997 with functions (SST, MLD, PAR and wind speed) characteristic of the colder 2001 year (Fig. 3.3). Fig. 4.8b shows the results of this experiment as compared with the SR (Fig. 4.8a) for the year 1997. *E. huxleyi* population and coccolith concentrations would be dramatically reduced if 1997 would have been a year with a climatic forcing typical of a cold year like 2001 (Fig. 4.8b).

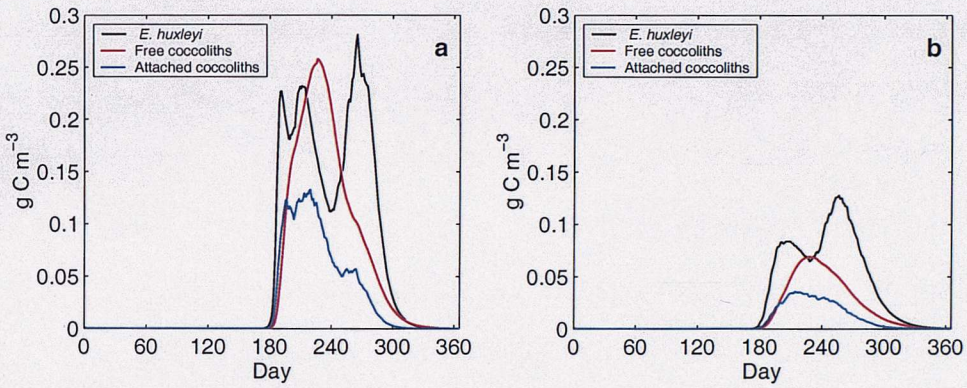

Figure 4.8: Snapshots of 1997 *E. huxleyi*, attached and free coccolith concentrations (solid, dashed and dotted lines respectively) as obtained a) in the SR configuration; and b) by forcing 1997 with functions typical of a cold year (i.e. 2001).

4.3.3 Phytoplankton impact on carbonate system

In subsection 1.5.6, the importance of the calcite saturation state on calcifying organisms and in particular on *E. huxleyi* was discussed. There is a strong relationship between both calcite and aragonite saturation states and temperature (Opdyke & Wilkinson, 1990, 1993) and each exhibits systematic variation with latitude (see for example Fig. 1.8). In equatorial regions (0° - 15°) saturation values are depressed relative to this correlation[1] (Fig. 1.8), but toward higher latitudes, temperature and carbonate saturation decrease more or less linearly. The underlying question relevant to this study is: could the unusually high SST of summer 1997 in the Bering Sea shelf have produced a higher than usual calcite saturation state? And if so, how

[1]Lower saturation state in equatorial regions is due to higher rainfall, lower rates of evaporation, and, in some areas, higher concentrations of CO_2 because of upwelling of deeper waters (Broecker & Takahashi, 1984).

might such a higher degree of saturation impacted on *E. huxleyi* success?

Given the novelty of the subject (it is the first time that the seasonal dynamics of the calcite saturation state has been investigated in relation to *E. huxleyi* abundance and its success), and due to the fact that there are only limited carbon chemistry data available to compare the model with, the results presented in this section are to be considered preliminary. However, the calcite saturation state depends mainly on the carbonate ion concentration, which in turn, is driven by DIC and alkalinity, at least to a first order approximation (see equation 2.1). Seasonality in phytoplankton growth impacts on DIC. Alkalinity, on the other hand, is not affected to a great degree by the processes of photosynthesis and respiration (see subsection 2.2.5). The remaining important factors impacting on the calcite saturation state are the carbonate speciation changes with temperature and salinity changes. The model is well constrained with temperature and the phytoplankton growth dynamics are also well captured, as shown above. The following results can be therefore considered realistic.

Carbonate system in the Bering Sea prior to *E. huxleyi* arrival

A typical phytoplankton spring bloom in the Bering Sea (Fig. 4.9a, red line) before the arrival of *E. huxleyi* (i.e. before 1997) would cause a ten-fold depletion of surface nitrate to less than $1\,\mu$M nitrate (Fig. 4.4c) and about $85\,\mu$M (5%) drawdown of DIC (Fig. 4.9a, black line). Such a change in DIC impacts on $[CO_3^{2-}]$ (the concentration of carbonate ion) by raising this variable by about 50% above its winter value (Fig. 4.9c). The degree of saturation state of calcium carbonate (Ω_{cal}) increases concomitantly, from about 2.5 (typical winter value) to about 3.5 (Fig. 4.9d).

Seasonal overturn of the water column in September evidently restocks both the pools of nitrate (Fig. 4.4c) and DIC (Fig. 4.9a, black line), when the winter light limitation halts the autumn bloom of 3-4 mg Chl m^{-3} (Fig. 4.9a, red line). In the absence of calcifying organisms, pCO_2 in seawater will remain undersaturated

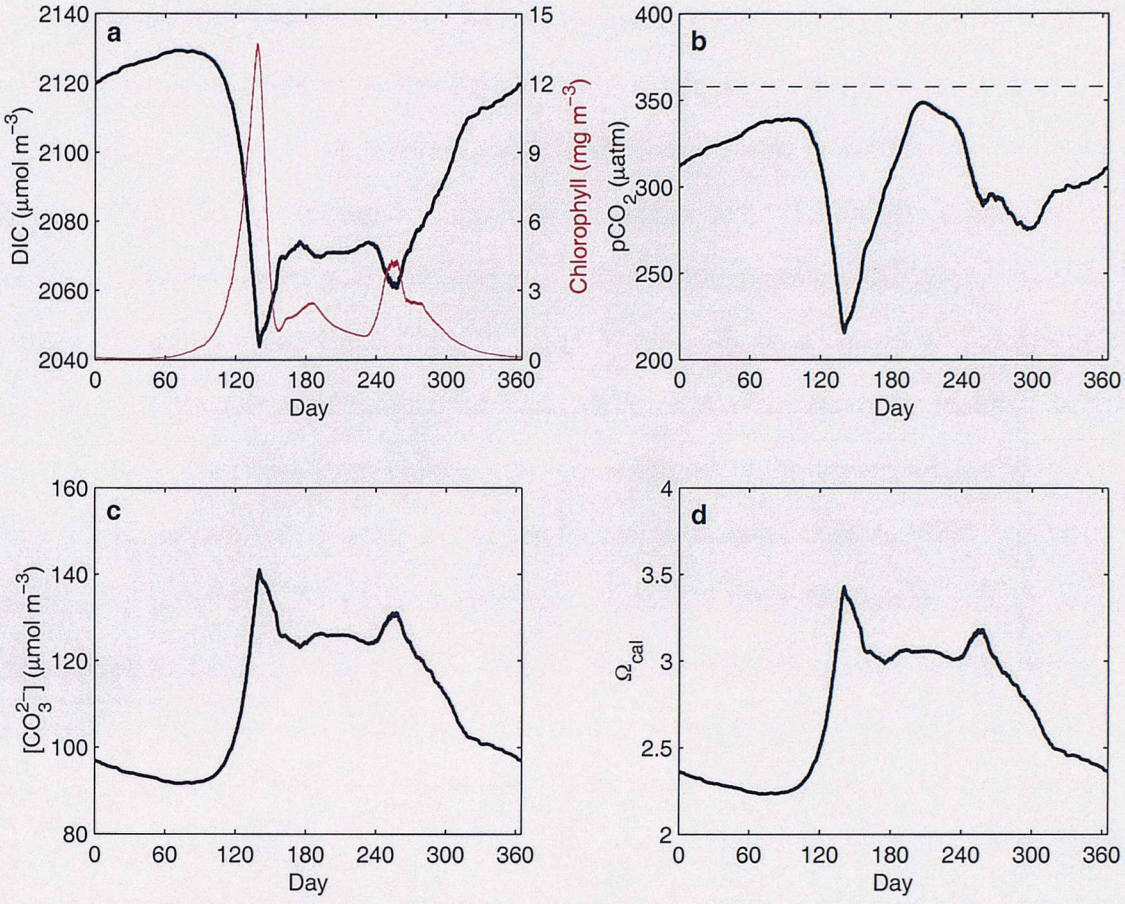

Figure 4.9: Seasonal cycles of carbonate variables in the Bering Sea before the arrival of *E. huxleyi*. a) DIC (black line) and total chlorophyll (red line); b) seawater pCO_2 (solid line) and pCO_2 in air (dashed line); c) carbonate ion concentration and d) calcite saturation state

throughout the year with respect to pCO_2 in air (Fig. 4.9b), as expected at these latitudes (Takahashi *et al.*, 1993).

The described DIC and pCO_2 dynamics predicted by the model are consistent with the general understanding of carbon cycling at high latitudes (Takahashi *et al.*, 1993) and agree very well with the earlier numerical analysis of carbon cycling in the southeastern Bering Sea done in the past by Walsh & Dieterle (1994). The seasonal variations of $[CO_3^{2-}]$ and Ω_{cal} in high latitude waters have not previously been calculated.

Carbonate system with *E. huxleyi*

The arrival of *E. huxleyi* in the Bering Sea caused a perturbation to the carbonate system with respect to non-*E. huxleyi* years. The model results suggest that the

intensive *E. huxleyi* bloom of 1997 caused seawater pCO_2 to become supersaturated with respect to atmospheric pCO_2 (Fig. 4.10d). Changes of this order of magnitude in pCO_2 have been observed in connections with these blooms (taking place at similar latitudes but different location) in the past (Holligan *et al.*, 1993a; Robertson *et al.*, 1994). The pCO_2 increase arises because, due to calcification, alkalinity decreases in 1997 of approximately $70\,\mu\mathrm{Eq\,kg^{-1}}$ (Fig. 4.10e). Such a decrease in alkalinity is in agreement with observations carried out during a bloom of *E. huxleyi* in the north Atlantic (see Fig. 13 in Holligan *et al.*, 1993a, where a drawdown in alkalinity of about $65\,\mu\mathrm{Eq\,kg^{-1}}$ is reported). Changes are also noticeable in DIC and other variables (Fig. 4.10). It appears, however, that the large change in SST (4-5 °C above climatological mean) in 1997 had no effect on the carbonate concentrations, contrary to what was hypothesised at the beginning of this study (see subsection 1.5.6). Indeed, this can be seen with a simple experiment, consisting of a run which does not include *E. huxleyi* in the ecosystem (Fig. 4.11). The higher SST of 1997 does not produce a higher calcite saturation state in 1997 with respect to other years. This experiment allows to decouple the effects that calcification and higher SST conditions have on the carbonate system and shows that yearly fluctuations in post-spring bloom carbonate ion concentrations appear more strongly connected to the intensity of the spring bloom rather than interannual SST variations (Fig. 4.11).

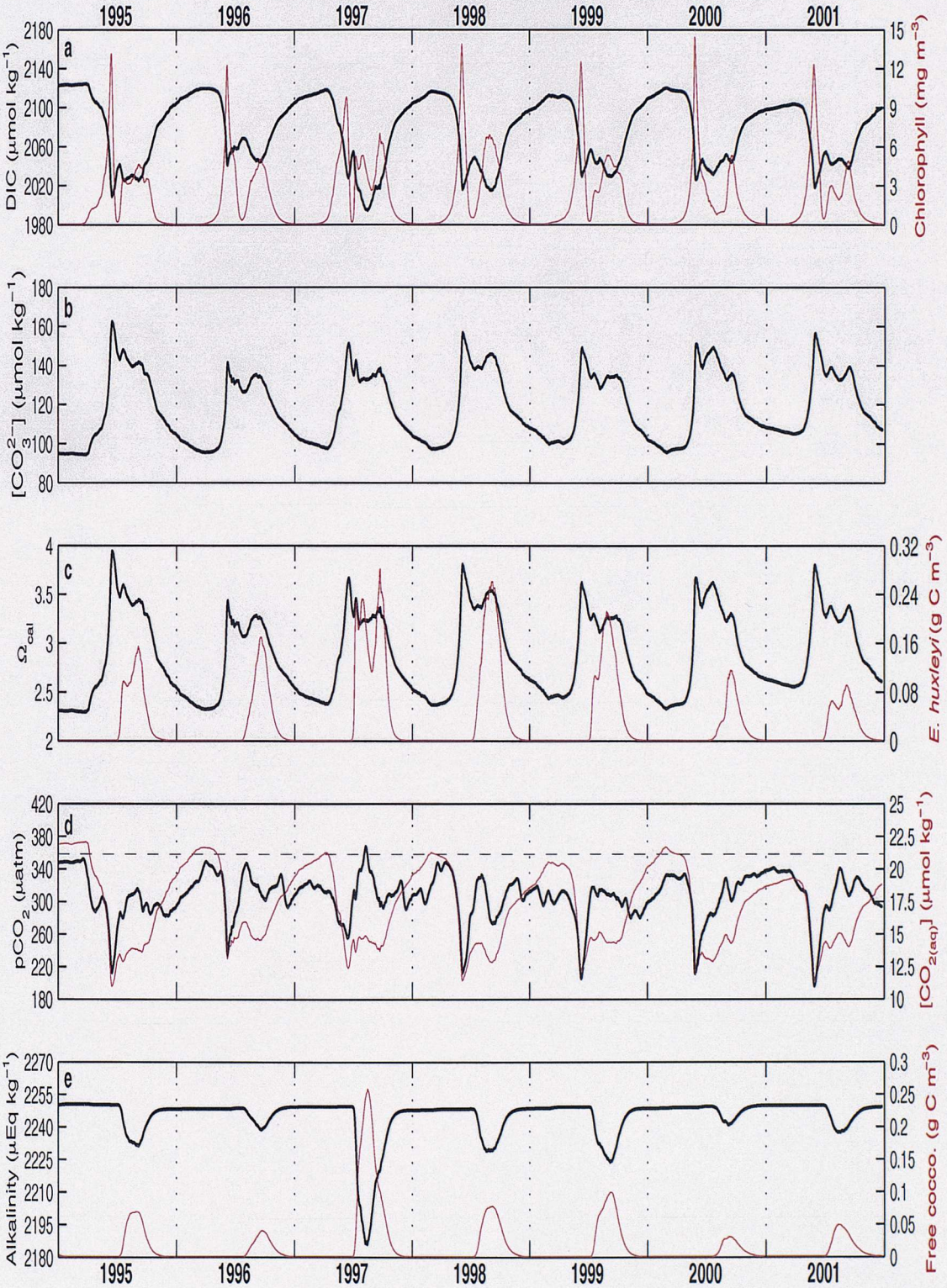

Figure 4.10: Modelled carbonate system variables from 1995 to 2001.

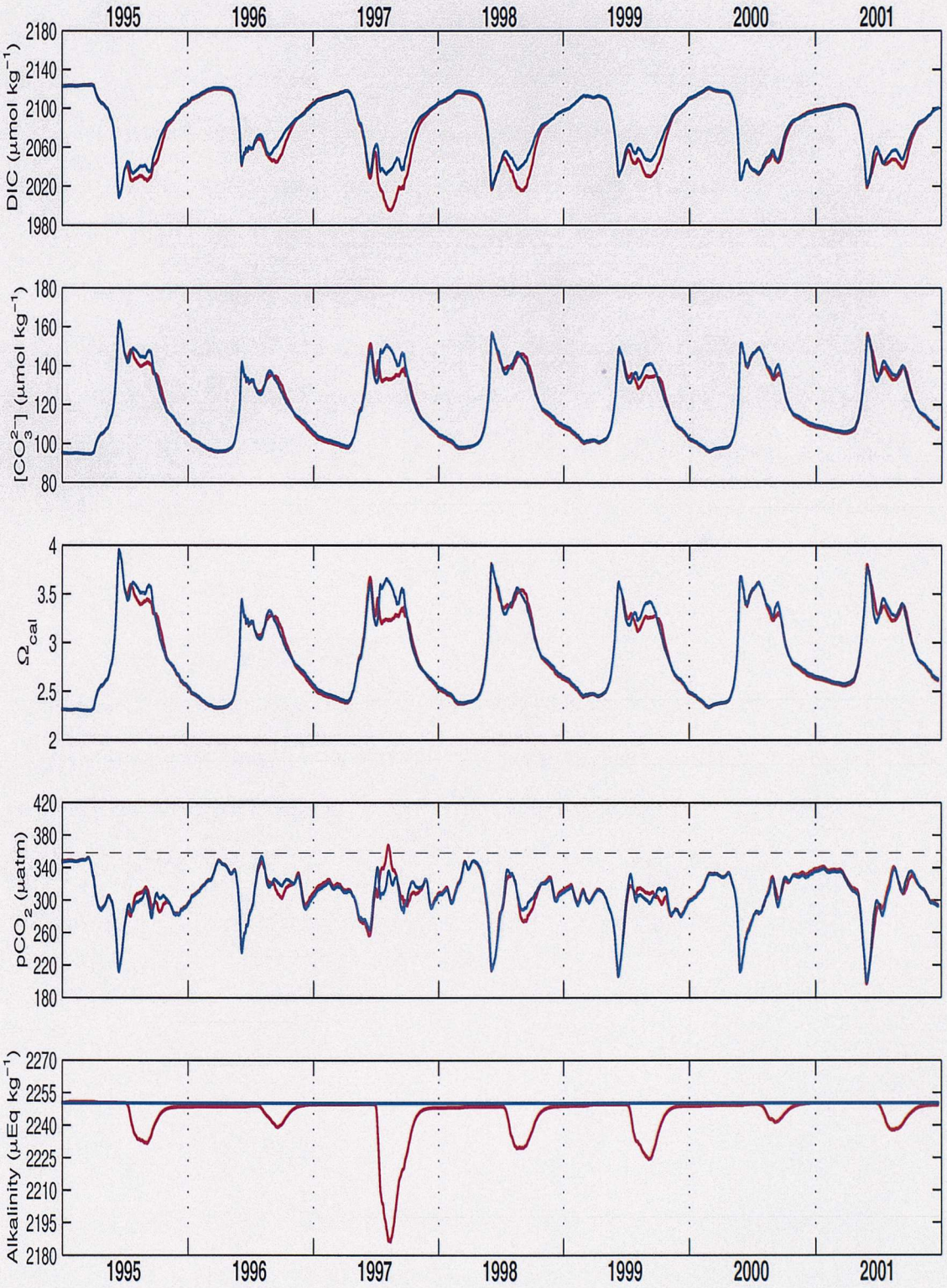

Figure 4.11: Modelled carbonate system variables from 1995 to 2001 with ecosystem including *E. huxleyi* (red) and with ecosystem not including *E. huxleyi* (blue). The dashed line in the pCO_2 plot represents the concentration of this variable in atmosphere.

Changes in alkalinity are mainly driven by the processes of calcification (i.e. the production of attached coccoliths), dissolution and upper to bottom box fluxes (see equation 2.26). Therefore, a good simulation of the process of production of attached coccoliths will result in a realistic prediction of alkalinity drawdown, provided that dissolution is negligible at the surface. However, since the details of how coccoliths are produced and afterward detached in nature are not fully understood (see subsection 2.2.4), it is a significant challenge to model these processes. The approach used here was to tune the amount of coccoliths produced in the model so that the concentrations of free coccoliths could fit reasonably well with the observations available (i.e. SeaWiFS-derived concentration of calcite). The satellite-derived concentrations of calcite for the summer periods from 1997 to 2000 are presented in Fig. 4.12. Coccoliths concentrations were also measured *in situ* in the Bering Sea on one occasion (September 1997) and a value of $0.1\,\mathrm{g\,C\,m^{-3}}$ was reported (Napp & Hunt Jr, 2001).

The model results of attached and free coccoliths for the year 1997 (shown in Fig. 4.13) are roughly consistent with the data just mentioned and also with observations carried out in the north Atlantic (see Fig. 6D in Holligan *et al.*, 1993a, where a value of about $0.2\,\mathrm{g\,C\,m^{-3}}$ is reported) and in the western English Channel (see Fig. 11A in Garcia-Soto *et al.*, 1995, where a value of about $0.3\,\mathrm{g\,C\,m^{-3}}$ is reported).

As for *E. huxleyi* abundances in 1995 and 2001, the model overestimates attached and free coccoliths. Moreover, attached and free coccoliths are probably underestimated by the model for the years 1998, 1999 and 2000. Possible explanations for these discrepancies are given in chapter 6.

An interesting result of this investigation is, however, that high concentrations of *E. huxleyi* are always coincidental with high calcite saturation state (see Fig. 4.10c). An ecological interpretation of this result is given in chapter 6.

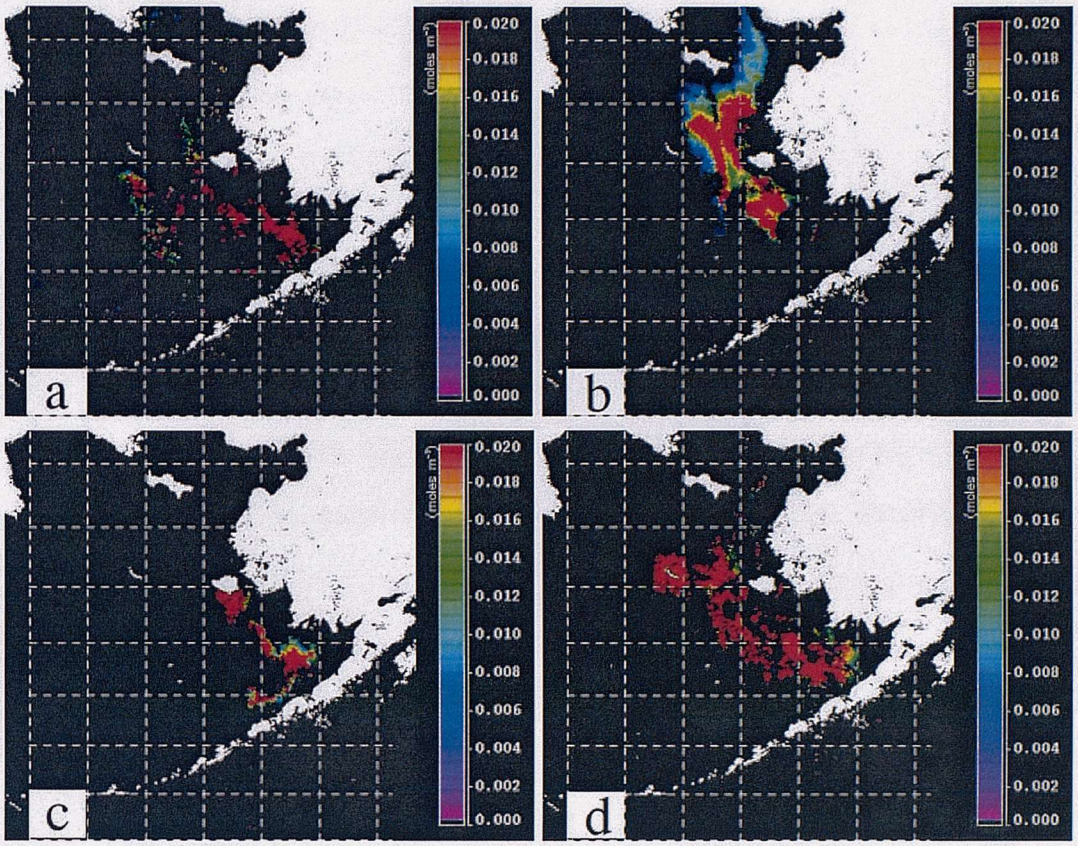

Figure 4.12: SeaWiFS-derived concentration of calcite (in $\mathrm{mol\,m^{-3}}$) for a) 16 September 1997, b) 20 July 1998, c) 11 September 1999 and d) 15 September 2000. Images produced by Tulay Cokacar.

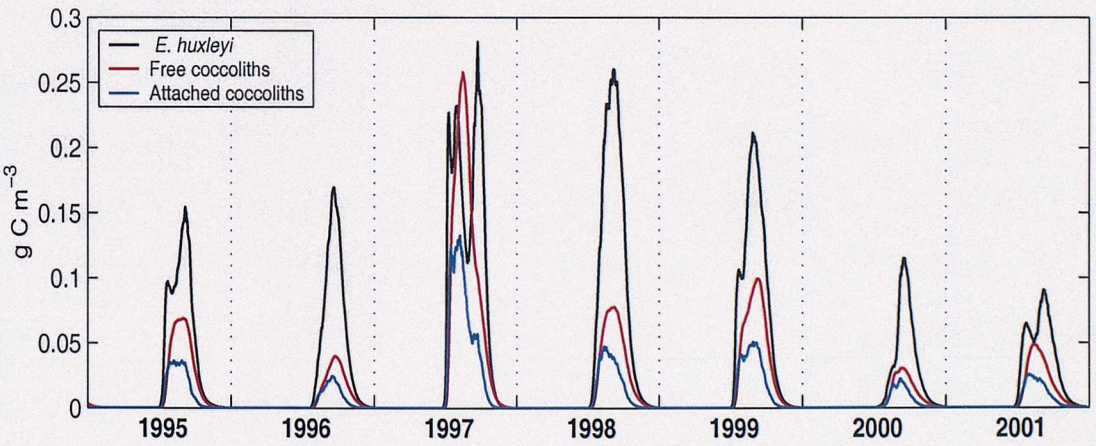

Figure 4.13: Modelled *E. huxleyi*, free and attached coccolith abundances.

4.4 N:P ratio and *E. huxleyi* blooms

One of the key environmental factors hypothesized to favour *E. huxleyi* blooms is phosphate limitation, classically identified as waters with a high Redfield ratio (N:P>16). Evidence for this is critically reviewed in the following subsection and

new insights are provided into the N:P conditions under which *E. huxleyi* blooms take place in the world ocean.

4.4.1 Experimental evidence for *E. huxleyi* success under high N:P conditions

In multi-species competition experiments, Riegman *et al.* (1992) found that *E. huxleyi* (isolated from the North Sea), along with the diatom species *Chaetoceros socialis*, outcompeted other species when N:P supply ratio was 100. At N:P of 1.5, *E. huxleyi* was outcompeted by other species (but notably, *E. huxleyi* still maintained a relatively high population). In a later study, Riegman *et al.* (2000) demonstrated that *E. huxleyi* has an unusually high affinity for phosphate under phosphorus stress (N:P of 300), with an extremely low half-saturation constant of about 1 nM. Further, Riegman *et al.* (2000) showed that *E. huxleyi* has two cell-surface bound alkaline phosphatase enzymes enabling it to use organic phosphate at nanomolar levels. Therefore, *E. huxleyi* would be expected to be particularly competitive at low phosphate concentrations and when the N:P ratio was high. Support for the idea of phosphorus stress being important for the competitive success of *E. huxleyi* has also come from mesocosm studies in a Norwegian fjord. In one experiment (May 1992), the most dense *E. huxleyi* blooms occurred in mesocosms receiving the highest N:P (16:0.2 μmol, N:P of 80) additions (Egge & Heimdal, 1994). Aksnes *et al.* (1994) developed a simulation model of *E. huxleyi* growth and compared it to the data from these mesocosm experiments and a set in May 1991, where *E. huxleyi* also bloomed most strongly in bags receiving the highest N:P additions. They found that they could best reproduce experimental results only by giving *E. huxleyi* an enhanced affinity for phosphate and adding a pool of organic phosphate that supplemented the inorganic phosphate pool. However, as Egge & Heimdal (1994) point out, an examination of mesocosm experiments over several years shows that *E. huxleyi* grew well in mesocosms receiving both high and low N:P additions. Taking all these mesocosms experiments together there is little correlation between nutrient ratios

or concentration and the abundance of *E. huxleyi*. This suggests that other factors other than N:P ratio were also critical to the growth of this species. It appears that *E. huxleyi* can take advantage of a wide range of nutrient concentrations and ratios in mesocosms where the nutrient environment is artificially altered.

4.4.2 Evidence for high N:P conditions in natural blooms

From a literature survey, there appears to be only one documented *E. huxleyi* bloom that occurred under high N:P conditions: the June/July 1991 bloom of the North Atlantic, south of Iceland (Holligan *et al.*, 1993a). Tyrrell & Taylor (1996) noted that the *E. huxleyi* bloom occurred only in areas north of 60° where N:P was >16, and reached its maximum abundances where N:P was >25. They were able to successfully model *E. huxleyi* dynamics only when giving it a phosphorus uptake advantage over other algal groups.

4.4.3 Re-evaluating the high N:P hypothesis

High N:P ratios, however, appear to be the exception rather than the rule in *E. huxleyi* blooms. In fact, most of the blooms studied to date occurred under low N:P conditions, where nitrate was low or nondetectable. High N:P ratios, for example, did not occur in the Bering Sea, nor was there an increase in N:P during the bloom years (1997 onward), as might be expected if phosphorus stress was a factor in the appearance of the bloom (see Fig. 1.7).

Table 4.1 lists all field studies to date of *E. huxleyi* blooms in various parts of the world oceans in which nitrate and phosphate were reported (after Lessard *et al.*, 2003). In all cases except the 1991 North Atlantic bloom, N:P ratios as well as nitrate concentrations are very low, indicating nitrogen rather than phosphorus stress. Most of these studies were done late in the bloom development, when the water was visibly coloured by shed coccoliths, and thus may not reflect growth conditions. However, low N:P was also the case in one study of an early bloom phase in the North Sea (Rees *et al.*, 2002). In fact, except for the North Atlantic, low N:P ratios are typical

Table 4.1: Nutrient levels (in mmol m^{-3}) and NO_3:PO_4 ratios measured during *E. huxleyi* blooms. Modified from Lessard *et al.* (2003).

	NO_3	PO_4	$NO_3 : PO_4$	NH_4	Urea	N uptake	Reference
North Atlantic							
June/July 1991	2-5	0.18-0.2	17-25	–	–	–	Tyrrell & Taylor (1996)
North Sea							
July 1993	0.08-0.15	0.1	0.8-1.5	0.4-1.0	–	–	van der Wal *et al.* (1995)
June/July 1994	nd-0.09	0.26-0.37	0.15	–	–	NH_4>NO_3>urea	Head *et al.* (1998)
June 1999	<0.13	0.03-0.1	0.1-1.2	<0.1	0.1-1.5	urea>NH_4>NO_3	Rees *et al.* (2002)
Norwegian fjords							
May 1992	<0.5	0.1	1-5	0.8-1.5	$\ll$0.5	NH_4>urea>NO_3	Kristiansen *et al.* (1994)
May 1993	nd	0.12-0.31	<1	0.23-0.54	0.1-0.87	NH_4>urea>NO_3	Fernández *et al.* (1996)
Gulf of Maine							
June 1989	0.2-0.6	0.02-0.16	~6	0.2-0.3	–	–	Townsend *et al.* (1994)
July 1990	0.1-0.4	0.3-0.8	~2	0.1-0.4	–	–	Townsend *et al.* (1994)
Eastern Bering Sea							
July/August 1997	2	0.4	5	–	–	–	Anonymous (2002)
July/August 1998	1.5	0.4	3.75	–	–	–	Anonymous (2002)
July/August 1998	0.2	0.4	0.5	–	–	–	Anonymous (2002)
July/August 1999	0.3	0.3	1	–	–	–	Anonymous (2002)

Table 4.2: NO_3:PO_4 average surface ratios at locations in the world ocean where satellite images suggest *E. huxleyi* blooms. Data from WOD98 (in mmol m^{-3}).

	NO_3		PO_4		$NO_3 : PO_4$	
Location	**annual**	**summer**	**annual**	**summer**	**annual**	**summer**
North Atlantic (South of Iceland)	8.0	4.0	0.5	0.3	16	13.3
South West Atlantic (Off Patagonia)	12.0	10.0	1.1	1.0	11	10
Bering Sea (Southeastern part)	10.0	2.0	1.2	0.6	8.3	3.3
North Sea (Off Norway)	4.5	1.0	0.3	0.2	15	5

of all the regions where satellites have suggested the presence of *E. huxleyi* blooms in the past, as shown in Table 4.2.

Chapter 5

Sensitivity analyses

5.1 Introduction

A sensitivity analysis of multi-species competition models of multi-annual cycles presents problems in terms of data presentation. The number of parameters to be studied would quickly lead to an unmanageable number of figures. Since the aim of the study was to investigate the reasons for *E. huxleyi* arrival and persistence in the Bering Sea, the attention was focused on 1) processes and 2) parameters that have a direct impact on the causative factors introduced in section 1.5. The importance of the processes of photoinhibition and microzooplankton selective grazing was investigated through a series of tests in which individual assumptions were omitted from the model. Sensitivity of the model outputs to selected parameters was conducted by varying each parameter in turn by $\pm 25\%$ (Saltelli, 2000). Sensitivity of the carbonate system to changes in the calcification parameters was examined independently.

5.2 Processes

The importance of individual assumptions related to the processes of photoinhibition and microzooplankton selective grazing is investigated here. In each test, a run is

performed by omitting an individual assumption. The results of these runs are then compared with the standard run (SR), which includes all the assumptions (Fig. 5.1). Each test was accompanied by a series of diagnostic plots (consisting of seasonal cycles of nitrate, silicate, ammonium and microzooplankton concentrations).

5.2.1 Test 1 - No photoinhibiting effect

This scenario has been implemented by assuming that all phytoplankton respond to light according to a Michaelis-Menten function (equation 2.7) rather than to a Steele function (equation 2.6). As in a previous study (Tyrrell & Taylor, 1996), *E. huxleyi* is assumed to have a higher half-saturation constant for light ($I_h = 45\ \mathrm{W\,m^{-2}}$) compared to all other groups ($I_h = 15\ \mathrm{W\,m^{-2}}$). The achieved growth also depends on the maximum growth rates. These parameters have been changed slightly in this run so that flagellates have an advantage with respect to *E. huxleyi* at light intensities lower than approximately $70\ \mathrm{W\,m^{-2}}$. This was done in order to produce P-I curves (shown in Fig. 5.2) similar to the ones obtained in the standard run configuration (Fig. 2.5) but now without photoinhibition.

Maximum growth rates and light half-saturation constants used in this run are reported in Table 5.1.

Table 5.1: Maximum growth rates and light half-saturation constants used to explore the sensitivity of the model results in the absence of photoinhibition.

	$\mu_{max,0}\ (\mathrm{d^{-1}})$	$I_h\ (\mathrm{W\ m^{-2}})$
Diatoms	1.3	15
Flagellates	0.8	15
Dinoflagellates	0.6	15
E. huxleyi	1.1	45

This run shows that no photoinhibition will cause the flagellates population to reach unrealistically high values and *E. huxleyi* concentrations to become too low (Fig. 5.1b). Note that diatoms are still under the pressure of the extra microzooplankton grazing term during summer, when silicate gets lower than $3\,\mu\mathrm{M}$.

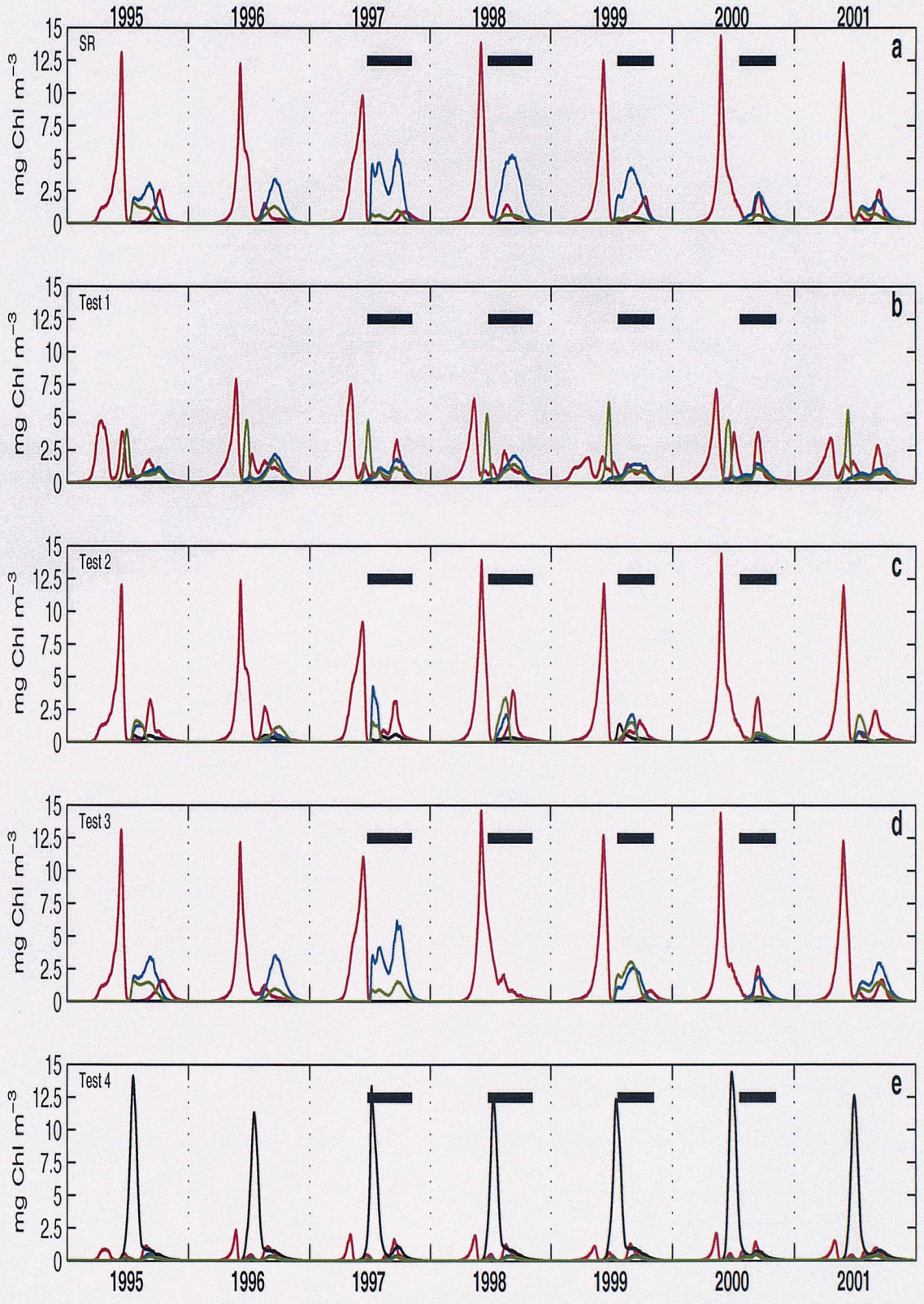

Figure 5.1: Sensitivity to processes. Phytoplankton succession from: a) standard run, b) no photoinhibition, c) microzooplankton not grazing diatoms, d) microzooplankton not grazing diatoms and only lightly grazing *E. huxleyi*, and e) microzooplankton grazing equally on diatoms, flagellates and *E. huxleyi*. In all plots the red line represents diatoms, the blue line *E. huxleyi*, the green line flagellates and the black line dinoflagellates. The horizontal black line indicates the duration of *E. huxleyi* blooms as observed in SeaWiFS true-colour images.

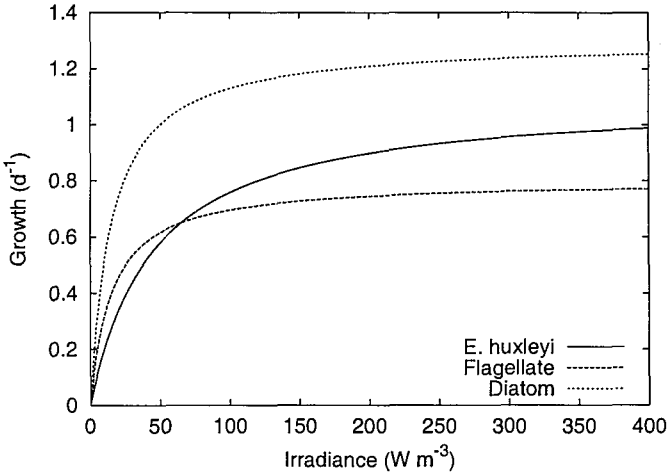

Figure 5.2: Comparison of PI-curves for *E. huxleyi*, flagellates and diatoms in the case of Michaelis-Menten light-limited growth. The parameters used to produce this scenario are given in Table 5.1.

5.2.2 Test 2 - Microzooplankton not grazing on diatoms

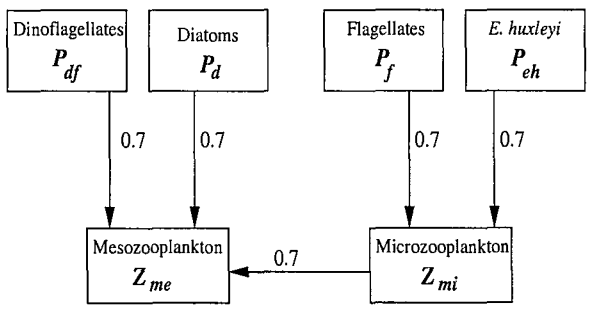

Figure 5.3: Schematic representation of the zooplankton-phytoplankton interactions used in Test 2.

The extra diatom loss term representing microzooplankton grazing on them ($G_{d,mi}P_d$ in equation 2.11) has been omitted in this run. For this case, the ingestion rate of microzooplankton feeding on *E. huxleyi* has been set to $0.7\,\mathrm{d}^{-1}$ year-round, as for the other phytoplankton. Figure 5.3 illustrates the zooplankton-phytoplankton interactions considered in this test (compare to Fig. 2.4 for the SR). As expected, the occurrence and magnitude of the spring bloom is not affected (see Fig. 5.1c). The impact is evident between late summer and beginning of autumn when silicate is depleted. Diatoms show a somewhat higher summer peak than in the standard run but more interestingly the durations of *E. huxleyi* blooms are very much reduced (see Fig. 5.1c) in this run, thus producing an unrealistic result.

5.2.3 Test 3 - Microzooplankton not grazing diatoms and lightly grazing *E. huxleyi*

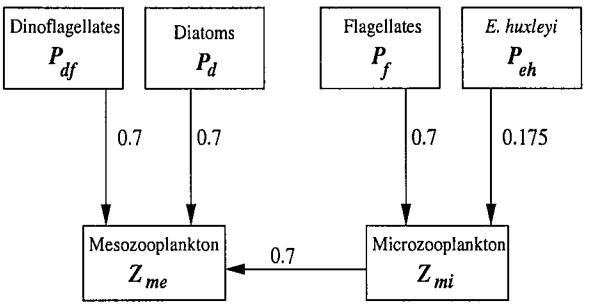

Figure 5.4: Schematic representation of the zooplankton-phytoplankton interactions used in Test 3.

This run is similar to the previous one but this time the microzooplankton grazing pressure on *E. huxleyi* has been reduced by setting the ingestion rate, $g_{eh,mi}$, to the lower level of $0.175\,\mathrm{d}^{-1}$ throughout the year, as shown in Fig. 5.4. Diatoms are again not grazed by microzooplankton. Although the result gets somewhat closer to the standard run, it still remains unrealistic. The 1998 *E. huxleyi* bloom disappears and the duration of the blooms after 1998 is reduced (Fig. 5.1d). This run shows that a reduced grazing pressure on *E. huxleyi* without having an extra grazing pressure of microzooplankton on diatoms is not enough to explain the success of *E. huxleyi*.

5.2.4 Test 4 - Microzooplankton grazing equally on diatoms and *E. huxleyi*

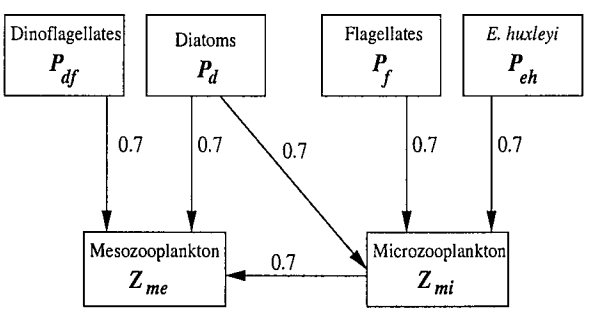

Figure 5.5: Schematic representation of the zooplankton-phytoplankton interactions used in Test 4.

This test has been carried out by putting diatoms, flagellates and *E. huxleyi*

under the same microzooplankton grazing pressure year-round (see Fig. 5.5). This has been realised by setting $g_{d,mi}$, $g_{f,mi}$ and $g_{eh,mi}$ all to $0.7\,d^{-1}$. Note that diatoms are still grazed by mesozooplankton with an ingestion rate, $g_{d,me}$, of $0.7\,d^{-1}$. Such a scenario also leads to an unrealistic result by favouring dinoflagellates (Fig. 5.1e).

5.2.5 Diagnostics

A series of diagnostic plots are presented here in order to provide further information about the model behaviour in the standard run configuration as compared with the configuration of the tests illustrated above. Nitrate, silicate, ammonium and microzooplankton concentrations are reported for the SR as compared to the different tests.

In Test 1, a lower diatom abundance tends to be produced every year with respect to the SR (Fig. 5.1b). The (smaller) spring blooms are also anticipated in time. Both these aspects are well reflected in a lower and earlier drawdown of nitrate and in an earlier ammonium peak (Fig. 5.6). Microzooplankton increasing also takes place earlier in Test 1 and higher abundances are reached (Fig. 5.6) in coincidence with the unusually high flagellates concentrations (Fig. 5.1b).

As regard to Test 2, very often (years 1995, 1997, 1998, 1999 and 2001), microzooplankton reaches higher and earlier abundances, which have the tendency to last for shorter time (Fig. 5.7) probably as a consequence of the shorter duration of *E. huxleyi* and flagellate blooms (Fig. 5.1c, they are subjected to the same microzooplankton grazing pressure). These two phytoplankton types appear to be outcompeted by a more active diatom population during summer (which is not subjected to the extra microzooplankton grazing pressure).

In Test 3, the microzooplankton population is generally smaller than in the SR, particularly from 1996 onwards (Fig. 5.8). This is due to the fact that the food sources for microzooplankton are reduced mainly to flagellates (*E. huxleyi* is only lightly grazed by microzooplankton). In 1998, the diatom bloom lasts unrealistically

longer than in other years. This leaves too short a time-window for flagellates and *E. huxleyi* (Fig. 5.1c) to bloom before light becomes limiting. The bigger microzooplankton population reached in 1999 is most likely a result of the bigger flagellate peak of that same year.

In Test 4, microzooplankton is able to crop down the spring blooms (Fig. 5.9). Silicate maintains high concentrations throughout the years and nitrate is drawdown appreciably only in summer when the dinoflagellate populations burst out (Fig. 5.1d).

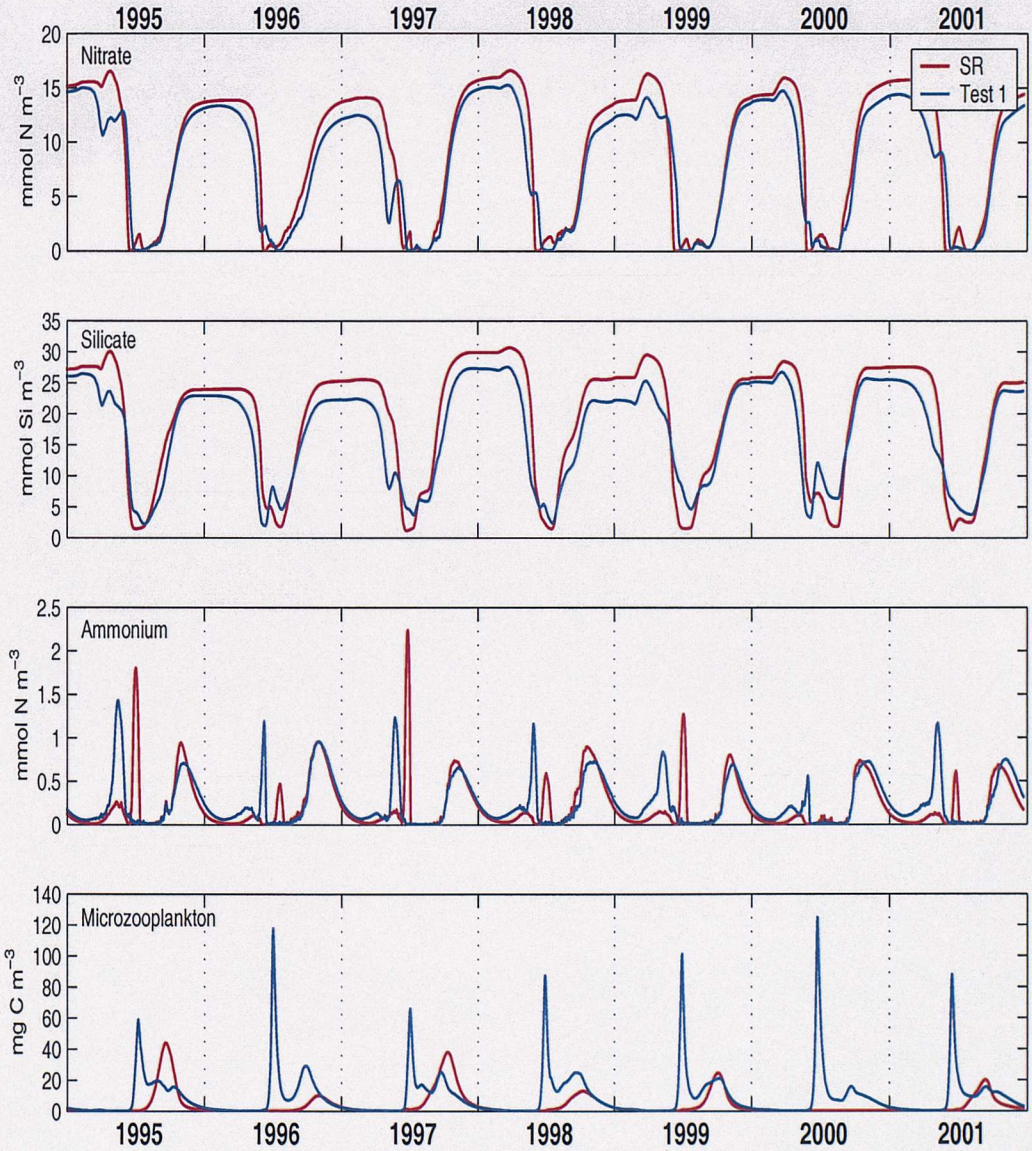

Figure 5.6: Nutrients and microzooplankton cycles for SR as compared with Test 1 - No photoinhibition.

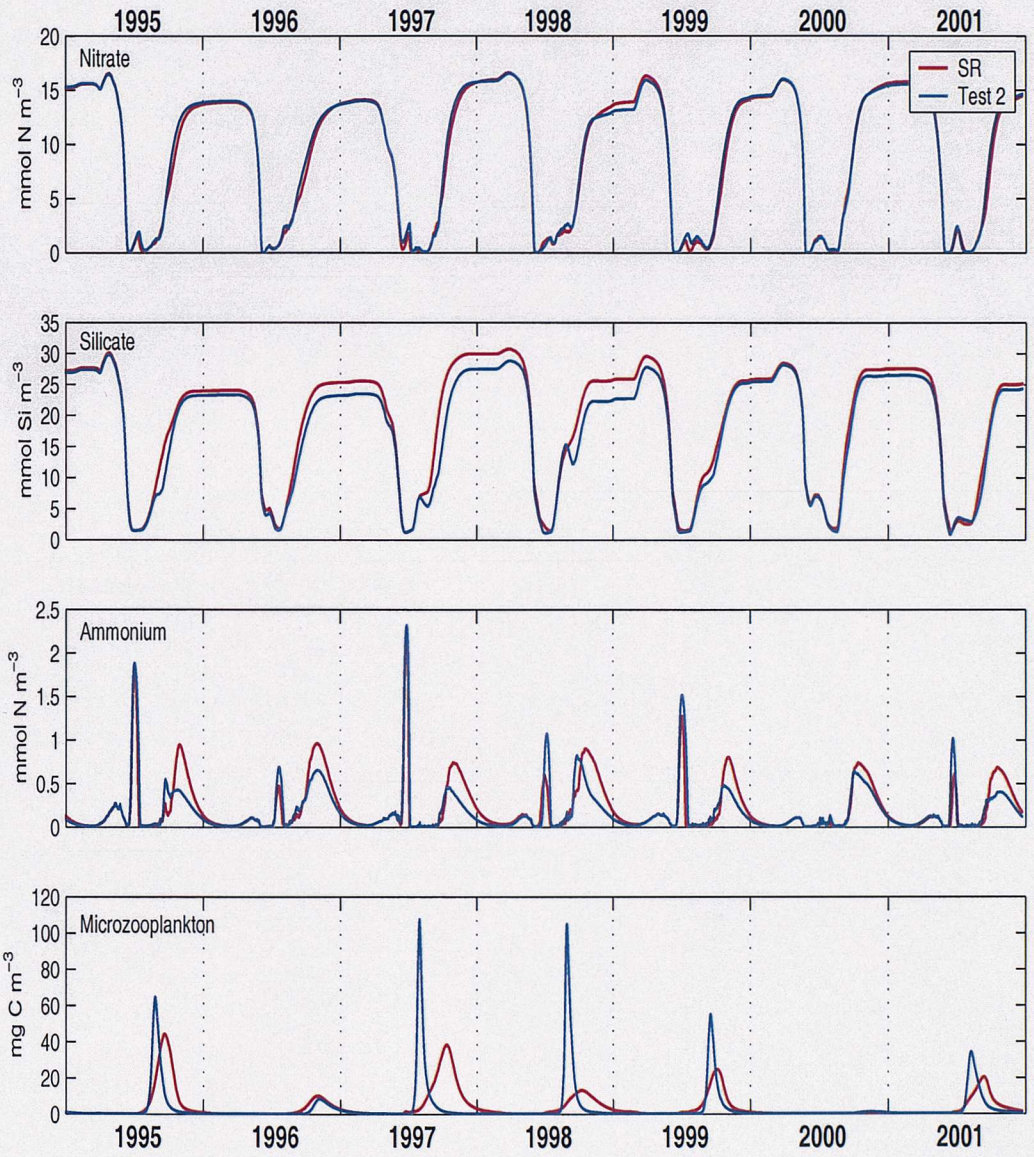

Figure 5.7: Nutrients and microzooplankton cycles for SR as compared with Test 2 - Microzooplankton not grazing on diatoms.

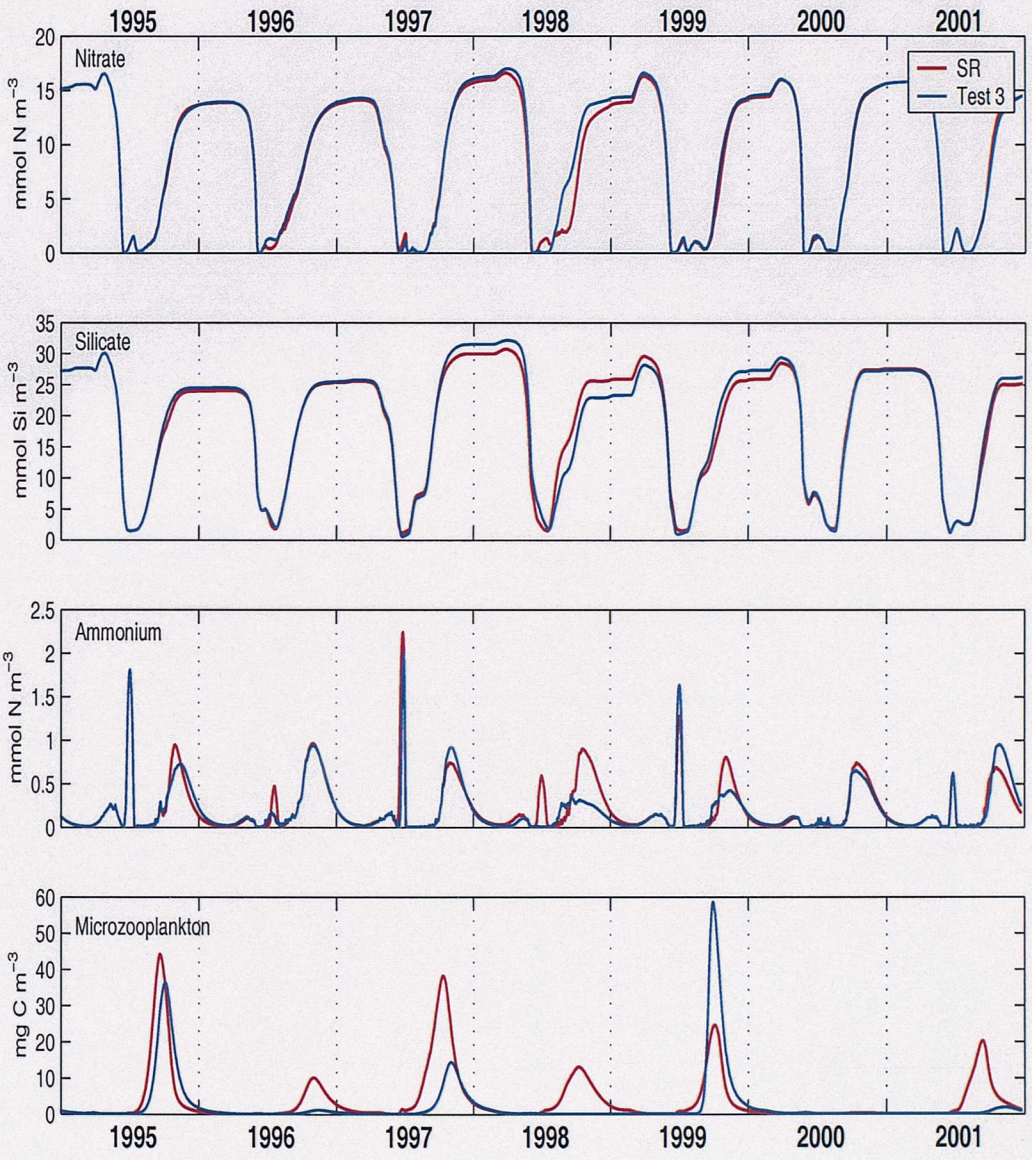

Figure 5.8: Nutrients and microzooplankton cycles for SR as compared with Test 3 - Microzooplankton not grazing on diatoms and lightly grazing *E. huxleyi*.

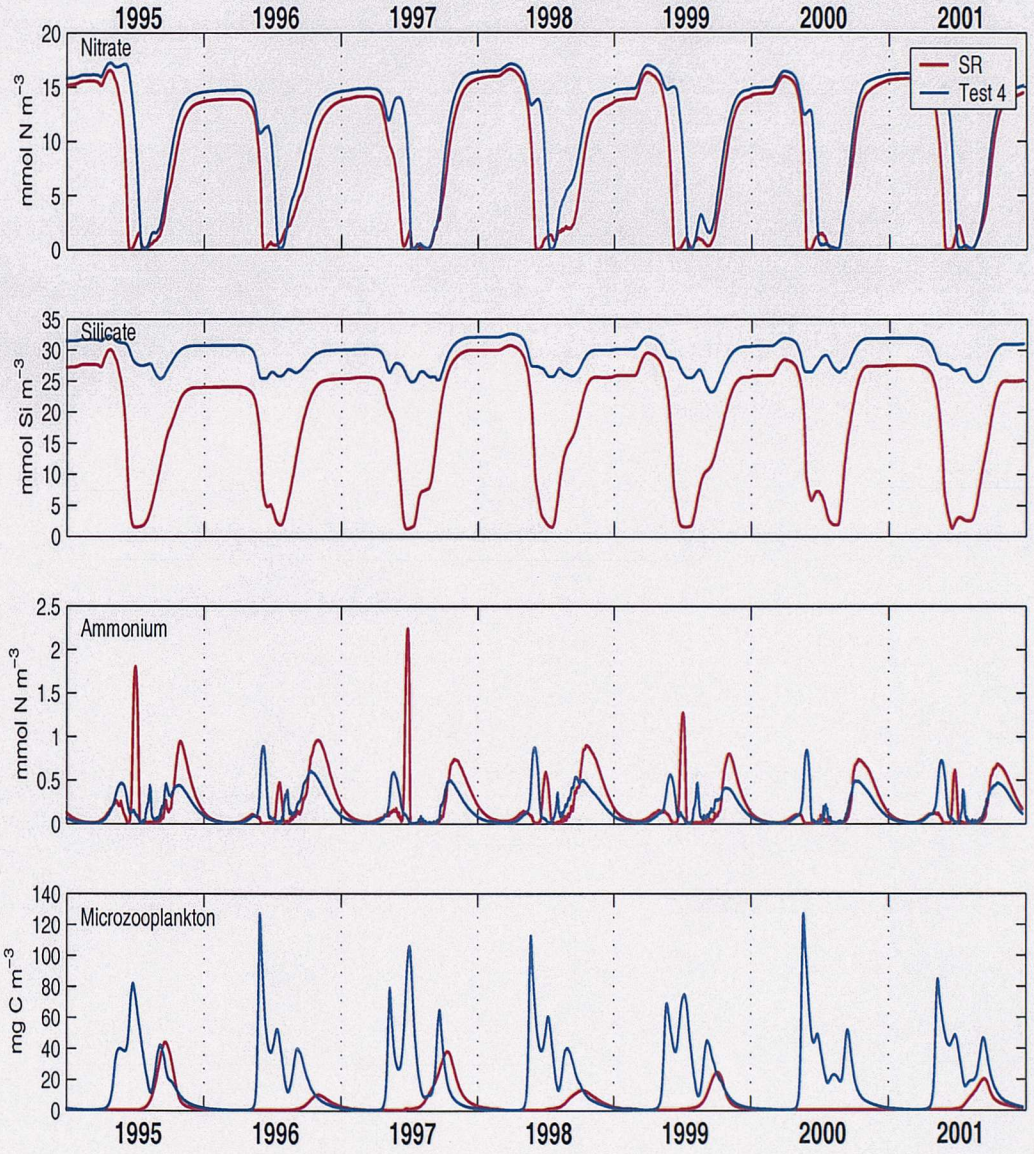

Figure 5.9: Nutrients and microzooplankton cycles for SR as compared with Test 4 - Microzooplankton grazing equally on diatoms and *E. huxleyi*.

5.3 Sensitivity to specific parameters

The model contains approximately 80 parameters (see Tables 2.1 and 2.2). It would be an impracticable task if the effect of changes to all parameters were to be examined and presented here. Extra difficulty is added by the fact that the analyses should be performed over several years (1995-2001). Therefore, the sensitivity of 1) the maximum values of five model variables (P_d, P_f, P_{eh}, Z_{mi} and Z_{me}) and 2) the timing of their maximum values to changes of $\pm 25\%$ of selected parameters (A_h, N_h, S_h, μ_{max}, m, I_{sat}, g_{mi} and g_{me}) has been examined only for the year 1997. Only the sensitivity of the model biological variables was calculated. The sensitivity of nutrients was not calculated because they tended to behave similarly in the calibration run (Fig. 4.4), the SR (Fig. 4.5) and the four tests (Figs. 5.6-5.8, although note Fig 5.6). Following Haefner (1996), the sensitivity of each model variable was characterised with a simple index S that compares the changes in model output relative to model responses for the set of parameters:

$$S = \frac{p}{Y}\frac{(Y' - Y)}{(p' - p)} \tag{5.1}$$

where Y' and Y are model responses for altered and nominal[1] parameters, respectively, and p' and p are the altered and nominal parameters, respectively. In the cases where one parameter has different values for different state variables (μ_{max}, I_{sat} and g_{mi}), the multi-parameter sensitivity formula has been used (Haefner, 1996):

$$S = \frac{\frac{Y'-Y}{Y}}{\sqrt{\frac{(p_1-p_1')^2+(p_2-p_2')^2}{p_1^2+p_2^2}}} \tag{5.2}$$

where p_1 and p_2 are the nominal values and p_1' and p_2' are the altered values. Note that in this case, since the denominator is always positive, the ability to distinguish between positive and negative parameter changes is lost. Note also that equation 5.2 is reduced to equation 5.1 for $p_1 = p_2$. In both cases (single- and multi-parameter

[1] "Nominal parameter" refers to the value of the parameter used for the standard run (given in Tab. 2.1).

sensitivity), a value of $S \approx 0.5$ indicates that the variable Y is robust with respect to changes in the parameter p, and Y is sensitive to changes in p if S is $\gg 1$ (Haefner, 1996).

In all runs, results have been checked to ensure that a stable equilibrium was reached and to avoid solutions with multi-year cycles. In all cases examined, the model has provided a stable solution.

Sensitivities of maximum values of model variables and timing of the maxima are shown in Figs. 5.10 and 5.11, respectively. In general, all parameters have a higher impact on the maximum concentrations rather than on the timing of maxima (compare Fig. 5.10 with 5.11). Moreover, nutrient half-saturation constants, changed simultaneously for all phytoplankton, have less impact than all other parameters both on achieved maximum concentrations of phytoplankton and zooplankton and on the timing of the maxima. Therefore, the brief discussion will be focused only on the impact that μ_{max}, m, I_{sat}, g_{mi} and g_{me} have on the achieved maximum plankton concentrations.

Increasing μ_{max} for all phytoplankton types does not have a big impact on the model results (Fig. 5.10). By contrast, all variables are generally more sensitive to a decrease in μ_{max}. A higher phytoplankton mortality (note that $m = m_d = m_f = m_{df} = m_{eh}$) causes a general decrease in both zooplankton groups. When m is decreased, however, there is a less noticeable effect on all variables. I_{sat}, also changed simultaneously for all phytoplankton, has its biggest impact on flagellates and *E. huxleyi*, particularly when this parameter is decreased. This is not surprising when considering the maximum irradiances levels that phytoplankton can experience in the Bering Sea at different times of the year (Fig. 3.3c). The effects of g_{mi} is somewhat more difficult to assess because microzooplankton ingestion rate of diatoms ($g_{d,mi}$) is switched from $0\,d^{-1}$ to $0.7\,d^{-1}$ according to silicate concentrations. Nevertheless, the model variables do not appear to be very sensitive to changes of $\pm 25\%$ of this parameter. Finally, g_{me} impacts mainly on diatoms.

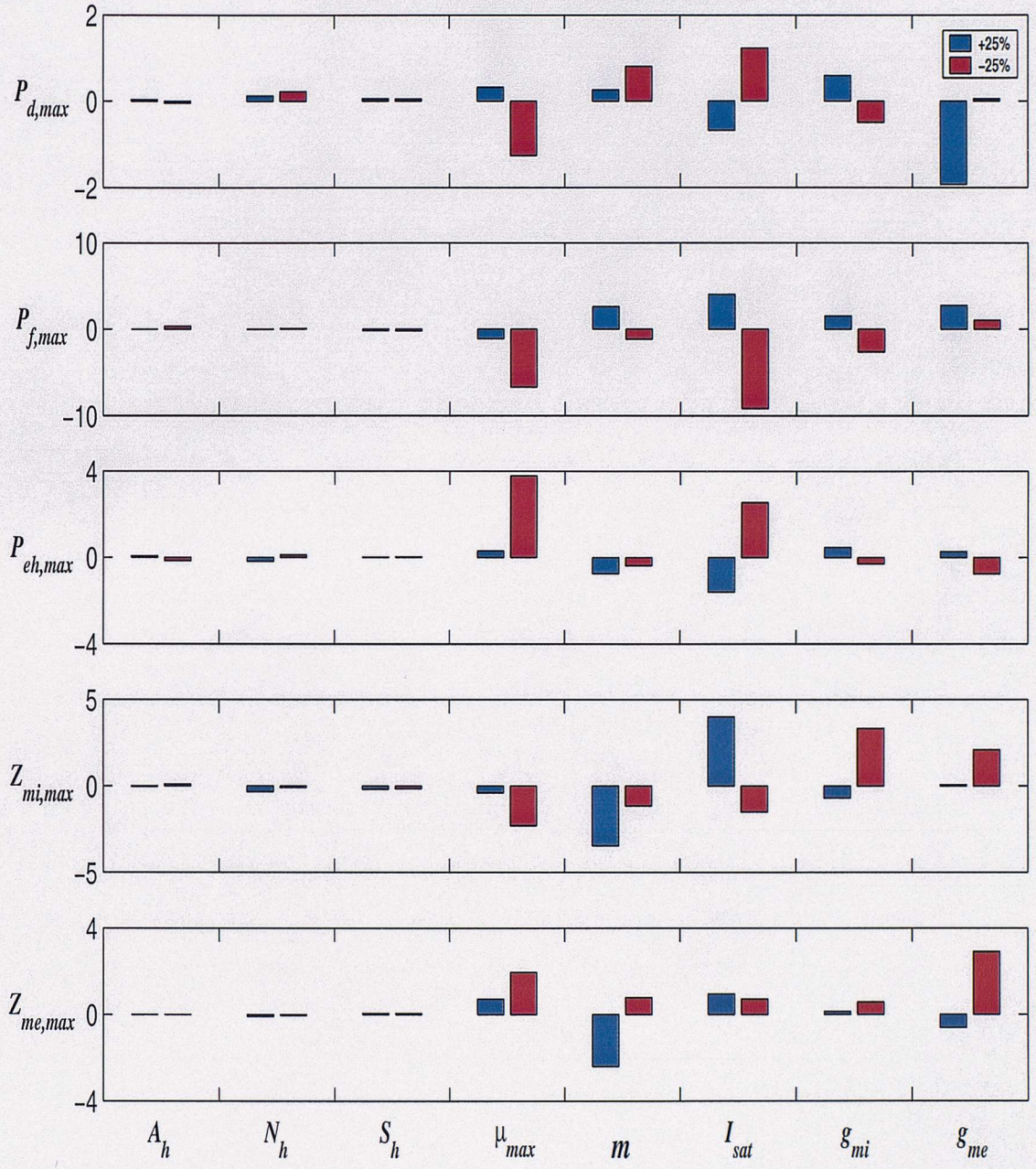

Figure 5.10: Sensitivity index of maximum values of five model variables (year 1997) to the variation of +25% (blue bar) and -25% (red bar) of various parameters. Model variables are: diatoms ($P_{d,max}$), flagellates ($P_{f,max}$), *E. huxleyi* ($P_{eh,max}$), microzooplankton ($Z_{mi,max}$) and mesozooplankton ($Z_{me,max}$). Parameters are: ammonium half-saturation (A_h), nitrate half-saturation (N_h), silicate half-saturation (S_h), maximum growth rates (μ_{max}), phytoplankton mortalities (m), light saturation levels (I_{sat}), maximum microzooplankton ingestion rates (g_{mi}) and maximum mesozooplankton ingestion rates (g_{me}).

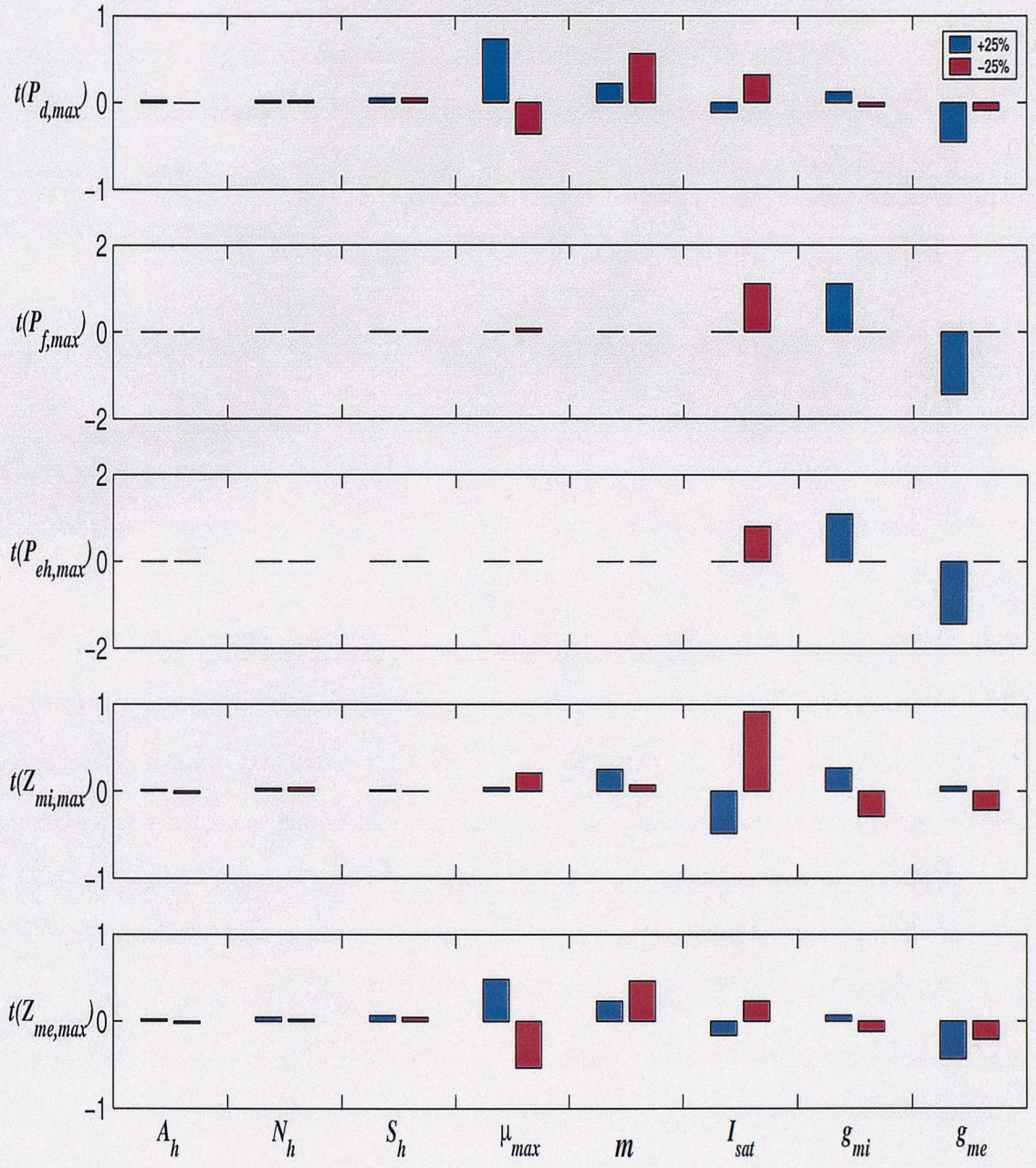

Figure 5.11: Sensitivity index of timing of maximum values of five model variables (year 1997) to the variation of +25% (blue bar) and -25% (red bar) of various parameters. Model variables are: diatoms ($P_{d,max}$), flagellates ($P_{f,max}$), *E. huxleyi* ($P_{eh,max}$), microzooplankton ($Z_{mi,max}$) and mesozooplankton ($Z_{me,max}$). Parameters are: ammonium half-saturation (A_h), nitrate half-saturation (N_h), silicate half-saturation (S_h), maximum growth rates (μ_{max}), phytoplankton mortalities (m), light saturation levels (I_{sat}), maximum microzooplankton ingestion rates (g_{mi}) and maximum mesozooplankton ingestion rates (g_{me}).

In conclusion, the sensitivity analysis for the year 1997 suggests that relatively big uncertainties (±25%) in important parameters do not greatly effect the timing of when the maximum concentrations of the model variables occur. So, for example, the impact on the timing of the diatom spring bloom or *E. huxleyi* peak concentration is fairly robust with respect to the changes discussed. Nonetheless, both μ_{max} and I_{sat} are critical (particularly for flagellates) to 1997 model results in terms of achieved maximum concentrations.

5.4 Different diffusivity regimes across the thermocline

A model sensitivity analysis of diffusive mixing (results not shown) showed that the ecosystem experiences low vertical diffusion when k is set to $0.01\,\mathrm{m\,d^{-1}}$ and lower, and in these cases any exchange of material between the two boxes is only driven by the dynamics of the mixed layer depth itself, by entrainment or detrainment (see equation 2.4). By increasing k, diffusive mixing becomes more and more important up to the limit of when the upper box is brought to the same nutrient concentration as in the bottom layer and with no more biological activity due to a complete loss of phytoplankton. A turbulent environment tends to favour diatoms and *E. huxleyi* due to their high maximum growth rates. However, conditions of reduced diffusive mixing in 1997 and 1998 with respect to other years did not produce any interesting results probably due to the complex dual effect of k in supplying nutrients but also in removing plant cells (Evans, 1988).

5.5 The calcification process

The changes of three parameters have been investigated in order to explore the sensitivity of the carbonate variables to the calcification process: the maximum calcification rate, C_{max}, the half-saturation constant of the light-dependent calcification, I_h (see Table 2.2) and the total number of attached coccoliths that an *E.*

huxleyi cell can hold, Π_{max}. All the parameters have been changed independently by $\pm 50\%$[2] and the effects of these changes have been investigated on free coccoliths (L_f), attached coccoliths (L_a), alkalinity (Alk), dissolved carbon dioxide (DIC) and carbonate ion concentration ($[CO_3^{2-}]$). Almost no effect can be observed on these variables due to changes in the total number of attached coccoliths (results not shown). Conversely, the impact of C_{max} is more important, as shown in Fig. 5.12, but the effect of I_h (see Fig. 5.13) is less important.

Given the great uncertainties related to this parameter and in general on the functioning of the calcification process (Paasche, 2002), the model results have to be interpreted with caution. However, despite these weaknesses in the quantitative predictions of the carbonate variables, the general patterns are consistent with previous studies, as explained in subsection 4.3.3. The calcification process has a first order impact on alkalinity but only a second order impact on DIC (see Figs. 5.12 and 5.13).

[2]It was decided to change the calcification parameters by $\pm 50\%$ because preliminary investigations showed that a $\pm 25\%$ change would produce small effects.

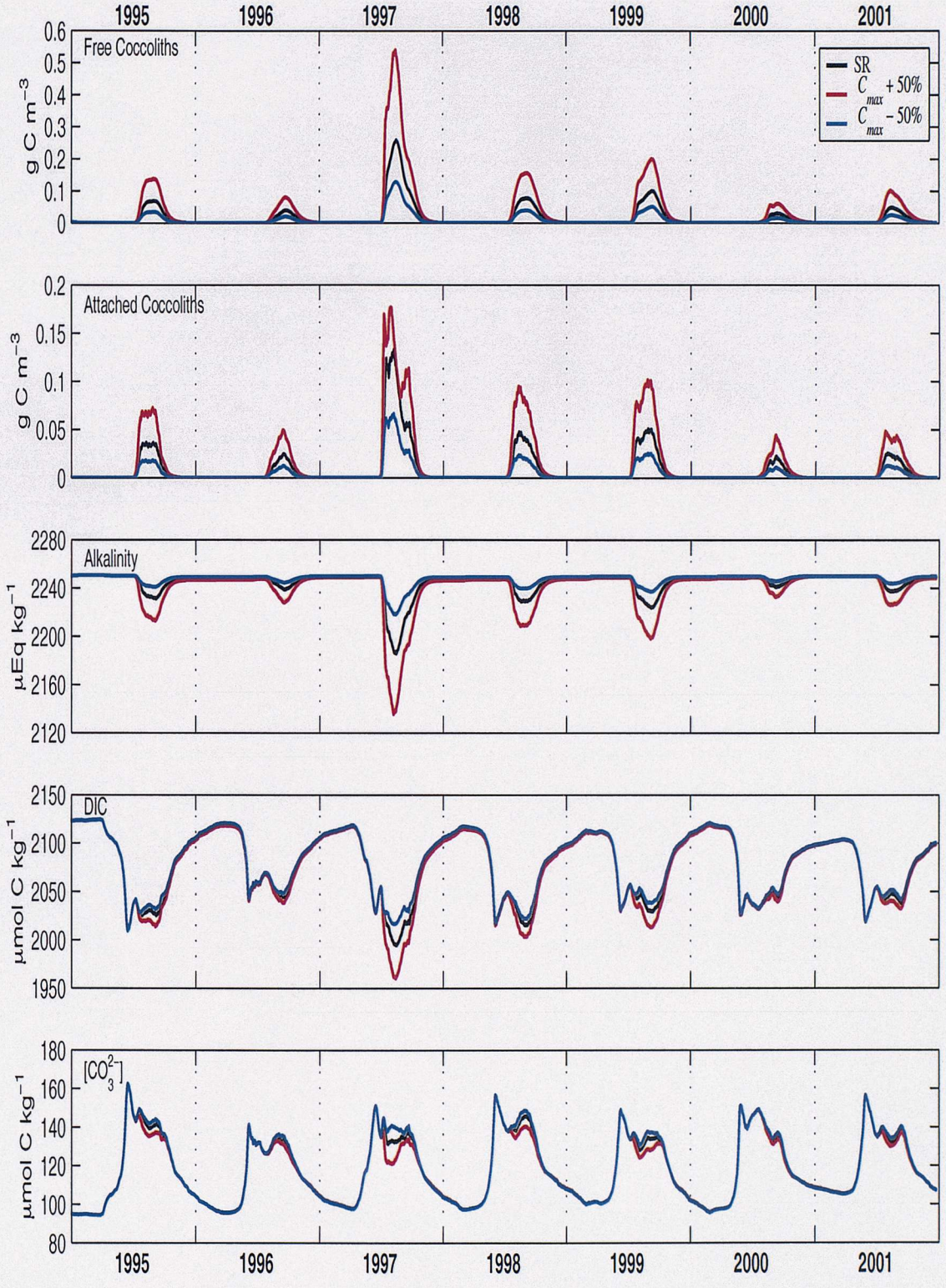

Figure 5.12: Sensitivity of free and attached coccoliths, alkalinity, DIC and carbonate ion concentrations to changes in maximum calcification rate C_{max}. In all plots the black line is with C_{max} as in the SR, the red line is with C_{max} increased by 50% from the SR value and the blue line is with C_{max} decreased by 50% from the SR value.

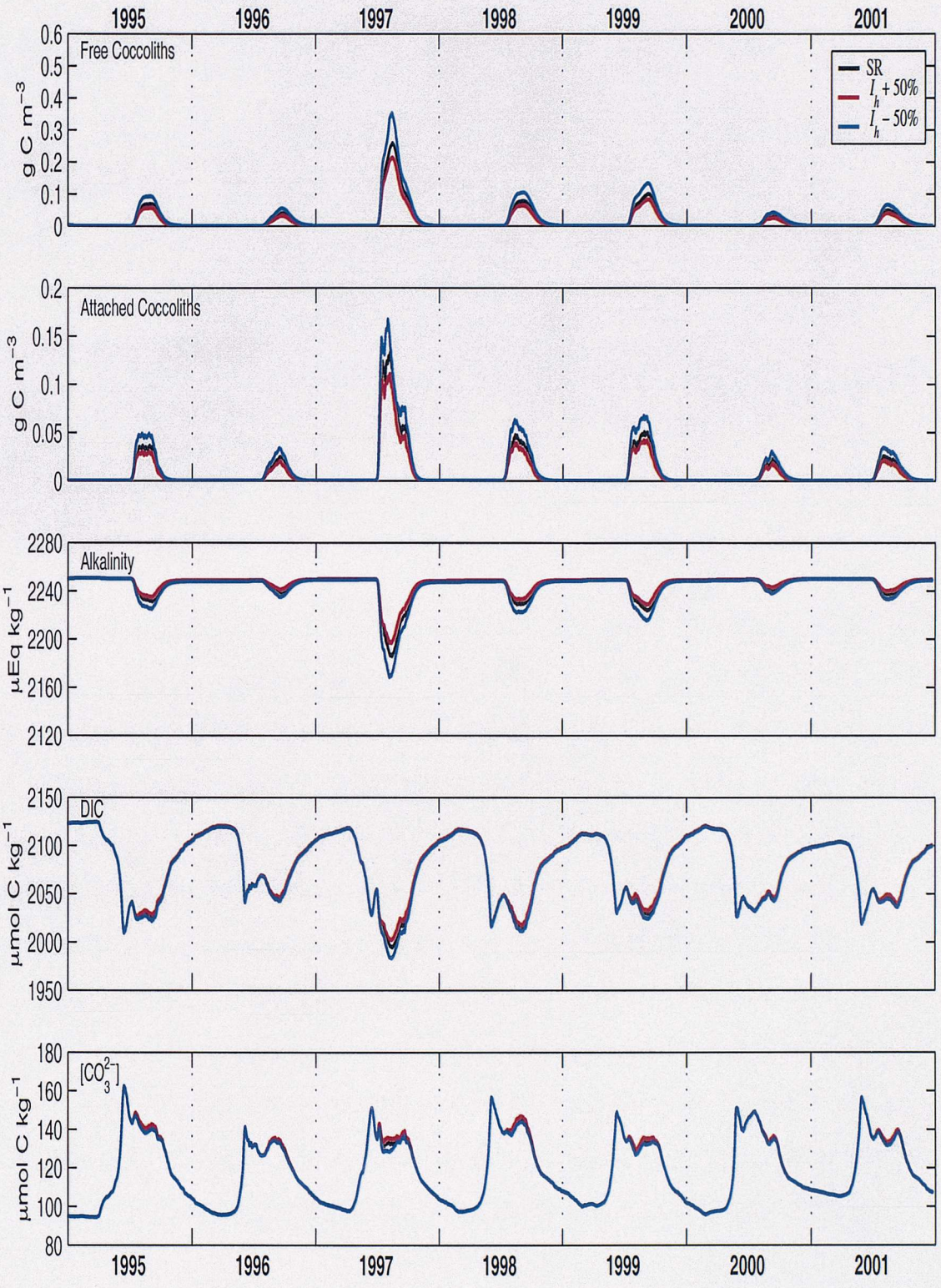

Figure 5.13: Sensitivity of free and attached coccoliths, alkalinity, DIC and carbonate ion concentrations to changes in the half-saturation constant of the light-dependent calcification (I_h). In all plots the black is with I_h as in the SR, the red line shows I_h increased by 50% from the SR value and the blue line is with I_h decreased by 50% from the SR value.

Chapter 6

Discussion

6.1 Introduction

A combination of tools have been used in this study. Satellite imagery (CZCS and AHVRR) have been used to determine the distribution of *E. huxleyi* in the Bering Sea from 1978 to 1996. The hypothesis that *E. huxleyi* may be favoured by high N:P ratio conditions has also been investigated in detail in those locations of the global ocean where *E. huxleyi* blooms are commonly observed. Such a study has been motivated by the evidence that the Bering Sea waters are characterised by N:P ratios lower than the Redfield ratio, both before and after the appearance of *E. huxleyi* in the area. Finally, numerous field (mooring and cruises) and satellite (SeaWiFS) data have been collected and then used in conjunction with an ecosystem model in order to understand the reasons for the success of *E. huxleyi* in the area from 1997 to 2000. All of these studies, whose results have been presented in chapter 4, are here discussed in the context of the scientific questions highlighted in chapter 1.

6.2 History of *E. huxleyi* in the Bering Sea

The diagram presented in Fig. 6.1 summarises the *E. huxleyi* bloom occurrences in the Bering Sea from 1978 to 2001 as ascertained by satellite imagery.

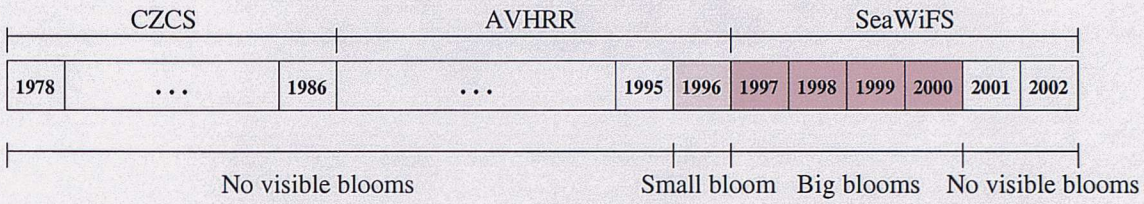

Figure 6.1: Diagram summarising *E. huxleyi* bloom occurrences in the Bering Sea as derived by satellite imagery.

Clear evidence has been found that the vast blooms taking place in 1997 and following years were not an instantaneous response of the Bering Sea ecosystem (on a time scale of one year or less) to climate anomalies, as proposed by previous studies (Napp & Hunt Jr, 2001). Most likely *E. huxleyi* appeared in the area more gradually as the precursor bloom of 1996 suggests (Fig. 4.3). Note, however, that the fact that no blooms have been found in the period from 1978 to 1995 is not sufficient to rule out the presence of this species in this region. Indeed, evidence suggests that *E. huxleyi* has been present in the Bering Sea since the early '90s, although not in blooming concentrations (M. Flint, unpublished observations).

The results of the satellite study are limited to the image coverage provided by satellites and the ability to detect *E. huxleyi* blooms in the imagery. The latter is a function of several variables, such as weather (i.e. presence of clouds) and sensor sensitivity.

6.2.1 Correspondence between blooms and PDO and ENSO

Hare & Mantua (2000) compiled oceanic indices of PDO and ENSO for the Bering Sea on the basis of sea surface temperature anomalies. The massive appearance of *E. huxleyi* in the Bering Sea in 1997 coincided with both PDO and ENSO positive summer indices (see Fig. 6.2). The apparent absence of *E. huxleyi* blooms in the

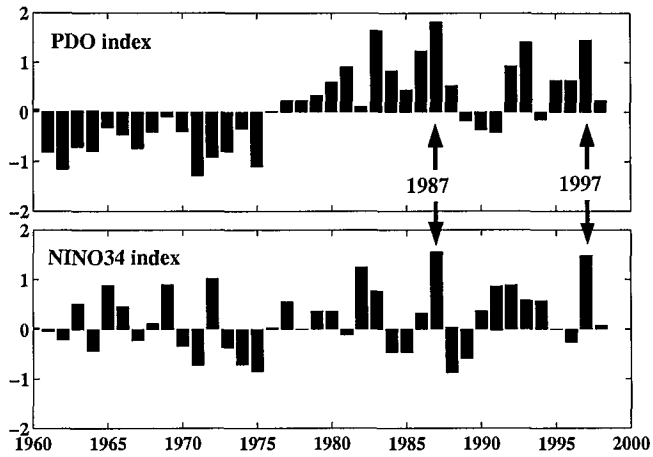

Figure 6.2: PDO and ENSO annual indices (data courtesy of Steven R. Hare).

Bering Sea between 1978-1995, based on this study, suggests that the sole combination of positive PDO and ENSO is not sufficient to stimulate *E. huxleyi* bloom formation in this area. Perhaps a monthly high pressure system is also required (Overland *et al.*, 2001), or perhaps additional triggers (of biological nature for example) are also required. For example, it was not possible to find evidence of any relevant *E. huxleyi* activity in 1987, a year which possessed the same characteristics in terms of PDO and ENSO indices as 1997 (Fig. 6.2).

6.3 N:P ratio requirements

E. huxleyi has been found to bloom under high N:P ratios in some mesocosm studies and in the oceanic northeast North Atlantic. The recent *E. huxleyi* blooms on the southeastern Bering Sea shelf, however, occurred under low N:P conditions (see Fig. 1.7), indicative of nitrogen stress. A review of field studies of blooms where nitrate and phosphate were measured indicates that N:P was always low. A survey of areas of the world ocean where satellite-detected *E. huxleyi* blooms occur also shows that N:P ratios are generally low.

High N:P ratios, however, may not be good indicators of phosphorus stress if other forms of nitrogen (inorganic and organic) and phosphorus (organic) are available to phytoplankton. Organic N and organic P are utilized by many phytoplankton and may be significant in their nutrition, but data on organic N and P concentra-

tions, bioavailability, and species-specific abilities to use them are still limited (e.g. Palenik & Dyrhman, 1998; Berman & Bronk, 2003). *E. huxleyi* has been found to be able to use some amino acids (Ietswaart *et al.*, 1994), amides, urea and purines such as hypoxanthine (Palenik & Henson, 1997). In the few studies that also examined the uptake of organic N during *E. huxleyi* blooms, *E. huxleyi* was found to primarily be using ammonium and urea (see Table 4.1). Therefore, *E. huxleyi* success may at least in part be due to a superior ability to use regenerated nitrogen. It is perhaps the combined ability of *E. huxleyi* to utilize non-nitrate N in addition to its exceptional phosphorus acquisition ability that provides a competitive edge in nutrient-depleted waters with shallow mixed layers and high light (Nanninga & Tyrrell, 1996).

These observations suggest that *E. huxleyi* is able to exploit situations where either phosphorus or nitrogen is limiting to competing species. These observations also suggest that attention should be directed to examination of the utilization of organic nitrogen by *E. huxleyi* to better understand the role nutrients play in blooms of this species. Moreover, the high N:P factor should not necessarily be assumed as a pre-requisite for *E. huxleyi* success in modelling studies.

6.4 Why did *E. huxleyi* first bloom in the Bering Sea in 1997?

It has been shown above that the massive appearance of *E. huxleyi* in the Bering Sea in 1997 was preceded by a small bloom in 1996 and that *E. huxleyi* has been present in the Bering Sea at least since the early '90s (M. Flint, unpublished observations), although not in high concentrations. Coccolithophores (*Pontosphaera* sp.) have also been observed in field studies carried out in the early '70s in the Subarctic Pacific and Bering Sea (Taniguchi *et al.*, 1976). Given this evidence, it seems plausible to assume that the Bering Sea has long been a potentially favourable place for coccolithophores. What then made a "sleeping" population gradually become more active in 1996 to

finally burst out in 1997 and persist until 2000? Unusual weather conditions, with persistent clear skies and weaker winds (Stockwell *et al.*, 2001) were the most evident anomalous factors in 1997, which caused SST to be 4° C above the climatological mean (Stabeno *et al.*, 2001). It has not been possible to reproduce a transition that goes from non-bloom year (1995) to small-bloom year (1996) to big-bloom years (1997-2000) with the model. However, in a simple experiment, in which the ecosystem was artificially forced in 1997 with functions (SST, MLD and PAR) typical of a colder year, a dramatic reduction in *E. huxleyi* activity was produced (Fig. 4.8). In other words, particularly good weather conditions in 1997, resulting in higher SST and weaker winds, have contributed to create a shallower MLD (Fig. 3.3b) and to keep the water column stable for longer (Fig. 1.4). These conditions, in conjunction with greater tolerance to high irradiances, seem to have favoured *E. huxleyi.* It should be noted that important parameters in the model are kept constant for all the years throughout which the model is run. Undoubtedly, phytoplankton mortalities, *E. huxleyi* calcification rates, zooplankton ingestion rates, etc. may all vary with time and location but our knowledge of their dynamical behaviour is up to now inadequate. Such a lack of information sets a limit on the model performance.

6.5 Why was *E. huxleyi* successful only in the period from 1997 to 2000?

The model results suggest that at least two different processes have combined to create favourable conditions for *E. huxleyi* in the Bering Sea. A lack of photoinhibition of *E. huxleyi* appears to be important. A high maximum growth rate combined with tolerance to high light intensities allow *E. huxleyi* to do better against flagellates. When photoinhibition is not included, the flagellate population becomes unrealistically high. Microzooplankton selective grazing "helped" *E. huxleyi* in the competition against diatoms. This result implies that microzooplankton can effectively control diatom populations during summer (Olson & Strom, 2002); this was achieved in the model by assuming that grazing intensified when silicate concentra-

tions were low (<3μM). This was hypothesized to be a consequence of the increased susceptibility of lightly silicified diatoms to grazing. However, it is also possible that diatoms become the most abundant preferred food in the presence of unpalatable *E. huxleyi*, and low silica conditions were simply coincidental with summer conditions. In any case, it appears that once conditions became favourable for the establishment of a consistent seeding population (in 1997) in the Bering Sea, *E. huxleyi* had the possibility to bloom again in the following years until it faded away once climate returned to its normal state.

6.6 Why did the blooms persist for so long?

The model strongly suggests that the bloom persistence (3-4 months) is related to the microzooplankton-diatom interaction. This finding is supported by studies showing microzooplankton capable of choosing their prey selectively (Burkill *et al.*, 1987) and by studies showing their ability to graze cells up to five times their own volume (Jacobson & Anderson, 1986; Hansen & Calado, 1999). The current model investigations were also based on results obtained with dilution experiments conducted in 1999 in the Bering Sea during an *E. huxleyi* bloom (Olson & Strom, 2002).

6.7 *E. huxleyi* and the carbonate system

As explained in subsection 4.3.3, the model predicts reasonably well the drawdown of alkalinity and the increase in $pCO_{2(sea)}$ during the *E. huxleyi* bloom of 1997. Similar good results are not reproduced in the following years (1998-2000). For instance, Murata & Takizawa (2002) examined the impact on the carbonate system of the *E. huxleyi* bloom taking place in the southeastern Bering Sea during September-October 2000. A maximum drawdown of alkalinity of 82 μmol kg^{-1} and a value of seawater pCO_2 of 400 μatm was reported for the bloom area, which is not in agreement with the model results for that year (see Fig. 4.10). However, sensitivity analysis (see section 5.5) has shown that alkalinity strongly depends on the maximum calcification

rate C_{max} (Fig. 5.12). Small changes in this parameter may lead to very different results. On the other hand, the poor knowledge of the calcification process sets a limit on our ability to model it. Possibly, discrepancies between observations and model results for only some of the years may also be due to the fact that these parameters are kept constant for all the duration of the main simulation run (from 1995 to 2001). As mentioned above, given that our knowledge of their dynamical behaviour is up to now inadequate, the model performance is clearly limited by such a lack of information. A year by year study, however, has not been attempted. This approach, although it might have produced better results by fine-tuning the crucial parameters differently for each year, would have prevented an exploration of the natural interannual evolution of the system.

6.8 Implications for the future

The atmospheric CO_2 concentration has increased from the preindustrial value of 280 ppmv to a value of 364 ppmv in 1997 (Indermühle *et al.*, 1999). According to calculations under the "business as usual" scenario (Houghton *et al.*, 2001), the CO_2 concentration will reach 700 ppmv by the year 2100 (see Fig. 1.9). What will be the consequences of this rapid increase for the calcifying organisms of the ocean? And in particular for coccolithophores? These changes may have important consequences for growth and calcification rates of both marine plankton and corals. For instance, regarding the production of $CaCO_3$ in the surface ocean, a decrease has to be expected in the future in corals (e.g. Gattuso *et al.*, 1999; Kleypas *et al.*, 1999; Langdon *et al.*, 2000), foraminifera (Wolf-Gladrow *et al.*, 1999; Spero *et al.*, 1997) and coccolithophores (Riebesell *et al.*, 2000; Zondervan *et al.*, 2001), as explained in subsection 1.5.6.

The study presented here confirms this scenario by providing strong evidence (Fig. 4.10c) that the $[CO_3^{2-}]$ seasonal peak (and therefore the calcite saturation state) is always coincident with *E. huxleyi* bloom timing. If the slowdown of calcification under increased acidification of seawater is confirmed, on a global scale, a

potential negative feedback effect on atmospheric pCO_2 may be expected.

The discussed disruptions may be accompanied by other possible consequences. For instance, the biogeographic distribution of individual coccolithophore species has changed substantially through geological time as a result of changes in the environment. McIntyre (1967) has demonstrated that the subpolar species *Coccolithus pelagicus* expanded its range further toward the equator during last glacial peak while tropical species like *Calcidiscus leptoporus*, *Umbilicosphaera irregularis* and others all had reduced biogeographic ranges withdrawing closer to the equator. It is reasonable to assume that under a global warming scenario, as high latitude seas become more stratified, calcifiers may move toward polar latitudes to find a more suitable environment. Initial evidence, including the Bering Sea case presented here, suggests that such a migration may well be a phenomenon that we are already starting to experience. In fact, a SeaWiFS composite (1997-2002) of *E. huxleyi* classified blooms as compared to a CZCS mission composite (1978-1986), both images created according to the method of Brown & Yoder (1994), indicates an increased *E. huxleyi* abundance in northern latitudes (see Fig. 6.3), most notably in the Bering and in the Barents Sea (north of Norway). It is somewhat striking that the increased *E. huxleyi* abundance coincides with increased sea surface temperatures at high latitudes, as data of the National Snow and Ice Data Center show (Fig. 6.4). The implied connection between global warming and *E. huxleyi* northward migration is not so unreasonable when considering, for instance, that vegetation belts on land are known to have shifted polewards in response to warming at the end of last ice age (e.g. Gates, 1993), and are likely to do so again in response to global warming[1] (Theurillant & Guisan, 2001). However, it appears from the model results (see Fig. 4.10) that there is no significant impact of increasing temperature on the carbonate ion concentration (or calcite saturation state), counter to the hypothesis put forward at the beginning of this study (see subsection 1.5.6).

[1]See for example `http://earthobservatory.nasa.gov/Study/BorealMigration` for evidence on ecotonal shifts involving the Boreal Forest

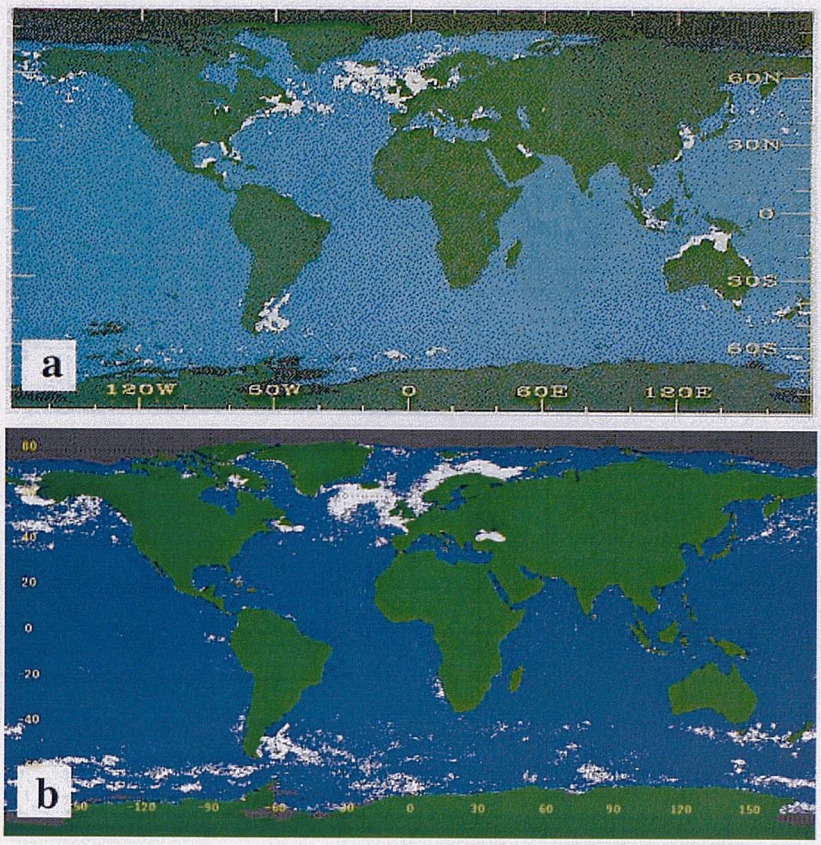

Figure 6.3: *E. huxleyi* classified blooms from a) CZCS mission composite (1978-1986), after Brown & Yoder (1994); and b) SeawiFS composite (1997-2002), courtesy of Chris Brown.

6.9 Summary

Several important results have been obtained with this study. The occurrences of *E. huxleyi* blooms in the Bering Sea (the previous absence of which was assumed on the basis of "non-reported blooms", i.e. on anecdotal reports from fishermen, T. Whitledge, personal communication) have been scientifically investigated with remote sensing techniques. *E. huxleyi* appeared to have arrived in the Bering Sea gradually. In fact, a small precursor bloom taking place in 1996 has been discovered. Observation suggest that alkaline phosphatase activity, which should give an advantage to this species under limiting phosphorus conditions (or at N:P ratios higher than the Redfield ratio) did not play any role in the Bering Sea. An investigation of nutrient and bloom data in the global ocean has also indicated that, in fact, this species may be able to exploit situations with different N:P ratio conditions.

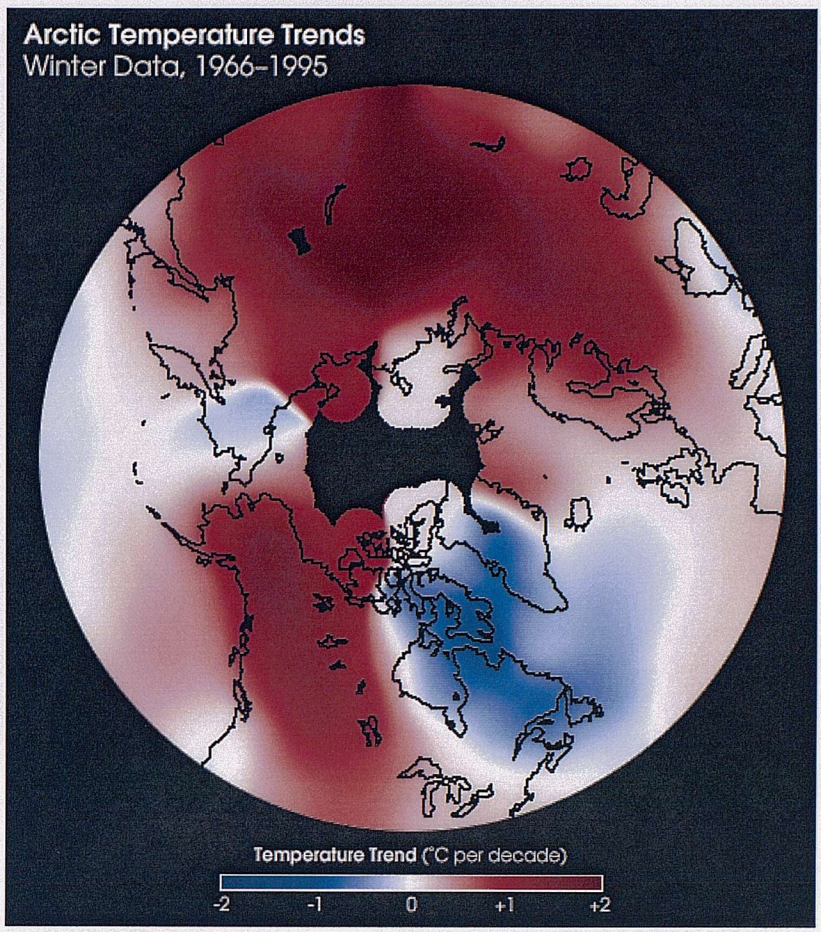

Figure 6.4: Winter temperature trend in the Arctic from 1966 to 1995. The scale is in degrees Celsius per decade. Image courtesy of National Snow and Ice Data Center.

The model results, on the other hand, suggest that climate conditions (clear skies, calmer winds, higher SST) have been important in allowing *E. huxleyi* to have such a dramatic success in 1997. The model also clearly indicates selective diatom grazing by microzooplankton (during the *E. huxleyi* blooms) as a possibly crucial factor for *E. huxleyi* seasonal persistence. Furthermore, it has been shown that periods of high abundance of this species always coincide with high calcite saturation state, after the spring diatom bloom. There is an ecologically important aspect suggested by these last results: weakly silicified frustules and high saturation state may be important controlling factors in the dynamics of diatom-coccolithophore succession through microzooplankton grazing. High $pCO_{2(sea)}$ predicted by the model within *E. huxleyi* blooms confirms that in such locations there may be a shift from sink to source of CO_2 ($pCO_{2(sea)} > pCO_{2(air)}$). The model is limited by the knowledge of the parameters involved in the different simulated processes. Nonetheless, this study is

a first attempt in trying to understand the functioning of a complex ecosystem like the Bering Sea during years of anomalous forcing. Finally, it has been pointed out that in coincidence with increasing Arctic temperatures, there has been an increased *E. huxleyi* activity at high latitudes. If confirmed, this will be the first evidence in the ocean of a species "on the move" in response to global warming.

Chapter 7

Conclusions

7.1 Summary of results

Anomalous climatic conditions in the Bering Sea during spring and summer 1997 caused a series of biological disruptions. Qualitative studies (Overland *et al.*, 2001; Stabeno *et al.*, 2001) have hypothesised that the anomalies in the local weather were due to a combination of three factors: 1) the Pacific decadal oscillation (PDO) in its warm phase; 2) a strong blocking ridge of higher-than-normal atmospheric pressure over the Gulf of Alaska (a monthly oscillation), which prevented weather systems from propagating towards the eastern Bering Sea; and 3) the strongly positive El Niño Southern Oscillation (ENSO) signal of 1997/98, which resulted in warmer and drier weather over the North Pacific and Alaska. Calm winds and reduced cloud cover in spring 1997 produced a very shallow mixed layer depth and SST raised 4 °C above the climatological mean in the southeastern Bering Sea (Stabeno *et al.*, 2001). By summer, most of the Bering Sea continental shelf was covered by an extensive (more than 200,000 km^2) and intensive (as high as 2.1-2.8x10^6 cells L^{-1}) bloom of the coccolithophore *E. huxleyi* (Sukhanova & Flint, 1998; Vance *et al.*, 1998). Such an event had never before been reported in this region. The characteristic milky waters, due to the calcium carbonate plates of the coccolithophore scattering light, were visible from September onwards to the newly launched SeaWiFS instrument.

The study presented here addressed the reasons both for the arrival and for the unusual seasonal persistence (from 3 to 4 months) of *E. huxleyi* in the Bering Sea ecosystem. Initially, archived satellite imagery were closely examined in order to ascertain whether the reported appearance of *E. huxleyi* in 1997 was indeed a new phenomenon for the area. CZCS and AVHRR images from 1978 to 1995 suggested the absence of *E. huxleyi* blooms in this period. The massive appearance of this species in 1997 coincided with both PDO and ENSO positive summer indices. Interestingly, a similar climatic condition took also place in 1987 but without any apparent *E. huxleyi* activity, according to the present study. This indicates the importance of other accompanying factors in stimulating the blooms in the Bering Sea such as, for example, the monthly oscillation mentioned above. The satellite imagery study revealed also that a small bloom of *E. huxleyi* took place in the Bering Sea in 1996. This discovery advances our understanding of how, and on what time scales, climate changes may impact on the Bering Sea ecosystem. In other words, the 'on/off' behaviour of the ecosystem (proposed by Napp & Hunt Jr, 2001) is not supported by this study (at least with respect to the occurrence of *E. huxleyi* blooms). Such insights are important if we are to understand for instance how global warming will increase stratification in high latitude seas and thereby affect bloom frequency in the future. The interannual *E. huxleyi* bloom dynamics (no blooms up to 1995, a small bloom in 1996 and big blooms from 1997 to 2000) identified by remote sensing tools represent important information for the part of this study related to modelling.

A 1/2-dimensional time-dependent phytoplankton competition model was developed for the Bering Sea, which included two main assumptions: 1) all phytoplankton are photoinhibited except *E. huxleyi* (Platt *et al.*, 1980; Kirk, 1994; Nanninga & Tyrrell, 1996), and 2) microzooplankton selectively graze diatoms rather than *E. huxleyi* at low silicate concentrations, $< 3\,\mu$M, (Olson & Strom, 2002). Results suggest that these two factors, photoinhibition and microzooplankton selective grazing, are responsible respectively for *E. huxleyi* increased activity and seasonal persistence.

A simple model experiment (Fig. 4.8) indicated that the unusual weather conditions of 1997, resulting in calmer winds, higher PAR, higher SST and shallower MLD, played an important role in generating the *E. huxleyi* bloom. The investigation of different selective grazing scenarios (Fig. 5.1), according to the general principle that selective predation can regulate the net increase of certain phytoplankton at certain times of the year, highlighted the impact that microzooplankton can have on diatoms under low silicate conditions. However, it is also possible that diatoms were the most abundant preferred food in the presence of unpalatable *E. huxleyi*, and low silicate conditions were simply coincidental with summer conditions.

The important ability of *E. huxleyi* to thrive in water conditions with high N:P ratios (Riegman *et al.*, 2000), which has been considered a crucial factor for the success of this species in past modelling studies (Aksnes *et al.*, 1994; Tyrrell & Taylor, 1996), did not have any relevance in the Bering Sea. A more detailed analysis of bloom conditions in most of the locations where this species is commonly found, and of mesocosm experiments, supports this conclusion. Indeed, this study suggests that *E. huxleyi* is able to exploit situations where either phosphorus or nitrogen is limiting to competing species. This result also suggests that *E. huxleyi*'s high phosphorus affinity should not be an *a priori* driving factor in ecosystem models that include this species.

Motivated by recent evidence that increasing sea water acidification (Caldeira & Wickett, 2003), due to increasing CO_2 concentrations in the atmosphere, may cause a calcification slowdown of the most important calcifying organisms (Kleypas *et al.*, 1999; Riebesell *et al.*, 2000; Spero *et al.*, 1997), the relation between phytoplankton seasonal succession and the relevant carbonate variables has also been a focus of this study. The increase of CO_2 in seawater translates to a decrease of carbonate ion concentration, $[CO_3^{2-}]$, (Zeebe & Wolf-Gladrow, 2001). The calcite saturation state (Ω_{cal}), mainly dependent on the carbonate ion concentration in today's ocean, is not only the crucial parameter driving dissolution processes in seawater but it also impacts on the ability of calcifying organisms to form $CaCO_3$ (Kleypas *et al.*,

1999; Riebesell *et al.*, 2000; Spero *et al.*, 1997). Given the strong latitudinal correlation between temperature and aragonite and calcite saturation states (Opdyke & Wilkinson, 1990, 1993), it was hypothesised at the beginning of this study that the big SST rise in the Bering Sea in 1997 might have affected the calcite saturation state so as to make it easier for *E. huxleyi* to synthesise more strongly calcified coccoliths. However, this hypothetical effect (i.e. higher temperature $\Rightarrow$ higher calcite saturation state) was not confirmed by the model results for 1997 (Fig. 4.10). Instead, it was shown that the period of high *E. huxleyi* abundance always coincides with high calcite saturation state, typically after the spring diatom bloom (due to the drawdown of DIC), and that the magnitude of the seasonal peak of Ω_{cal} depends on the intensity of spring blooms (Fig. 4.10).

A new mechanism, which is suggested to be at work in the Bering Sea during the blooms of *E. huxleyi*, is therefore put forward as potentially responsible for the typical diatom-coccolithophore succession sequence observed in regions with strong seasonal cycles: **"microzooplankton grazing responds to frustule silicification and coccosphere calcification"** so that lightly (or heavily) silicified frustules make diatoms susceptible of higher (or lower) grazing pressure by microzooplankton and lightly (or heavily) calcified coccospheres make coccolithophore susceptible of higher (or lower) grazing pressure by microzooplankton.

7.2 Challenging aspects of this study

Two parts of the present work will be considered in this section: the satellite imagery investigation (from 1978 to 1996) and the modelling studies.

The satellite investigation has two main caveats: the temporal coverage provided by the satellites and the ability of the instruments to detect *E. huxleyi* blooms. The latter is a function of weather conditions (i.e. presence of cloud) and sensor sensitivity. Due to various instrument and power problems, CZCS data collection rates varied greatly over the life of the CZCS mission, as did the spatial distribution which

was non-uniform and highly variable[1]. Moreover, CZCS scenes with excessively high aerosol content or cloud cover were excluded during an initial browsing. In total, 177 daily composites from 1978 to 1986 were examined but with a highly variable number of scenes per year. AVHRR temporal coverage was much more consistent than CZCS and hence it was possible to examine an average of 3 daily scenes per day from June to October during 1987-1996 (for a total of about 4,500 images). Therefore, CZCS temporal coverage and cloudiness was the main limitation of this study. The fact of not having detected *E. huxleyi* blooms in the Bering Sea from 1978 to 1995 cannot be considered as proof of the "absence" of this species throughout the whole time interval.

Simulation modelling allows one to integrate many factors, processes, and interactions in a framework that can greatly assist in addressing important questions. Nonetheless, there are many uncertainties in this exercise. A key problem in ecosystem modelling is that there is no single modelling approach, or even a single model that can include all relevant processes (and scales). Furthermore, although ecosystem modelling presents its own challenges, the utilization of observations also has its own problems. Measurements and modelled concentrations are often expressed in different units. Conversion factors are then required but are often poorly known. Measured concentrations and rates can be overestimated or underestimated as a result of the measurement technique. Ecosystem models are also affected by the difficulty of constraining a large number of biogeochemical, physiological and physical parameters. All these complications must be taken in mind when interpreting model results. The main aim of this study has been to simulate the interannual pattern of *E. huxleyi* bloom occurrences from 1995 to 2001 so that it is consistent with observations. A crucial limit to this target was set by the lack of knowledge of the inter-annual variability of the important environmental conditions affecting the ecosystem. However, a simple experiment and several tests have provided possible answers to the questions posed at the beginning of this work.

[1] More detailed information on CZCS temporal and spatial resolution and coverage can be found at `http://daac.gsfc.nasa.gov/CAMPAIGN_DOCS/OCDST/CZCS_Starter_kit.html`.

A final remark. Despite all the modelling challenges, this study "offers" some explanations on the base of certain assumptions, which in turn are derived from observations. It is certainly arguable whether the explanations can be trusted. But yet, can those assumptions be trusted? A model can never be better than the modeller's understanding of the system. As Botkyn (1977) nicely put it:

> *"By operating the model the computer faithfully and faultlessly demonstrates the implications of our assumptions and information. It forces us to see the implications, true or false, wise or foolish, of the assumptions we have made. It is not so much that we want to believe everything that the computer tells us, but that we want a tool to confront us with the implications of what we think we know".*

7.3 Ideas for future work

With the work presented here a new ecological factor as a possible cause of phytoplankton succession has been introduced which opens an exciting ground of research connected to its experimental testing. It was proposed that the typical diatom-coccolithophore succession sequence may be driven by seasonal variation in frustule and coccosphere thickness. After the spring diatom bloom, when dissolved silicate concentrations are very low, the diatom intra-specific competition should favour those species with weakly silicified frustules. The ability of *E. huxleyi* to build up strongly calcified coccoliths may be crucial for this species at this time of the year[2]. This ability may in fact be the factor influencing microzooplankton grazing selection. Some evidence, as discussed previously, supports this mechanism. An interesting experiment therefore would be the setting up of such a microzooplankton-diatom-*E. huxleyi* system, in a culture or in a mesocosm environment.

A literature survey of the N:P ratio conditions during *E. huxleyi* blooms has shown that this species is able to exploit situations with different nutrient limita-

[2]Note, however, that despite previously being considered as a possibility, the role of coccoliths as a protection against grazing has never yet been demonstrated (Young, 1994)

tions. However, little is known on the utilization of organic forms of either nitrogen or phosphorus. A sampling campaign targeted to the understanding of this feature may certainly help to clarify the nutrient requirements of this species.

Is *E. huxleyi* on the move towards more northern latitudes? Some evidence suggests that increased *E. huxleyi* in high latitude seas may not be limited to the Bering Sea. Such a phenomenon, if confirmed, might have dramatic implications for the future of high latitude seas' ecosystems. A sampling campaign, in order to ground-proof satellite evidence, is certainly desirable for those regions suspected of being the place of an augmented activity of this species in recent years. More modelling studies such as the one presented here may also help in understanding the relations between the carbonate system and the occurrences of this species on a global scale.

In conclusion, some of the complex interactions among phytoplankton, zooplankton and their environment in the Bering Sea have been elucidated by this study. Nevertheless, in order to explore further the findings reported here, it is important that detailed time-series measurements of photosynthetically active radiation and nutrients, along with phytoplankton species abundance and their N- or C-content, are made so that the results of studies such as this one can be substantiated further. Moreover, a grazing experiment where a microzooplankton-diatom-*E. huxleyi* system can be investigated at different dissolved silicon concentrations and degree of calcite saturation state is desirable.

Appendix A

Carbon chemistry in seawater

When gaseous CO_2 dissolves in water, it first gets hydrated to form aqueous carbon dioxide, $CO_{2(aq)}$, which reacts with water to form carbonic acid, H_2CO_3. This acid can then dissociate in two steps to form bicarbonate, HCO_3^-, and carbonate, CO_3^{2-}, ions. These reactions are very fast, so that for all practical purposes it can be assumed that thermodynamic equilibrium between the species is established. These four reactions can be summarised as follows:

$$\begin{aligned} CO_{2(aq)} &\rightleftharpoons CO_2 \\ CO_2 + H_2O &\rightleftharpoons H^+ + HCO_3^- \\ HCO_3^- &\rightleftharpoons H^+ + CO_3^{2-} \\ H_2O &\rightleftharpoons H^+ + OH^- \end{aligned}$$

Since it is very difficult to distinguish analytically between the two species $CO_{2(aq)}$ and H_2CO_3, it is usual to combine the two together and express this sum as the concentration of a hypothetical species, CO_2^* (Zeebe & Wolf-Gladrow, 2001). The

equilibrium relationships of the reactions outlined above are given by:

$$k_0 = \frac{[CO_2^*]}{[CO_{2(aq)}]} \tag{A.1}$$

$$k_1 = \frac{[H^+][HCO_3^-]}{[CO_2^*]} \tag{A.2}$$

$$k_2 = \frac{[H^+][CO_3^{2-}]}{[HCO_3^-]} \tag{A.3}$$

$$k_w = [H^+][OH^-] \tag{A.4}$$

$[CO_2^*]$ can be expressed as:

$$[CO_2^*] = S_{CO_2} pCO_2 \tag{A.5}$$

where S_{CO_2} is the solubility of CO_2 in seawater. The value of S_{CO_2} can be computed using the expression given by Weiss (1974):

$$\begin{aligned} \ln S_{CO_2} = & -60.2409 + \frac{9345.17}{T_K} + 23.3585 \ln\left(\frac{T_K}{100}\right) + \\ & +0.023517S - 0.023656S\left(\frac{T_K}{100}\right) + 0.0047036S\left(\frac{T_K}{100}\right)^2 \end{aligned}$$

where T_K is temperature in Kelvin, S is salinity and ln is the natural logarithm. The values for k_1 and k_2 are computed using the expressions for the data obtained by Mehrbach *et al.* (1973) and by Millero (1995):

$$\log k_1 = 13.7201 - 0.031334T_K - \frac{3235.76}{T_K} - 1.3\ 10^{-5} S\ T_K + 0.1032(S)^{1/2} \tag{A.6}$$

$$\begin{aligned} \log k_2 = & -5371.9645 - 1.671221T_K + \frac{128375.28}{T_K} + 2194.3055 \log T_K - 0.22913S \\ & -18.3802 \log S + 8.0944\ 10^{-4} S\ T_K + 5617.11\frac{\log S}{T_K} - 2.136\frac{S}{T_K} \end{aligned} \tag{A.7}$$

$$\begin{aligned} -\ln K_w = & 148.96502 + \frac{-13847.26}{T_k} - 236521 \ln T_k + \\ & \left(-5.977 + \frac{118.67}{T_K} + 1.0495 \ln T_K\right) S^{1/2} - 0.01615S \end{aligned} \tag{A.8}$$

where log represents the base 10 logarithm. The CO_2 system so far consists of 6

unknowns (pCO_2, $[CO_2^*]$, $[HCO_3^-]$, $[CO_3^{2-}]$, $[H^+]$ and $[OH^-]$) and four equations (A.1, A.2, A.3 and A.4). In order to determine the system, any two of the six unknowns have to be specified. The two parameters used in models are dissolved inorganic carbon and total alkalinity, defined as:

$$[DIC] = [CO_2^*] + [HCO_3^-] + [CO_3^{2-}] \quad \text{(A.9)}$$

$$[Alk] = [HCO_3^-] + 2[CO_3^{2-}] + [OH^-] - [H^+] + [B(OH)_4^-] + \text{minor bases} \quad \text{(A.10)}$$

where $[OH^-]$ is the concentration of hydroxide ion, and $[B(OH)_4^-]$ is the concentration of the borate ion. The total alkalinity is a measure of the excess of bases (protons acceptors) over acids (proton donors), and is operationally defined by the titration with H^+ of all weak bases present in the solution (Dickson, 1981). Alternatively, total alkalinity can be viewed as the charge balance of all strong acids and bases unaffected by this titration, i.e.:

$$[Alk] = [Na^+] + [K^+] + 2[Mg^{2+}] + 2[Ca^{2+}] + \text{minor cations} - [Cl^-] - 2[SO_4^{2-}] - [Br^-] - [NO_3^-] - \text{minor anions} \quad \text{(A.11)}$$

The contribution of variations in the concentration of the minor bases like phosphate, silicate, and sulphate to the variations in total alkalinity are usually well below one percent, and therefore their contribution is neglected. The definition of dissolved inorganic carbon and total alkalinity introduces three new unknowns ($[DIC]$, $[Alk]$ and $[B(OH)_4^-]$) for a total of 9, but only two equations for a total of 6. Additional constraints on the system of equations are needed. Borate is formed by the dissociation of boric acid by the reaction:

$$H_3BO_3 + H_2O \rightleftharpoons H^+ + B(OH)_4^- \quad \text{(A.12)}$$

with the dissociation constant:

$$k_B = \frac{[H^+][B(OH)_4^-]}{[H_3BO_3]} \tag{A.13}$$

k_B is computed using (Dickson, 1990):

$$\begin{aligned} -\ln k_B = {} & (-8966.9 - 2890.53S^{1/2} - 77.942S + 1.728S^{3/2} - 0.0996S^2)\frac{1}{T_K} \\ & 148.0248 + 137.1942S^{1/2} + 1.62142S + 0.053105S^{1/2}T_K \\ & +(-24.4344 - 25.085S^{1/2} - 0.2474S)\ln T_K \end{aligned} \tag{A.14}$$

The total boron concentration is nearly conservative within the ocean and its concentrations changes only with net exchange of water at the sea surface by evaporation and precipitation. Since these processes control salinity, the total boron concentration can be assumed to be proportional to the salinity, S (Millero, 1996):

$$[B(OH)_4^-] + [H_3BO_3] = 1.2\ 10^{-5}\ S \tag{A.15}$$

Equations A.13 and A.15 add two new equations and one new unknown, H_3BO_3. There are now 8 equations and ten unknowns. Again the specification of two unknowns completely determines the carbon system. The system of eight equations cannot be solved analytically, because a higher order polynomial equation has to be solved. Iterative methods are commonly used (see for example Peng *et al.*, 1987).

Solving the equations for global mean surface seawater properties (i.e. by using mean values of temperature, salinity, DIC, Alk, pCO_2, CO_2^*, HCO_3^- and CO_3^{2-} in the world oceans based on data collected during the GEOSECS campaign, Takahashi *et al.*, 1981) yields:

$$\begin{aligned} [DIC] &= [CO_2^*] + [HCO_3^-] + [CO_3^{2-}] \\ &= 0.5\% + 88.6\% + 10.9\% \end{aligned}$$

$$\begin{aligned}
[Alk] &= [HCO_3^-] + 2[CO_3^{2-}] + [OH^-] - [H^+] + [B(OH)_4^-] \\
&= 76.8\% + 18.8\% + 0.2\% + 4.2\%
\end{aligned}$$

This shows that only a very small fraction of the dissolved inorganic carbon exists as dissolved CO_2, and that the majority of the carbon exists as bicarbonate ion and a smaller amount in the form of carbonate ion, therefore, DIC can be approximated as the sum of bicarbonate and carbonate ions only:

$$[DIC] \approx [HCO_3^-] + [CO_3^{2-}] \tag{A.16}$$

This computation also reveals that the contribution of the dissociation of water to variations in alkalinity is negligible and that the contribution of borate is of the order of a few percent. Therefore, alkalinity can be reasonably well approximated by the carbonate alkalinity, i.e.:

$$[Alk] \approx [\text{carbonate alkalinity}] = [HCO_3^-] + 2[CO_3^{2-}] \tag{A.17}$$

Combining equations A.16 and A.17, the concentration of bicarbonate and carbonate can be expressed in terms of DIC and Alk:

$$\begin{aligned}
[HCO_3^-] &\approx 2[DIC] + [Alk] \\
[CO_3^{2-}] &\approx [Alk] - [DIC]
\end{aligned}$$

Appendix B

Anderson's model for light attenuation

The phytoplankton groups of this model are assumed to respond to light according to the Michaelis-Menten function. A numerical integral through depth is used to calculate the averaged limitation. The total limitation is then given by the following:

$$\psi(I) = \frac{1}{M} \int_0^M \frac{I(z)}{I_h + I(z)} \, \mathrm{d}z \tag{B.1}$$

where M is the mixed layer depth and I_h is the light half-saturation constant (see, however, subsection 2.3.1). The most frequently used form of attenuation of photosythetically active radiation (PAR) in ecosystem models (see, for instance, Fasham, 1993, 1995) is probably expressed by the Beer's law: $I(z) = I_0 \, e^{-k_{par} z}$, with z actual depth; I_0 being the PAR just beneath the surface and calculated by means of astronomical formulae and then assuming a clear or cloudy sky (Kirk, 1994); k_{par} the vertical attenuation coefficient. But this single exponential is a poor approximation of the irradiance distribution since k_{par} is influenced by several different components of the optical system like water, phytoplankton and other substances. Red wavelengths, for instance, are almost completely extinguished in the top few metres of the water, and so attenuation is higher for this case. The most accurate

method to compute the attenuation of light through depth is perhaps (Simpson & Dickey, 1981) to divide the PAR into a large number of spectral wavebands, each of which is independently attenuated. This has been achieved with Morel's model (Morel, 1988) where the photosynthetic spectrum is split in 61 wavebands. In order to reduce the computation time that is required by Morel's model, Anderson (1993) introduced a numerical approximation of it, where the water column is divided into three homogeneous vertical layers and thus the attenuated light as a function of depth and vertical pigment profile is given by:

$$I(z) = I_0 \; exp\left\{\sum_{i=1}^{r-1}[-k_i(u_i - u_{i-1})]\right\} \; exp\left\{[-k_r(z - u_{r-1})]\right\} \tag{B.2}$$

with z in the r^{th} layer, $r > 1, u_0 = 0, u_1 = 5$ and $u_2 = 23$

k_i (with $i = 1, 2, 3$), which depend on the pigment concentration, were found to be:

$$k_i = b_{0,i} + b_{1,i}c + b_{2,i}c^2 + b_{3,i}c^3 + b_{4,i}c^4 + b_{5,i}c^5 \tag{B.3}$$

where $c = G^{1/2}$ mg m^{-3} is the square root transformation of the pigment concentration to ensure a bias toward smaller values which are more frequently encountered in nature. The b coefficients were obtained by Anderson (1993) by running Morel's model and then by looking at the least squares best-fit values with equation B.2.

Note, therefore, that the light attenuation in relation to varying chlorophyll is given by G but the attenuation in relation to coccolith concentrations is neglected for the reasons explained in subsection 1.5.4.

References

Aksnes, D.L., Egge, J.K., Rosland, R. & Heimdal, B.R. (1994). Representation of *Emiliania huxleyi* in phytoplankton simulation models. A first approach. *Sarsia*, **79**, 291–300.

Aksnes, D.L., Ulvestad, K.B., Baliño, B.M., Berntsen, J., Egge, J.K. & Svendsen, E. (1995). Ecological modelling in coastal waters: towards predictive physical-chemical-biological simulation models. *Ophelia*, **41**, 5–36.

Anderson, T.R. (1993). A spectrally averaged model of light penetration and photosynthesis. *Limnology and Oceanography*, **38**, 1,403–1,419.

Anonymous (2002). Data record of the oceanographic observations and exploratory fishing. Tech. Rep. 41, 42 (part 2), 43, 44, 45, Faculty of Fisheries, Hokkaido University, Hakodate, Japan.

Archer, S.D., Widdecombe, C.E., Tarran, G.A., Rees, A.P. & Burkill, P.H. (2001). Production and turnover of particulate dimethylsulphonioprionate during a coccolithophore bloom in the northern North Sea. *Aquatic Microbial Ecology*, **24**, 225–241.

Baduini, C.L., Hyrenbach, K.D., Coyle, K.O., Pinchuk, A., Mendenhall, V. & Hunt Jr, G.L. (2001). Mass mortality of short-tailed shearwaters in the south-eastern Bering Sea during summer 1997. *Fisheries Oceanography*, **10**, 117–130.

Baith, K., Linsday, R., Fu, G. & McClain, C.R. (2001). SeaDAS: data analysis system developed for ocean color satellite sensors. *EOS Transactions of the American Geophysical Union*, **82**, 202–205.

Balch, W.M., Holligan, P.M., Ackleson, S.G. & Voss, K.J. (1991). Biological and optical properties of mesoscale coccolithophore blooms in the Gulf of Maine. *Limnology and Oceanography*, **36**, 629–643.

Balch, W.M., Holligan, P.M. & Kilpatrick, K.A. (1992). Calcification, photosynthesis and growth of the bloom-forming coccolithophore, *Emiliania huxleyi. Continental Shelf Research*, **12**, 1,353–1,374.

Balch, W.M., Kilpatrick, K.A., Holligan, P.M. & Cucci, T. (1993). Coccolith production and detachment by *Emiliania huxleyi* (Prymnesiophyceae). *Journal of Phycology*, **29**, 566–575.

Berge, G. (1962). Discolouration of the sea due to *Coccolithus huxleyi* "bloom". *Sarsia*, **6**, 27–40.

Berman, T. & Bronk, D.A. (2003). Dissolved organic nitrogen: a dynamic partner in aquatic ecosystems. *Aquatic Microbial Ecology*, **31**, 279–305.

Berry, L., Taylor, A.R., Lucken, U., Ryan, K.P. & Brownlee, C. (2002). Calcification and inorganic carbon acquisition in coccolithophores. *Functional Plant Biology*, **29**, 289–299.

Birkenes, E. & Braarud, T. (1952). Phytoplankton in the Oslo Fjord during a *"Coccolithus huxleyi*-summer*"*. *Avh. Nor. Videnskap. Akad. Oslo*, **2**, 1–23.

Botkyn, D.B. (1977). Life and death in a forest community: the computer as an aid to understanding. In C. Hall & J. Day, eds., *Models as ecological tools: Theory and case histories*, 213–234, Wiley, New York.

Brand, L.E. (1994). Physiological ecology of marine coccolithophores. In A. Winter & W.G. Siesser, eds., *Coccolithophores*, 39–49, Cambridge University Press.

Brodeur, R.D., Sugisaki, H. & Hunt Jr., G.L. (2002). Increases in jellyfish biomass in the Bering Sea: implications for the ecosystem. *Marine Ecology Progress Series*, **233**, 89–103.

Broecker, W.S. (1974). *Chemical Oceanography*. Harcourt Brace Jovanovich, Ins., Mew York.

Broecker, W.S. & Takahashi, T. (1984). Is there a tie between atmospheric CO_2 content and ocean circulation? In J.E. Hansen & T. Takahashi, eds., *Climate processes and climate sensitivity*, 314–326, American Geophysical Union, Washington D.C.

Broerse, A.T.C., Tyrrell, T., Young, J.R., Poulton, A.J., Merico, A., Balch, W.M. & Miller, P.M. (2003). The cause of bright waters in the Bering Sea in winter. *Continental Shelf Research*, **23**, 1579–1596.

Brown, C.W. & Yoder, J.A. (1993). Blooms of *Emiliania huxleyi* (Prymnesiophyceae) in surface waters of the Nova Scotian shelf and the Grand Bank. *Journal of Plankton Research*, **15**, 1429–1438.

Brown, C.W. & Yoder, J.A. (1994). Coccolithophorid blooms in the global ocean. *Journal of Geophysical Research*, **99**, 7,467–7,482.

Brownlee, C. & Taylor, A. (2003). Calcification in coccolithophores: A cellular perspective. In H.R. Thierstein & J.R. Young, eds., *Coccolithophore: from molecular processes to global impact*, Springer-Verlag, Germany, IN PRESS.

Brzezinski, M.A. (1985). The Si:C:N ratio of marine diatoms: interspecific variability and the effect of some environmental variables. *Journal of Phycology*, **21**, 347–357.

Burkill, P.H., Mantoura, R., Llewellyn, C.A. & Owens, N.J.P. (1987). Microzooplankton grazing and selectivity of phytoplankton in coastal waters. *Marine Biology*, **93**, 581–590.

Burkill, P.H., Archer, S.D., Robinson, C., Nightingale, P.D., Groom, S.B., A., G. & Zubkov, M.V.T. (2002). Dimethyl sulphide biogeochemistry within a coccolithophore bloom (DISCO): an overview. *Deep-Sea Research Part II*, **49**, 2863–2885.

Caldeira, K. & Wickett, M.E. (2003). Anthropogenic carbon and ocean pH. *Nature*, **425**, 365–365.

Coachman, L.K. (1986). Circulation, water masses, and fluxes on the southeastern Bering Sea shelf. *Continental Shelf Research*, **5**, 23–108.

Codispoti, L.A., Friederich, G.E. & Hood, D.W. (1986). Variability in the inorganic carbon system over the southeastern Bering Sea shelf during spring 1980 and spring-summer 1981. *Continental Shelf Research*, **5**, 133–160.

Cokacar, T., Kubilay, N. & Oguz, T. (2001). Structure of *Emiliania huxleyi* blooms in the Black Sea surface waters as detected by SeaWiFS imagery. *Geophysical Research Letters*, **28**, 4607–4610.

Cokacar, T., Oguz, T. & Kubilay, N. (2003). Satellite-detected early summer coccolithophore blooms and their interannual variability in the Black Sea. *Deep-Sea Research Part I*, SUBMITTED.

Denman, K.L. (2003). Modelling plankton ecosystems: parameterizing complexity. *Progress in Oceanography*, **57**, 429–452.

Dickson, A.G. (1981). An exact definition of total alkalinity and a procedure for the estimation of alkalinity and total inorganic carbon from titration data. *Deep-Sea Research Part I*, **28**, 609–623.

Dickson, A.G. (1990). Thermodynamics of the dissociation of boric acid in synthetic seawater from 273.15 to 318.15 K. *Deep-Sea Research Part I*, **37**, 755–766.

Dugdale, R.C., Wilkerson, F. & Minas, H.J. (1995). The role of a silicate pump in driving new production. *Deep-Sea Research Part I*, **42**, 697–719.

Edwards, A.M. & Yool, A. (2000). The role of higher predation in plankton population models. *Journal of Plankton Research*, **22**, 1085–1112.

Egge, J.K. & Aksnes, D.L. (1992). Silicate as regulating nutrient in phytoplankton competition. *Marine Ecology Progress Series*, **83**, 281–289.

Egge, J.K. & Heimdal, B.R. (1994). Blooms of phytoplankton including *Emiliania huxleyi* (Haptophyta). Effects of nutrient supply in different N:P ratios. *Sarsia*, **79**, 333–348.

Eppley, R.W. (1972). Temperature and phytoplankton growth in the sea. *Fishery Bulletin*, **70**, 1,063–1,085.

Eslinger, D.L. & Iverson, R.L. (2001). The effect of convective and wind-driven mixing on spring phytoplankton dynamics in the southeastern Bering Sea middle shelf domain. *Continental Shelf Research*, **21**, 627–650.

Evans, G.T. (1988). A framework for discussing seasonal succession and coexistence of phytoplankton species. *Limnology and Oceanography*, **33**, 1027–1036.

Fasham, M.J.R. (1993). Modelling the marine biota. In M. Heimann, ed., *The global carbon cycle*, vol. I15 of *NATO ASI Series*, 457, Springer-Verlag.

Fasham, M.J.R. (1995). Variations in the seasonal cycle of biological production in subarctic oceans: a model sensitivity analysis. *Deep-Sea Research Part I*, **42**, 1,111–1,149.

Fernández, E., Boyd, P., Holligan, P.M. & Harbour, D.S. (1993). Production of organic and inorganic carbon within a large-scale coccolithophore bloom in the northeast Atlantic ocean. *Marine Ecology Progress Series*, **97**, 271–285.

Fernández, E., Maranon, E., Harbour, D.S., Kristiansen, S. & Heimdal, B.R. (1996). Patterns of carbon and nitrogen uptake during blooms of *Emiliania huxleyi* in two Norwegian fjords. *Journal of Plankton Research*, **18**, 2349–2366.

Fileman, E.S., Cummings, D.G. & Llewellyn, C.A. (2002). Microzooplankton community structure and the impact of microzooplankton grazing during an *Emiliania huxleyi* bloom, off the Devon coast. *Journal of Marine Biological Association*, **82**, 359–368.

Furnas, M.J. (1990). In situ growth-rates of marine phytoplankton as approaches to measurement, community and species growth-rates. *Journal of Plankton Research*, **12**, 1117–1151.

Garcia-Soto, C., Fernández, E., Pingree, R.D. & Harbour, D.S. (1995). Evolution and structure of a shelf coccolithophore bloom in the western English Channel. *Journal of Plankton Research*, **17**, 2011–2036.

Gates, D.M. (1993). *Climate change and its biological consequences*. Sinauer Associates Inc., Sounderland, Massachusetts.

Gattuso, J.P., Allemand, D. & Frankignoulle, M. (1999). Photosynthesis and calcification at cellular, organismal and community levels in coral reefs: A review on interactions and control by carbonate chemistry. *American Zoology*, **39**, 160–183.

Goering, J.J. & Iverson, R.L. (1981). Phytoplankton distribution on the southeastern Bering Sea shelf. In D.W. Hood & J.A. Calder, eds., *The eastern Bering Sea shelf: Oceanography and resources*, vol. 2, 933–946, University of Washington Press.

Gordon, H.R., Boynton, G.C., Balch, W.M., Groom, S.B., Harbour, D.S. & Smyth, T.J. (2001). Retrieval of coccolithophore calcite concentration from SeaWiFS imagery. *Geophysical Research Letters*, **28**, 1587–1590.

Green, J.C., Perch-Nielsen, K. & Westbroek, P. (1990). Prymnesiophyta. In L. Margulis, J.O. Corliss, M. Melkonian & D.J. Chapman, eds., *Handbook of Protoctista*, 293–317, Jones and Bartlett, Boston, Massachusetts.

Groom, S.B. & Holligan, P.M. (1987). Remote sensing of coccolithophore blooms. *Advanced Space Research*, **7**, 73–78.

Haefner, J.W. (1996). *Modeling biological systems: principles and applications.* Chapman and Hall.

Hansen, P.J. & Calado, A.J. (1999). Phagotrophic mechanisms and prey selection in free-living dinoflagellates. *Journal of Eukaryotic Microbiology*, **46**, 382–389.

Hare, S.R. & Mantua, N.J. (2000). Empirical evidence for North Pacific regime shifts in 1977 and 1989. *Progress in Oceanography*, **47**, 103–145.

Harris, R.P. (1994). Zooplankton grazing on the coccolithophore *Emiliania huxleyi* and its role in inorganic carbon flux. *Marine Biology*, **119**, 431–439.

Head, R.N., Crawford, D.W., Egge, J.K., Harris, R.P., Kristiansen, S., Lesley, D.J., Marañón, E., Pond, D. & Purdie, D.A. (1998). The hydrography and biology of a bloom of the coccolithophorid *Emiliania huxleyi* in the northern North Sea. *Journal of Sea Research*, **39**, 255–266.

Holligan, P.M., Viollier, M., Harbour, D.S., Camus, P. & Champagne-Philippe, M. (1983). Satellite and ship studies of coccolithophore production along a continental shelf edge. *Nature*, **304**, 339–342.

Holligan, P.M., Fernández, E., Aiken, J., Balch, W.M., Boyd, P., Burkill, P.H., Finch, M., Groom, S.B., Malin, G., Muller, K., Purdie, D.P., Robinson, C., Trees, C.C., Turner, S.M. & van der Wal, P. (1993a). A biogeochemical study of the coccolithophore, *Emiliania huxleyi*, in the North Atlantic. *Global Biogeochemical Cycles*, **7**, 879–900.

Holligan, P.M., Groom, S.B. & Harbour, D.S. (1993b). What controls the distribution of the coccolithophore, *Emiliania huxleyi*, in the North Sea? *Fisheries Oceanography*, **2**, 175–183.

Honjo, S. (1976). Coccoliths: production, transportation and sedimentation. *Marine Micropaleontology*, **1**, 65–79.

Honjo, S. & Roman, M.R. (1978). Marine copepod faecal pellets: production transportation and sedimentation. *Journal of Marine Research*, **36**, 45–57.

Houghton, J.T., Ding, Y., Griggs, D.J., Noguer, M., van der Linden, P.J., day, X., Maskell, K. & Johnson, C.A., eds. (2001). *Climate change 2001: The scientific basis. Contribution of Working Group I to the Third Assessment Report of the Intergovernmental Panel on Climate Change*, 1–881. Cambridge University Press, U.K.

Hurlburt, E.M. (1990). Description of phytoplankton and nutrient in spring in the western north Atlantic ocean. *Journal of Plankton Research*, **12**, 1–28.

Ietswaart, T., Schneider, P.J. & Prins, R.A. (1994). Utilization of organic nitrogen-sources by 2 phytoplankton species and a bacterial isolate in pure and mixed cultures. *Applied and Environmental Microbiology*, **60**, 1554–1560.

Iglesias-Rodríguez, M.D., Brown, C.W., Doney, S.C., Kleypas, J., Kolber, D., Kolber, Z., Hayes, P.K. & Falkowski, P.G. (2002). Representing key phytoplankton functional groups in ocean carbon cycle models: Coccolithophorids. *Global Biogeochemical Cycles*, **16**, 47–67.

Iida, T., Saitoh, S.I., Miyamura, T., Toratami, M., Fukushima, H. & Shiga, N. (2002). Temporal and spatial variability of the coccolithophore blooms in the eastern Bering Sea. *Progress in Oceanography*, **55**, 165–175.

Indermühle, A., Stocker, T.F., Joos, F., Fisher, H., Smith, H.J., Wahlen, M., Deck, B., Mastroianni, D., Tschumi, J., Blunier, T., Meyer, R. & Stauffer, B. (1999). Holocene carbon-cycle dynamics based on CO_2 trapped in ice at Taylor Dome, Antarctica. *Nature*, **328**, 121–126.

IOCCG (1999). *Status and plans for Satellite Ocean-Colour Missions: Considerations for Complementary Missions. Yoder J. A. (ed.), Reports of the International Ocean-Colour Coordinating Group, No. 2, IOCCG, Dartmouth, Canada.*

Jacobson, D.M. & Anderson, D.M. (1986). Thecate heterotrophic dinoflagellates: feeding behaviour and mechanisms. *Journal of Phycology*, **22**, 249–258.

Kirk, J.T.O. (1994). *Light and photosynthesis in aquatic ecosystems.* Cambridge University Press.

Kleypas, J.A., Buddemeier, R.W., Archer, D., Gattuso, J.P., Langdon, C. & Opdyke, B.N. (1999). Geochemical consequences of increased atmospheric carbon dioxide on coral reefs. *Science*, **284**, 118–120.

Kristiansen, S., Thingstad, T.F., van der Wal, P., Farbrot, T. & Skjoldal, E.F. (1994). An *Emiliania huxleyi* dominated subsurface bloom in Samnangerfjorden, western Norway - Importance of hydrography and nutrients. *Sarsia*, **79**, 357–368.

Kuenzler, E.J. & Perras, J.P. (1965). Phosphatases of marine algae. *Biological Bulletin*, **128**, 271–284.

Lampert, L., Queguiner, B., Labasque, T., Pichon, A. & Lebreton, N. (2002). Spatial variability of phytoplankton composition and biomass on the eastern continental shelf of the Bay of Biscay (north-east Atlantic ocean). Evidence for a bloom of *Emiliania huxleyi* (Prymnesiophyceae) in spring 1998. *Continental Shelf Research*, **22**, 1225–1247.

Langdon, C., Takahashi, T., Sweeny, C., Chipman, D., Goddard, J., Marubini, F., Aceves, H., Barnett, H. & Atkinson, M.J. (2000). Effect of calcium carbonate saturation state on the calcification rate of an experimental coral reef. *Global Biogeochemical Cycles*, **14**, 639–654.

Le Fevre, J., Viollier, M., Corre, P.L., Dupouy, C. & Grall, J.R. (1983). Remote sensing observation of biological material by Landsat along a tidal thermal front and their relevancy to the available field data. *Estuarine, Coastal and Shelf Science*, **16**, 37–50.

Lessard, E.J. & Murrell, M.C. (1998). Microzooplankton herbivory and phytoplankton growth in the northwestern Sargasso Sea. *Aquatic Microbial Ecology*, **16**, 173–188.

Lessard, E.J., Merico, A. & Tyrrell, T. (2003). NO3:PO4 ratios and *Emiliania huxleyi* blooms. *Limnology and Oceanography*, SUBMITTED.

Levasseur, M., Michaud, S., Egge, J., Cantin, G., Nejstgaard, J.C., Sanders, R., ans P. T. Solber, E.F., Heimdal, B. & Gosselin, M. (1996). Production of DMSP and DMS during a mesocosm study of an *Emiliania huxleyi* bloom: influence of bacteria and *Calanus finmarchicus* grazing. *Marine Biology*, **126**, 609–618.

Macklin, S.A. (1999). Report on the FOCI International Workshop on recent condition in the Bering Sea. Tech. rep., Pacific Marine Environmental Laboratory, Seattle, WA, NOAA ERL Special Report.

Magley, W.C. (1990). *A phytoplankton-zooplankton model of the middle and outer shelf domains of the Bering Sea shelf during spring bloom conditions*. Ph.D. thesis, Florida State University.

Malin, G., Turner, S., Liss, P., Holligan, P.M. & Harbour, D. (1993). Dimethylsulphide and dimethylsulphoniopropionate in the northeast Atlantic during the summer coccolithophore bloom. *Deep-Sea Research Part I*, **40**, 1487–1508.

McIntyre, A. (1967). Coccoliths as paleoclimatic indicators of Pleistocene glaciation. *Science*, **158**, 1314–1317.

McRoy, C.P., Hood, D.W., Coachman, L.K., Walsh, J.J. & Goering, J.J. (1986). Processes and resources on the Bering Sea shelf (PROBES): the development and accomplishments of the project. *Continental Shelf Research*, **5**, 5–21.

Medlin, L.K., Barker, G.L.A., Campbell, L., Green, J.C., Hayes, P.K., Marie, D., Wrieden, S. & Vaulot, D. (1996). Genetic characterisation of *Emiliania huxleyi* (Haptophyta). *Journal of Marine Systems*, **9**, 13–31.

Mehrbach, C., Culberson, C.H., Hawley, J.E. & Pytkowicz, R.M. (1973). Measurement of the apparent dissociation constants of carbonic acid in seawater at atmospheric pressure. *Limnology and Oceanography*, **18**, 897–907.

Menden-Deuer, S. & Lessard, E. (2000). Carbon to volume relationships for dinoflagellates, diatoms and other protist plankton. *Limnology and Oceanography*, **45**, 569–579.

Merico, A., Tyrrell, T., Brown, C.W., Groom, S.B. & Miller, P.I. (2003a). Analysis of satellite imagery for *Emiliania huxleyi* blooms in the Bering Sea before 1997. *Geophysical Research Letters*, **30**, 1337–1340.

Merico, A., Tyrrell, T., Lessard, E.J., Oguz, T., Stabeno, P.J., Zeeman, S.I. & Whitledge, T.E. (2003b). Modelling the Bering Sea shelf ecosystem: role of climate influences and trophic interactions in generating *Emiliania huxleyi* blooms 1997-2000. *Deep-Sea Research Part I*, SUBMITTED.

Mihnea, P.E. (1997). Major shifts in the phytoplankton community (1980-1994) in the Romanian Black Sea. *Oceanologica Acta*, **20**, 119–129.

Millero, F.J. (1995). Thermodynamics of the carbon dioxide system in the oceans. *Geochimica et Cosmochimica Acta*, **59**, 661–677.

Millero, F.J. (1996). *Chemical Oceanography*. Marine Scince Series, CRC Press, 2nd edn.

Milliman, J.D., Troy, P.J., Balch, W.M., Adams, A.K., Li, Y.H. & Mackenzie, F.T. (1999). Biologically mediated dissolution of calcium carbonate above the chemical lysocline? *Deep-Sea Research Part I*, **46**, 1653–1669.

Morel, A. (1988). Optical modelling of the upper ocean in relation to its biogenous matter content (case 1 waters). *Journal of Geophysical Research*, **93**, 10,749–10,768.

Murata, A. & Takizawa, T. (2002). Impact of a coccolithophorid bloom on the CO_2 system in surface waters of the eastern Bering Sea shelf. *Geophysical Research Letters*, **29**, 1–4.

Nanninga, H.J. & Tyrrell, T. (1996). Importance of light for the formation of algal blooms of *Emiliania huxleyi*. *Marine Ecology Progress Series*, **136**, 195–203.

Napp, J.M. & Hunt Jr, G.L. (2001). Anomalous conditions in the south-eastern Bering Sea 1997: linkages among climate, weather, ocean, and biology. *Fisheries Oceanography*, **10**, 61–68.

Nejstgaard, J.C., Gismervik, I. & Solberg, P.T. (1997). Feeding reproduction by *Calanus finmarchicus*, and microzooplankton grazing during mesocosm blooms of diatoms and the coccolithophore *Emiliania huxleyi*. *Marine Ecology Progress Series*, **147**, 197–217.

Niebauer, H.J., Alexander, V. & Henrichs, S. (1990). Physical and biological oceanographic interaction in the spring bloom at the Bering Sea marginal ice edge zone. *Journal of Geophysical Research*, **95**, 22,229–22,241.

Niebauer, H.J., Bond, N.A., Yakunin, L.P. & Plotnikov, V.V. (1999). An update on the climatology and sea ice of the Bering Sea. In T.R. Loughlin & K. Ohtani, eds., *Dynamics of the Bering Sea*, chap. 2, 29–59, University of Alaska Sea Grant.

Olson, M.B. & Strom, S.L. (2002). Phytoplankton growth, microzooplankton herbivory and community structure in the southeast Bering Sea: insight into the formation and temporal persistence of an *Emiliania huxleyi* bloom. *Deep-Sea Research Part II*, **49**, 5,969–5,990.

Opdyke, B.N. & Wilkinson, B.H. (1990). Paleolatitude distribution of Phanerozoic marine ooids and cements. *Palaeogeography, Palaeoclimatology, Palaeoecology*, **78**, 135–148.

Opdyke, B.N. & Wilkinson, B.H. (1993). Carbonate mineral saturation state and cratonic limestone accumulation. *American Journal of Science*, **293**, 217–234.

Overland, J.E., Bond, N.A. & Adams, J.M. (2001). North Pacific Atmospheric and SST Anomalies in 1997: Links to ENSO? *Fisheries Oceanography*, **10**, 69–80.

Paasche, E. (1967). Marine plankton algae grown with light-dark cycles. I. *Coccolithus huxleyi*. *Physiologia Plantarum*, **20**, 946–956.

Paasche, E. (2002). A review of the coccolithophorid *Emiliania huxleyi* (Prymnesiophyceae), with particular reference to growth, coccolith formation, and calcification-photosynthesis interactions. *Phycologia*, **40**, 503–529.

Palenik, B. & Dyrhman, S. (1998). Recent progress in understanding the regulation of marine productivity by phosphorus. In J.P. Lynch & J. Deikman, eds., *Phosphorus in plant biology: regulatory roles in molecular, cellular, organismic and ecosystem processe*, American Society of Plant Physiologists.

Palenik, B. & Henson, S.E. (1997). The use of amides and other organic nitrogen sources by the phytoplankton *Emiliania huxleyi*. *Limnology and Oceanography*, **42**, 1544–1551.

Pease, C.H. (1980). Eastern Bering Sea ice processes. *Monthly Weather Review*, **108**, 2015–2023.

Peng, T.H., Takahashi, T., Broecker, W.S. & Olafsson, J. (1987). Seasonal variability of carbon dioxide, nutrients and oxygen in the northern North Atlantic surface water: observation and a model. *Tellus*, **39B**, 439–458.

Platt, T., Gallegos, C.L. & Harrison, W.G. (1980). Photoinhibition of photosynthesis in natural assemblages of marine phytoplankton. *Journal of Marine Research*, **38**, 687–701.

Quevedo, M. & Anadón, R. (2001). Protist control of phytoplankton growth in the subtropical north-east Atlantic. *Marine Ecology Progress Series*, **221**, 29–38.

Ragueneau, O., Tréguer, P., Leynaert, A., Anderson, R.F., Brzezinski, M.A., DeMaster, D.J., Dugdale, R.C., Dymond, J., Fischer, G., François., R., Heinze, C., Maier-Reimer, E., Martin-Jézéquel, V., Nelson, D.M. & Quéguiner, B. (2000). A review of the Si cycle in the modern ocean: recent progress and missing gaps in the application of biogenic opal as a paleoproductivity proxy. *Global Planetary Change*, **26**, 317–365.

Raymont, J.G.E., ed. (1983). *Plankton and productivity in the oceans. Vol. 2. Zooplankton*. Pergamon Press, 2nd edn.

Rees, A.P., Malcolm, E., Woodward, S., Robinson, C., Cummings, D.G., Tarran, G.A. & Joint, I. (2002). Size-fractionated nitrogen uptake and carbon fixation during a developing coccolithophore bloom in the North Sea during June 1999. *Deep-Sea Research Part II*, **49**, 2905–2927.

Richardson, K., Beardall, J. & Raven, J.A. (1983). Adaptation of unicellular algae to irradiance: an analysis of strategies. *New Phytologist*, **93**, 157–191.

Riebesell, U., Zondervan, I., Rost, B., Tortell, P.D., Zeebe, R.E. & Morel, F.M.M. (2000). Reduced calcification of marine plankton in response to increased atmospheric CO_2. *Nature*, **407**, 364–367.

Riegman, R., Noordeloos, A.A. & Cede, G.C. (1992). *Phaeocystis* blooms and eutrophication of the continental coastal zones of the North Sea. *Marine Biology*, **112**, 479–484.

Riegman, R., Stolte, W., Noordeloos, A.A.M. & Slezak, D. (2000). Nutrient uptake and alkaline phosphatase (EC 3:1:3:1) activity of *Emiliania huxleyi* (Prymnesiophyceae) during growth under N and P limitation in continuous cultures. *Journal of Phycology*, **36**, 87–96.

Robertson, J.E., Robinson, C., Turner, D.R., Holligan, P., Watson, A.J., Boyd, P., Fernández, E. & Finch, M. (1994). The impact of a coccolithophore bloom on oceanic carbon uptake in the northeast Atlantic during summer 1991. *Deep-Sea Research Part I*, **41**, 279–314.

Rousseau, V., Leynaert, A., Daoud, N. & Lancelot, C. (2002). Diatom succession, silicification and silicic acid availability in Belgian coastal waters (southern North Sea). *Marine Ecology Progress Series*, **236**, 61–73.

Saltelli, A. (2000). What is sensitivity analysis? In A. Saltelli, K. Chan & E.M. Scott, eds., *Sensitivity analysis*, Wiley Series in Probability and Statistics, chap. 1, 3–13, John Wiley and Sons LTD.

Sambrotto, R.N., Niebauer, H.J., Goering, J.J. & Inverson, R.L. (1986). Relationships among vertical mixing, nitrate uptake, and phytoplankton growth during the spring bloom in the southeast Bering Sea middle shelf. *Continental Shelf Research*, **5**, 161–198.

Sambrotto, R.N., Savidge, G., Robinson, C., Boyd, P., Takahashi, T., Karl, D.M., Langdon, C., Chipman, D., Marra, J. & Codispoti, L. (1993). Elevated consumption of carbon relative to nitrogen in the surface ocean. *Nature*, **363**, 248–250.

Schlitzer, R. (2002). Ocean Data View. `http://www.awi-bremerhaven.de/GEO/ODV`.

Schumacher, J.D. & Stabeno, P.J. (1998). The continental shelf of the Bering Sea. In A.R. Robinson & K.H. Brink, eds., *The Sea: the global coastal ocean regional studies and synthesis*, vol. XI, 869, John Wiley and Sons, New York.

Sciandra, A., Harlay, J., Lefèvre, D., Lemée, R., Rimmelin, P., Denis, M. & Gattuso, J. (2003). Response of coccolithophorid *Emiliania huxleyi* to elevated partial pressure of CO_2 under nitrogen limitation. *Marine Ecology Progress Series*, **261**, 111–122.

Simpson, J.J. & Dickey, T.D. (1981). Alternative parameterisation of downward irradiance and their dynamical significance. *Journal of Physical Oceanography*, **11**, 876–882.

Smayda, T.J. (1997). Harmful algal bloom: their physiology and general relevance to phytoplankton blooms in the sea. *Limnology and Oceanography*, **42**, 1137–1153.

Spero, H.J., Bijma, J., Lea, D.W. & Bemis, B.E. (1997). Effect of seawater carbonate concentration on foraminiferal carbon and oxygen isotopes. *Nature*, **390**, 497–500.

Stabeno, P.J., Schumacher, J.D. & Ohtani, K. (1999a). The physical oceanography of the Bering Sea. In T.R. Loughlin & K. Ohtani, eds., *Dynamics of the Bering Sea*, chap. 1, 1–28, University of Alaska Sea Grant.

Stabeno, P.J., Schumacher, J.D. & Salo, S.A. (1999b). Physical environment around the Pribilof Islands. In T.R. Loughlin & K. Ohtani, eds., *Dynamics of the Bering Sea*, chap. 9, 193–215, University of Alaska Sea Grant.

Stabeno, P.J., Bond, N.A., Kachel, N.B., Salo, S.A. & Schumacher, J.D. (2001). On the temporal variability of the physical environment over the south-eastern Bering Sea. *Fisheries Oceanography*, **10**, 81–98.

Steele, J.H. & Henderson, E.W. (1992). The role of predation in plankton models. *Journal of Plankton Research*, **14**, 157–172.

Stockwell, D.A., Whitledge, T.E., Zeeman, S.I., Coyle, K.O., Napp, J.M., Brodeur, R.D., Pinchuk, A.I. & Hunt Jr., G.L. (2001). Anomalous conditions in the south-eastern Bering Sea, 1997: nutrients, phytoplankton and zooplankton. *Fisheries Oceanography*, **10**, 99–116.

Strom, S., Wolfe, G., Holmes, J., Stecher, H., Shimeneck, C., Lambers, S. & Moreno, E. (2003). Chemical defense in the microplankton I: Feeding and growth rates of heterotrophic protists on the DMS-producing phytoplankter *Emiliania huxleyi*. *Limnology and Oceanography*, **48**, 217–229.

Strom, S.L., Brainard, M.A., Holmes, J.L. & Olson, M.B. (2001). Phytoplankton blooms are strongly impacted by microzooplankton grazing in coastal North Pacific waters. *Marine Biology*, **138**, 355–368.

Stumm, W. & Morgan, J.J. (1981). *Aquatic chemistry: an introduction emphasizing chemical equilibria in natural waters*. John Wiley and Sons, New York, 2nd edn.

Sukhanova, I.N. & Flint, M.V. (1998). Anomalous blooming of coccolithophorids over the eastern Bering Sea shelf. *Oceanology*, **38**, 502–505.

Sukhanova, I.N., Semina, H.J. & Venttsel, M.V. (1999). Spatial distribution and temporal variability of the phytoplankton in the Bering Sea. In T.R. Loughlin & K. Ohtani, eds., *Dynamics of the Bering Sea*, chap. 22, 453–483, University of Alaska Sea Grant.

Sverdrup, H.U. (1953). On conditions for the vernal blooming of phytoplankton. *Journal du Conseil Permanent International pour l'Exploration de la Mer*, **18**, 287–295.

Takahashi, T., Broecker, W.S. & Bainbridge, A.E. (1981). The alkalinity and total carbon dioxide concentration in the world oceans. In B. Bolin, ed., *Scope 16: Carbon Cycle Modelling*, 271–286, John Wiley, New York.

Takahashi, T., Olafsson, J., Goddard, J.G., Chipman, D.W. & Sutherland, S.C. (1993). Seasonal variability of CO_2 and nutrients in the high-latitude surface oceans: a comparative study. *Global Biogeochemical Cycles*, **7**, 843–878.

Taniguchi, A., Saito, K., Koyama, A. & Fukuchi, M. (1976). Phytoplankton communities in the Bering Sea and adjacent seas I. Communities in early warming season in southern areas. *Journal of the Oceanographical Society of Japan*, **32**, 99–106.

Taylor, A.H., Geider, R.J. & Gilbert, F.J.H. (1997). Seasonal and latitudinal dependencies of phytoplankton carbon-to-chlorophyll *a* ratios: results of a modelling study. *Marine Ecology Progress Series*, **152**, 51–66.

Theurillant, J.P. & Guisan, A. (2001). Potential impact of climate change on vegetation in the European Alps: a review. *Climate Change*, **50**, 77–109.

Townsend, D.W., Keller, M.D., Holligan, P.M. & Balch, S.G.A.W.M. (1994). Blooms of the coccolithophore *Emiliania huxleyi* with respect to hydrography in the Gulf of Maine. *Continental Shelf Research*, **14**, 979–1000.

Tynan, C.T., DeMaster, D.P. & Peterson, W.T. (2001). Endangered right whales on the southeastern Bering Sea shelf. *Science*, **294**, 1,894.

Tyrrell, T. & Merico, A. (2003). *Emiliania huxleyi*: bloom observations and the conditions that induce them. In H.R. Thierstein & J.R. Young, eds., *Coccolithophore: from molecular processes to global impact*, Springer-Verlag, Germany, IN PRESS.

Tyrrell, T. & Taylor, A.H. (1996). A modelling study of *Emiliania huxleyi* in the NE Atlantic. *Journal of Marine Systems*, **9**, 83–112.

Tyrrell, T., Holligan, P.M. & Mobley, C.D. (1999). Optical impacts of oceanic coccolithophore blooms. *Journal of Geophysical Research*, **104**, 3,223–3,241.

van der Wal, P., Kempers, R.S. & Veldhuis, M.J.W. (1995). Production and downward flux of organic matter and calcite in a North Sea bloom of the coccolithophore *Emiliania huxleyi*. *Marine Ecology Progress Series*, **126**, 247–265.

Vance, T.C., Baier, C.T., Brodeur, R.D., Coyle, K.O., Decker, M.B., Hunt Jr., G.L., Napp, J.M., Schumacher, J.D., Stabeno, P.J., Stockwell, D., Tynan, C.T., Whitledge, T.E., Wyllie-Echeverria, T. & Zeeman, S. (1998). Aquamarine waters recorded for first time in eastern Bering Sea. *EOS Transactions of the American Geophysical Union*, **79**, 121–126.

Verity, P.G. & Smetacek, V. (1996). Organism life cycles, predation, and the structure of marine pelagic ecosystems. *Marine Ecology Progress Series*, **130**, 277–293.

Vidal, J. & Smith, S.L. (1986). Bioass, growth and development of populations of herbivorous zooplankton in the southeastern Bering Sea during spring. *Deep-Sea Research Part I*, **33**, 523–556.

Walsh, J.J. & Dieterle, D.A. (1994). CO_2 cycling in the coastal ocean. I - A numerical analysis of the southeastern Bering Sea with applications to the Chukchi Sea and the northern Gulf of Mexico. *Progress in Oceanography*, **34**, 335–392.

Walsh, J.J., Rowe, G.T., Iverson, R.L. & McRoy, C.P. (1981). Biological export of shelf carbon is a sink of the global CO_2 cycle. *Nature*, **191**, 196–201.

Walsh, J.J., McRoy, C.P., Coachman, L.K., Georing, J.J., Nihoul, J.J., Whitledge, T.E., Blackburn, T.H., Parker, P.L., Wirick, C.D., Shuert, P.G., Grebmeir, J.M., Springer, A.M., Tripp, R.D., Hansell, D.A., Djenidi, S., Deleersnijder, E., Henriksen, K., Lund, B.A., Andersen, P., Muller-Karger, F.E. & Dean, K. (1989). Carbon and nitrogen recycling with the Bering/Chukchi Seas: source regions for organic matter effection AOU demands of the Arctic Ocean. *Progress in Oceanography*, **22**, 277–359.

Wanninkhof, R. (1992). Relationship between wind speed and gas exchange over the ocean. *Journal of Geophysical Research*, **97**, 7373–7382.

Ward, B.B. (2000). Nitrification and the marine nitrogen cycle. In D.L. Kirchman, ed., *Microbial ecology of the oceans*, 427–453, Wiley-Liss, New York.

Weiss, R.F. (1974). Carbon dioxide in water and seawater: the solubility of non-ideal gas. *Marine Chemistry*, **2**, 203–215.

Westbroek, P., Brown, C.W., van Bleijswijk, J.D.L., Brownlee, C., Brummer, G.J., Conte, M., Egge, J., Fernandez, E., Jordan, R., Knappertsbusch, M., Stefels, J., Veldhuis, M., van der Wal, P. & Young, J. (1993). A model system approach to biological climate forcing: the example of *Emiliania huxleyi*. *Global Planetary Change*, **8**, 27–46.

Whitledge, T.E. & Luchin, V.A. (1999). Summary of chemical distributions and dynamics in the Bering Sea. In T.R. Loughlin & K. Ohtani, eds., *Dynamics of the Bering Sea*, chap. 10, 217–249, University of Alaska Sea Grant.

Whitledge, T.E., Reeburgh, W.S. & Walsh, J.J. (1986). Seasonal inorganic nitrogen distributions and dynamics in the southeastern Bering Sea. *Continental Shelf Research*, **5**, 109–132.

Whitledge, T.E., Bidigare, R.E., Zeeman, S.I., Sambrotto, R.N., Roscigno, P., Jensen, P.R., Brooks, J.M., Trees, C. & Veidt, D.M. (1988). Biological measurements and related chemical features in Soviet and United States regions of the Bering Sea. *Continental Shelf Research*, **8**, 1,299–1,319.

Winter, A., Jordan, R.W. & Roth, P.H. (1994). Biogeography of living coccolithophores in ocean waters. In A. Winter & W.G. Siesser, eds., *Coccolithophores*, 39–49, Cambridge Univ. Press.

Wolf-Gladrow, D., Riebesell, U., Burkhardt, S. & Bijma, J. (1999). Direct effects of CO_2 concentration on growth and isotopic composition of marine plankton. *Tellus*, **51**, 461–476.

Wyllie-Echeverria, T. & Wooster, W.S. (1998). Year-to-year variations in Bering Sea ice cover and some consequences for fish distributions. *Fisheries Oceanography*, **7**, 159–170.

Young, J.R. (1994). Functions of coccoliths. In A. Winter & W.G. Siesser, eds., *Coccolithophores*, 63–82, Cambridge University Press.

Zeebe, R.E. & Wolf-Gladrow, D. (2001). *CO_2 in seawater: equilibrium, kinetics, isotopes*, vol. 65 of *Elsevier Oceanography Series*. Elsevier.

Zondervan, I., Zeebe, R.E., Rost, B. & Riebesell, U. (2001). Decreasing marine biogenic calcification: a negative feedback on rising atmospheric pCO_2. *Global Biogeochemical Cycles*, **15**, 507–516.